UAV AND IRS-AIDED WIRELESS COMMUNICATIONS:

MODELING, ANALYSIS, AND OPTIMIZATION

By

TANIYA SHAFIQUE

A Thesis submitted to the Faculty of Graduate Studies of
The University of Manitoba
in partial fulfillment of the requirements of the degree of

DOCTOR OF PHILOSOPHY

UNIVERSITY OF MANITOBA

Department of Electrical and Computer Engineering

DECEMBER 2021

Supervisor: Ekram Hossain

Abstract

With the roll-out of 5G in many countries e.g. South Korea, Canada, etc, the discussions on the development of 6G are overtaking the attention of both academia and industry. In comparison to 5G, 6G will bring a wider frequency band, higher coverage and spectral efficiency, higher data rate, low latency and more, to enhance communication for the massive number of users/devices. Two of the emerging enablers for beyond (5G) B5G and 6G communications are unmanned aerial vehicles (UAV) and intelligent reflecting surfaces (IRSs). When UAVs have already become an integral part of 5G and B5G to meet the high data rate requirement by offering better communication links due to the proactive placement at heights (i.e., flexible deployment in all the three dimensions (3D)), the IRSs have emerged as a key enabler for realizing 6G to provide better coverage by tuning the wireless environment through an intelligent reflection of the incoming signal at very little power cost. In addition, B5G networks are expected to support aerial user communications in accordance with the expanded requirements of data transmission for an aerial user. However, there are some challenges and unaddressed issues that need attention before accommodating the enablers like UAVs and IRSs in future wireless standards such as the consideration of different radio wave propagation properties between terrestrial areas and aerial areas, the effect of product path-loss experienced by IRS for both ground and aerial communication, gains associated with 3D IRS installation in static (on fixed location e.g. building height) and dynamic (on mobile UAV) environment are still unknown, and providing service to remote or un-served users on both small and large scale.

In order to address the technical issues in the above context, the thesis develops few

innovative enabling frameworks regarding UAV and/or IRS-assisted communication. In particular, (i) I begin with the optimal UAV-assisted data ferrying scheme to provide coverage to hard-to-reach or remote areas for delay-tolerant applications by taking aerial and ground channel model and rotary-wing UAV power consumption into account, (ii) Second, an integrated UAV-IRS scheme is proposed where IRS is installed on the UAV and therefore, can benefit from 3D deployment similar to UAV, taking important factors e.g. aerial and ground channel, height and number of IRS elements for UAV and IRS, respectively, and power consumption of both UAV and IRS in to account. Finally, (iii) to incorporate massive devices of different kinds in to consideration, I proposed large-scale IRS-assisted downlink communication for multi-BS and multi-IRS setup. For the very setup, the user association with indirect IRS-assisted communication and user association with direct BSs are studied. The impact of the fraction of each type of user, number of IRS elements and its power consumption, large-scale deployment intensity of UAV and IRS in to account. Additionally, the performance of the proposed schemes are investigated through the derivation of closed-form exact and/or accurate approximate expression of the performance metrics that include coverage/outage probability, spectral and energy efficiency, bit-error rate, etc. Finally, the provided expressions are utilized in the various optimization problem and optimization solutions are either convexified by reformulation and using approximations or by designing low complexity algorithms. The insights are drawn related to available operation modes and other critical network parameters. Finally, the results are validated through Monte-Carlo simulations.

Dedication

This dissertation is dedicated to my loving parents, beloved husband, and my adventurous little son Faateh.

ACKNOWLEDGMENT

Contents

List of Tables

List of Figures

List of Abbreviations

Acronym	Description
UAV	Unmanned aerial vehicle
BS	Base station
BEP	Bit error probability
LoS	Line of sight
NLoS	Non-line of sight
DC	Difference of convex funtion
LCAD	Load carry and deliver
SNR	Signal-to-noise ratio
SINR	Signal-to_interference plus noise ratio
QoS	Quality of service
DF	Decode and forward
EE	Energy efficiency
EE^{MC}	Overall energy efficiency of the multicasting system
CDF	Cumulative distribution function
PDF	Probability density function
5G	Fifth-generation of Internet
6G	Fifth-generation of Internet
IRS	Intelligent reflecting surface
CSI	Channel state information
IBFD	In-band full duplex
SI	Self interference
AWGN	All white Gaussian noise
SC	Selection combining
CTL	Central limit theorem
LT	Laplace transform
GG	Generalized Gamma random variable
MGF	Moment generating function
SDP	Semidefinite program

Chapter One

Introduction

Cellular communication has been evolving in stages from first-generation (1G) technologies to fifth-generation (5G) and beyond (B5G), which is also referred to as the sixth generation (6G) technology. The 1G cellular wireless communication technologies first introduced voice communication in analog form. 2G technologies enhanced voice communication and brought data and digital communication, e.g., sending messages into the picture. They also started the Internet with a limited average speed below 0.5 Mbps. 3G technologies significantly improved the downlink speed and data transmission. With 3G technologies, video communication become real in the form of video calling, video conferencing, and live video chat. 3G had four-fold data transfer capacity than 2G. 4G technologies targeted enhancing the video quality, smoothing the Internet browsing and playing video games. 5G technologies are being deployed now which are expected to support a very large number of wireless devices to realize the Internet of Things (IoT). The major features of 5G are enhanced speed, high bandwidth between (30GHz -300GHz) and low latency [1].

1.1 Future Wireless Networks and Enabling Technologies

6G is a successor technology of 5G. While 5G is in the roll-out stage, the advancement in the 6G research is being done throughout the world. The 6G standardization is estimated to be sorted out by the international standardization bodies by the year 2030 [2], which will potentially enable the Internet of Everything (IoE). With 6G, an extravagant number of devices/machines would be connected the each other to achieve massive connectivity. 6G technologies will also use higher spectrum bands (e.g. millimeter wave [mmWave] and tera Hertz [THz] bands), achieve lower latency, and higher speed than 5G [3]. 6G will bring improved battery lifetime, wireless charging, aerial as well as underwater wireless communication, machine learning (ML), and artificial intelligence (AI)-enabled wireless communications systems and networks [4].

Some of the enabling technologies for 6G systems are shown in Figure 1.1. These technologies will provide coverage to remote area users, build 3D communication and aerial interface to enhance coverage by leveraging the line of sight (LoS) communication. One innovation of 6G is smart intelligent surfaces, also called intelligent re-configurable surfaces or intelligent reflecting surfaces (IRSs) that can reconfigure the communication channel by intelligently reflecting the incident wireless signal. Since the 6G vision is to support millions of devices, different enabling technologies will coexist to serve a massive number of devices. Lastly, for real-time and intelligent decision-making, machine learning (ML) and artificial intelligence (AI) techniques will be vital in 6G.

1.1.1 Remote Area Communication

It is becoming increasingly important to provide coverage to remote area users that lack the terrestrial cellular wireless infrastructure. The coverage requirement can arise for on-demand applications and disaster management scenarios. For instance, short-term coverage
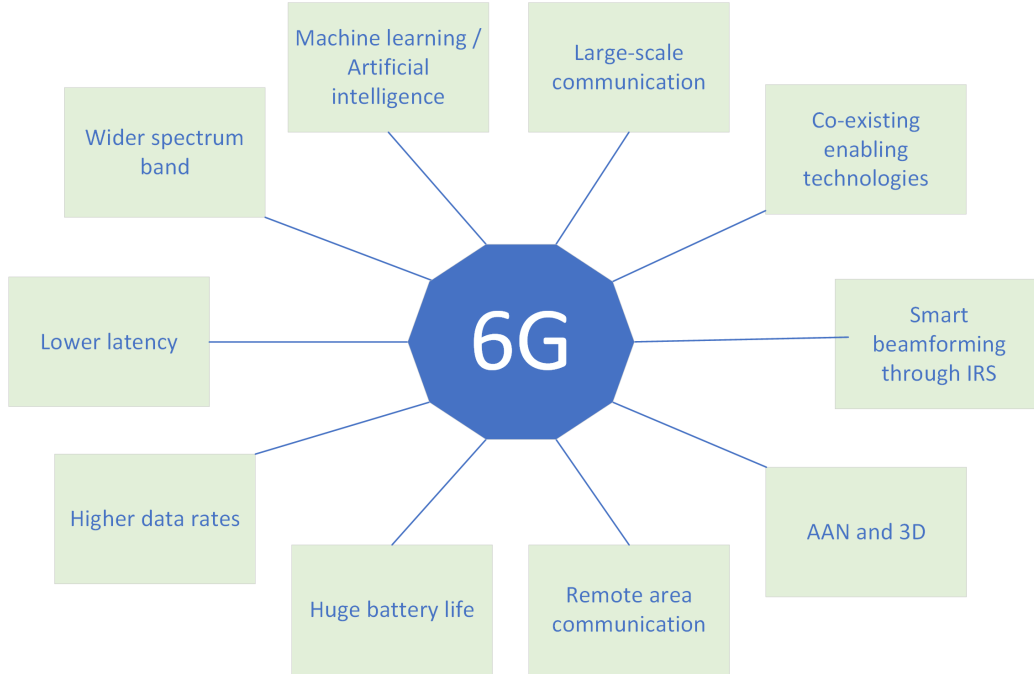
Figure 1.1 6G technologies.

requirement in a certain area for broadcasting a hockey match is an example of on-demand communication. In a scenario where massive destruction has caused the loss in the existing communication infrastructure (e.g., due to earth quack). In such a situation deployment of the terrestrial infrastructure such as BSs are economically expensive and time-consuming. 6G requires addressing such situations at a low cost.

1.1.2   Aerial Access Network and 3D Communication

The expected demand of providing the coverage to 'Everything' brings an aerial access network (AAN) as a potential candidate in the 6G communication system that can establish a line-of-sight (LoS) communication link between the ground and aerial users. The elements of AANs are unmanned aerial vehicles (UAVs), also known as drones, satellites, high and low altitude platforms [5]. In contrast to terrestrial infrastructure, the AAN elements such as UAVs, high and low altitude platforms have the potential to change their locations in all

three dimensions proactively. This helps to establish better and LoS communication links that will lead to coverage enhancement in 6G.

1.1.3 Intelligent Beamforming Through Intelligent Reflecting Surfaces

An intelligent reflecting surface (IRS) can steer the incident wireless signals in the desired direction that extends the communication range between sender and the receiver. This is unlike an omni-directional transmission that spreads the transmission energy in all directions. Additionally, the construction of IRS includes multiple small passive metasurfaces and does not require any additional transmission power. Also, since IRS mostly acts as a reflecting surface that does not spend any time in processing the incoming signal, it does not introduce any delays in the system. Besides the flexibility in the beamforming, the energy efficiency is also an important feature of IRS that makes IRS an enabling technology for 6G communication. The functionality of IRS will be discussed further in Chapter IV.

1.1.4 Co-Existence of Enabling Technologies

In a 6G network, different enabling technologies will co-exist and users should intelligently decide and switch to the best enabling technology available based on the channel conditions and quality of service (QoS) requirement. The examples of the enabling technologies are terrestrial cellular BS, aerial BSs, i.e., UAV, IRS-enabled communication, visible light communication (VLC), etc. Therefore, 6G needs to provide such hardware and infrastructure that is capable of combining all the enabling technologies [6] together.

1.1.5 Large-Scale Communication

5G and beyond 5G is an era of IoE where millions of devices will communicate to each other through different access networks within a small geographical area leading to large-scale networks. [7] expects to have 10 million devices per square kilometer which is ten folds larger than the 5G devices. The massive number of connecting devices will bring a list of new challenges for the 6G network such as blocking, non-line of sight channel, and spectrum sharing, resource allocation, and interference management. This will require modeling and characterization of large-scale 6G systems, e.g., using the tools of stochastic geometry.

1.1.6 Machine Learning and Artificial Intelligence

The applications such as automated cars and voice assistance are the ML innovations in 5G and B5G. However, the core of 6G will lie in handling continuous gigantic real-world data, its processing, demand-based decision making, and providing secure communication [8]. ML and AI will assist 6G in the decision-making by designing algorithms to obtain knowledge of fast varying changes in the channel condition which can not be taken care by the conventional mathematical modeling. ML and AI will also provide potential solutions for the user decision-making problem in presence of coexisting enabling technologies. Also, machine learning will provide an alternative to achieve solutions to optimization problems, especially where the conventional optimization method fails to provide an optimal solution due to high complexity, e.g., in combinatorial optimization problems.

1.2 Key Challenges of Future Wireless Networks

With the expected advancement in future wireless networks as described in previous section, there exist variety of challenges that needs to be taken in to account which are discussed

next.

i. Providing Coverage to Remote Area Users: The advancement in future network features providing coverage to the user in rural areas or hard-to-reach locations that may not have well-established cellular infrastructure [9]. Future networking should essentially provide a coverage solution to remote area users in such a way that solution is easy to deploy, power-efficient, cost-effective and has significantly lower time consumption.

ii. 3D Supported Modeling: 6G is required to support the 3D aerial communication because of the integration of airborne (such as UAVs) and terrestrial networks (terrestrial BS) in to the architecture. This requires modeling the 3D propagation environment and channel modeling between air and ground by taking environmental factors such as rain, fog, and humidity, etc. This also requires consideration of placement design, mobility management, and resource management, etc due to the mobility feature of UAVs.

iii. IRS Modeling and Utilization of IRS to Full Capacity: As described above, IRS-aided communication is gaining attention in both research and academia as a 6G candidate. The key features of IRS are as follows: (i) IRS can be deployed anywhere from clothes to the building wall and airplanes, and (ii) IRSs consist of the arrays of multiple low-cost metasurfaces and each surface individually has the potential to steer the incident signal in the desired direction. Besides the IRS functionality as a reflector, it is also capable to perform other functions such as transmission, switching, and refraction. Therefore, to utilize the IRS in full capacity for the future wireless generation, understanding IRS-functionality, IRS channel modeling, and integrating IRS with other technologies is highly needed. The understanding of IRS will answer the research questions such as how IRSs should be deployed to obtain maximum throughput or energy efficient solutions under different existing deployment setups. How IRS will behave when mounted on the mobile surface for instance on UAVs. Under what situation IRS

6

extend the communication range although it suffers from product path loss, and the behavior of IRSs in the IRS-assisted communication setup in the existence of random blocking objects, etc.

iv. Hardware Design for Co-existing Technologies: As 6G is will support billions of devices that are connected through different access networks and also utilize different enabling technologies, there is a need for designing such infrastructure that supports all the existing and new technologies to keep the transition to future generations smooth and cost efficient. Also, the devices in the future generation would be able to sense the channel conditions and will be able to decide and select the optimal network depending on the availability of the other channels, channel conditions, and QoS requirements. Therefore, it is a challenge to design such switching-supported hardware where all the enabling methods can be merged.

v. Large-Scale Network Modeling: With the massive connectivity in 6G modeling and analyzing large-scale networks is inevitable. With all the devices connected to each other and through different enabling technologies, the role of interference becomes even more significant than previous generations. Therefore, accurate modeling of the system interference and blockages for all kinds of devices should be taken into account. Also, analyzing the overall system performance such as outage and bit error probability, achievable data rate, and energy efficiency is a fundamental challenge for future communication networks.

In general, in this work, the common challenges for the thesis are noted below.

vi. Mathematically Tractable Performance Analysis: One of the common open problem that is not thoroughly studied and well-analyzed performance measures (e.g., for the communication setup I defined above). Also, the existing derived expression for the performance measure such as outage probability and capacity, etc are not in closed form

or represented in the form of integrals. Therefore, their application to the optimization of network parameters is a fundamental challenge.

vii. Statistical/Analytical Optimization: The existing works consider typical computationally intensive instantaneous optimization frameworks in which the objective function and constraints are defined for each fading channel realization (which typically assume perfect knowledge of channel state information (CSI)) and, subsequently, to understand the impact of a variety of fading channels, an instantaneous optimization problem needs to be solved for a large number of channel realizations.

1.3 Scope of Thesis and Motivation

The following enabling techniques for 6G wireless communications are within the scope of this thesis.

1.3.1 UAV-Assisted Communication

Unmanned aerial vehicles (UAVs), also referred to as drones, are expected to be an integral component of fifth generation (5G)/beyond 5G (B5G) wireless cellular networks [10]. UAVs have a wide range of applications to civilian and commercial domains [11]. UAVs can work as flying base stations (BSs) to provide wireless connectivity among users/devices which otherwise might not be served using the traditional cellular networks. A UAV can also work as a relay between two BSs and provide backhaul connectivity for cellular BSs. Due to their ease in deployment and ability to provide good air-to-ground (AtG) communication links (mainly due to line of sight [LoS] propagation), UAV enabled wireless communication has recently attracted significant interests in both industry and academia. For example, Facebook and Google has initiated the project 'Aquila' and 'Wing', respectively, to provide

UAV based internet/communication services [10]. Amazon has introduced 'Amazon Prime Air' to deliver items using UAV and tested its first successful air delivery in Dec 2016.

UAV related researches are categorized in three types based on the mobility of the UAVs, i.e., static-UAV, mobile-UAV networks, and data ferrying. Static-UAV approach majorly focuses on UAV placement and optimization [12] while the mobile-UAV networking pivot around shorting the distance significantly between UAV and ground users by proper path planning. For instance, in [13] circular UAV trajectory centered on ground BS is proposed. In data ferrying approach the UAV loads the data from source, carries it to the destination and delivers the data on reaching sufficiently close to the destination.

UAVs are classified into two categories based on their design structure: (i) fixed wing UAVs and (ii) rotary wing UAVs. There exist pros and cons associated with both types. For example, the fixed-wing UAVs are high speed and have heavy payload, but the limitation is that they need to maintain their motion in forward to remain aloft, therefore, fixed wing UAVs do not fit for the for stationary applications. However, the rotary-wing can move in any direction as well as they can hover or stay stationary in the air with the limitation on having limited mobility and limited payload. Therefore, the UAV should be selected wisely based on the application. The rotary wing UAVs are suitable for data ferrying application.

There main **technical challenges** that need to be taken into account when considering UAV-assisted communications are follows:

- *Energy consumption*: The energy consumed in UAV-communication are data transmission and the propulsion energy required by the UAV to remain aloft or maintain its movement [13, 14]. The propulsion energy is directly proportional to the size of the UAV and the distance the UAV travels that require precise energy consumption model.

- *Aerial channel modeling*: The UAV assisted aerial communication are expected to have line-of-sight (LoS) links in most scenarios, but occasionally the links could be

blocked by the obstacles and buildings etc, specially when variable height of a UAV is considered.

- *UAV path planning and trajectory design:* UAV path planning or trajectory design is one of the crucial aspect to consider. In particular, the appropriate path planning can significantly reduce the communication distance and traveling time of a UAV and hence the throughput gain and energy efficient system can be obtained. Optimizing the path and trajectory is more crucial and challenging when the UAV is in dynamic environment. For instance, due to on-boarding energy limitation, time assigned to complete the task, collision avoidance etc.

Another challenge to UAV communication is *UAV mobile relaying and memory requirement.* The UAV assisted relaying also referred as mobile BS leveraging the wireless communication because the UAV flies between the source and destination with the intend to reduce the link distances when UAV receives the data and when the UAV relays the data. A common approach used for UAV relaying is half duplex decode-and-forward (DF) mobile relaying, in which UAV receives data, process and store it in to a buffer in one time slot and in the next slot UAV sends the data to the desired node. The larger the buffer size the less number of cycles UAV need to complete the task e.g., for heavy data dispatch. Therefore, the trade-off between on-board buffer size and achievable throughput in the UAV assisted mobile relaying needs to be studied in detail.

1.3.2 UAV-Assisted Data Ferrying

In the conventional data ferrying approach, UAV loads the data from a source, carry, and then deliver data to the destination after reaching to the final location [15]. However, the optimal data ferrying system considers the traveling time delay (i.e. duration in which UAV travels and carries the data) and minimizes this delay by allowing the UAV to travel only to

a minimum distance (i.e. a distance where the desired quality of service (QoS) can be met). The conventional data ferrying is power-inefficient in the existence of good quality channel since unnecessary flight of UAV adds in propulsion power consumption and adds extra delay specially when the UAV has back to back tasks to perform.
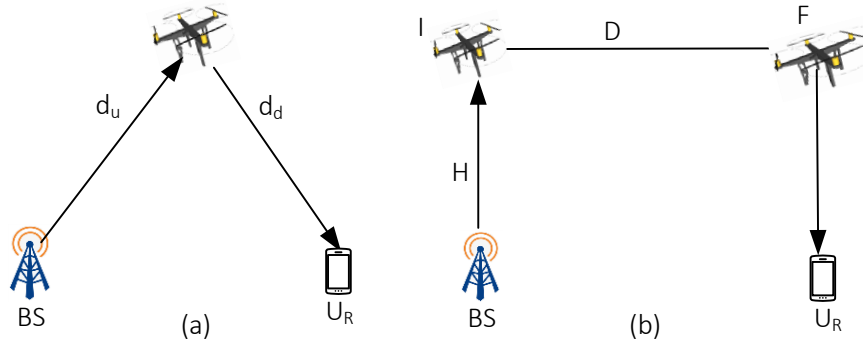
Figure 1.2 (a) UAV-assited communication between BS and user receiver (a) when UAV is at fixed location, and (b) when UAV is performing conventional data ferrying.

Figure 1.2 presents the UAV-assisted communication for two scenarios. In (a) when UAV is static and placed at the middle of the source (i.e, BS) and a destination (i.e U_R) and has the BS to UAV distance d_u and UAV to user distance d_d. In (b) when UAV performs conventional data ferrying that has data loading where UAV loads the data from height H above the BS, UAV travelling where UAV travels a distance D to reach closer to the destination, and data delivery phases where the information is being delivered to the destination U_R.

Applications of UAV-assisted data ferrying: The two main applications of data ferrying are as follow: *(i) UAV-assisted data ferrying for wireless backhauling:* Wireless backhauling is among one of the primary backhauling techniques in which wireless connections are typically established between base-stations (BSs) and the core network aggregators [16,17]. Since the backhaul requirements can significantly vary depending on the locations of the

BSs (e.g. BSs in rural areas or hard-to-reach locations may not have well-established backhaul infrastructure [9]), the wireless backhauling is becoming popular alternative to wired backhauling. Also, wireless backhauling is generally cost-effective compared to wired backhauling. In this context, UAV-assisted data ferrying provides a promising solution to assist wireless backhauling infrastructure through flexible on-demand UAV deployment and mobility in three dimensions [18,19], especially for delay-tolerant services and applications. *(ii) UAV-assisted data ferrying to ground users in disaster situations:* UAV-assisted data ferrying enables an instant communication infrastructure on demand. For example, consider a disaster situation in which the existing communication infrastructure including BSs has collapsed. Also, in scenarios where the communication infrastructure is not sufficient to fulfill the user requirements (i.e. most of the terrestrial BSs are congested). In such circumstances, communication of essential data and in turn UAV-assisted data ferrying becomes vital, even with higher transmission latencies [15]. A similar idea referred to as "Message ferrying" was studied in [20] for adhoc networks. Please note that, the proposed UAV data ferrying technique can also be perceived as a UAV that assists data dispatching to multiple ground nodes as shown in [21].

The phases and power consumption of conventional data ferrying : There are three phases of data-ferrying. (i): Uplink Data Loading Phase, (ii): UAV Travelling Phase (iii): Downlink Transmission Phase. In first phase, the UAV hovers above the source for a duration T_u to load the data from source. The energy consumption due to hovering of UAV and communication of the source BS in the uplink [21] is given as: $E^u = (P_h + p_u)T_u$, where p_u is the uplink power consumption of source BS and P_h is the propulsion power consumption of UAV (details in next chapter). In UAV Travelling Phase, the energy consumption is due to the UAV travelling for a distance D with a constant velocity V i.e, $E^t = P(V)D/V$, where $P(V)$ is the power consumed in travelling by UAV (details in next chapter). In the final Downlink Transmission Phase, The UAV experiences energy consumption due to

communication and hovering. The UAV hovering time T_d to deliver the data to destination BS which is given as $E^d = (P_h + p_d)T_d$. The end-to-end energy consumption of UAV is $E_{tot} = E^u + E^t + E^d$.

It is important to highlight that the energy efficiency and latency of a UAV-assisted data-ferrying network are primary concerns. Please note that minimizing the travel distance will also minimize the energy consumption of the UAV. The energy consumption model for optimal data ferrying is provided in next chapter in detail. In the following, we discuss two network scenarios in which data ferrying is applicable and can potentially yield benefits to network operators.

1.3.3 IRS-Assisted Communication

Intelligent reflecting surfaces (IRS) are emerging as a key enabling technique to smartly re-configure wireless propagation environment in beyond 5G or 6G wireless networks [22]. The IRS consists of multiple small meta-surfaces that are also referred to as *IRS elements*. IRS enables smart reconfiguration via software-controlled reflections and is energy-efficient since meta-surfaces contain low-cost polymer diode/switch and conductive square patches [23] [24]. The comprehensive intelligent functionality of each element includes reflection, refraction, transmittance and absorption [22, 25]. The functionalities can be used all together or in separate based on the application requirement. In contrast to conventional relays that re-quire active transmission and reception, the IRSs do not require any additional radio chan-nel/frequency for signal transmission or reception which makes IRS cost-effective. Note that, IRS usually act as a passive device and does not need any transmission power. However, its power consumption is due to the number of IRS elements and the phase resolution [23].

In conventional IRS relaying, IRS is usually mounted on building facade, furniture, and overall any objects in indoor or outdoor environments to establish communication between BS to the users in three different ways in general. In the presence of direct link, in the absence
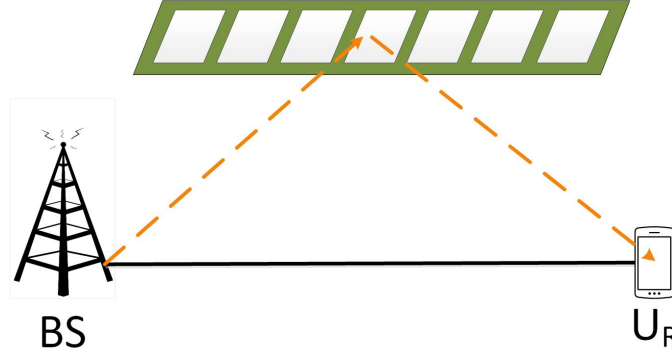
Figure 1.3 IRS-assited communication between BS and user when IRS is deployed at some building or wall.

of direct link and/or by jointly combine both direct and IRS-assisted link. Moreover, one important factor behind the emerging IRS-assisted communication is the power consumption. The power consumption of each IRS element is low, the overall power consumption may become significant for a large number of active IRS elements depending on the phase resolution power consumption $P_r(b)$. For instance, $P_r(b) = 5$dBm for 1-bit resolution and $P_r(b) = 45$dBm for infinite resolution [26]. The $P_r(b)$ depends on the operating frequency and the type of power amplifier [27]. The IRS power consumption is given as $P_{IRS} = NP_r(b)$.

Figure 1.3 presents the IRS-assisted communication when IRS is placed at the middle of the source (i.e, BS) and a destination (i.e U_R).

1.3.4   Integrated UAV-IRS Relaying

Unlike conventional IRS relaying, integrating IRS with the UAVs will not only improve the channel by optimizing the IRS angle for reflection but it will also allow flexible deployment of metasurfaces in three dimensional environment while minimizing the on-board UAV energy consumption [28, 29]. The proactive placement of integrated UAV-IRS system offers a cost-effective solution with minimal energy consumption and reduced network-wide spectrum resources. In future, I will consider the mathematical performance characterization and
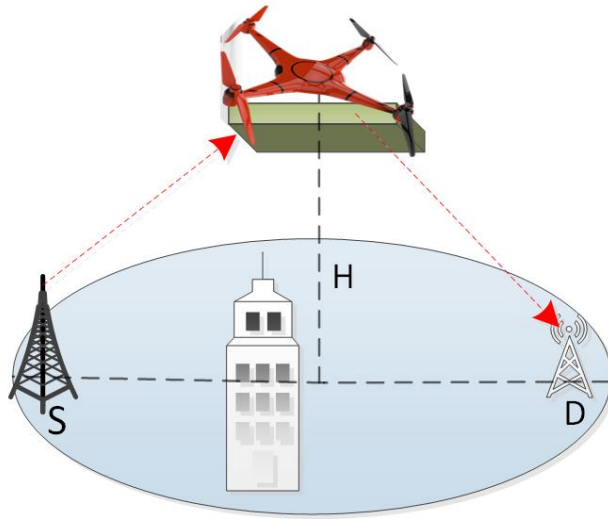
Figure 1.4 Integrated UAV-IRS communication when IRS is mounted on UAV and placed between source and destination receiver.

optimization of an integrated UAV-IRS system.

To develop the efficient integrated UAV-IRS system, the optimization of the number of IRS elements (N) is crucial due to two reasons, **(i)** given the limited UAV size, the number of IRS elements that can be deployed on a UAV is limited[1] and **(ii)** due to the power consumption associated with each IRS element. Although the power consumption of each IRS element is low, the overall power consumption may become significant for a large number of active IRS elements depending on $P_r(b)$ [27].

The Figure 1.4 represents the integrated UAV-IRS setup when UAV-borne IRS in 3D at height H is assisting the communication between S and D.

---

[1]The size of one IRS element is typically in the range $\lambda/10 - \lambda/5$ [24], where λ denotes the wavelength of the transmitted wave. As such, this limitation becomes more evident in low frequencies.

1.3.5 Large-Scale IRS-assisted communication

With the advances in the wireless technology and extravagant demand of higher data rate to millions of indoor/outdoor devices, it has become inevitable to utilize the resources wisely to enable massive connectivity. In this context, IRSs operate as a low cost solution to extend the communication range and to provide service to more users. To this end, IRS communication can hapen in three possible way, (i) *IRS-only Transmission:* When the direct link is blocked and only IRS-assisted signal is received by the user, (iii) *Direct Transmission:* in which a user gets served only through direct transmissions because of unavailability of IRS with in the cell radius, and (iii) *Joint Transmission:* When user received both direct and IRS-assisted signal. Similarly, in such setups user may experience different interference coming from interfering BSs and interference coming from other BSs reflected from other IRSs. Therefore, accurate consideration of interference is required for large scale IRS-setup.
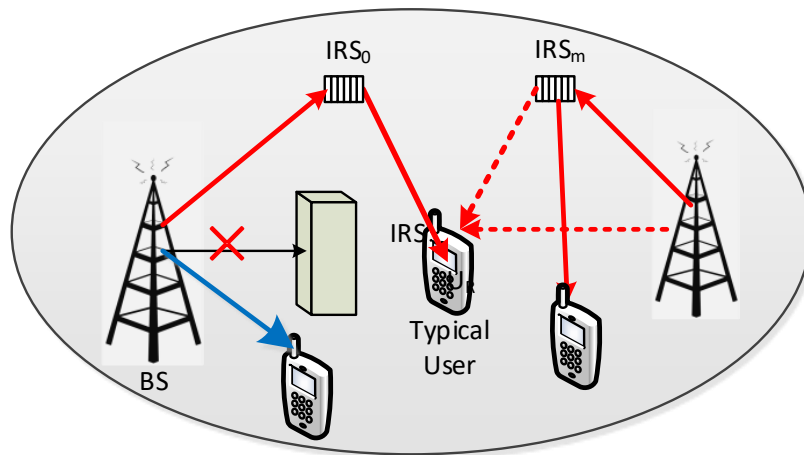
Figure 1.5 IRS-assisted communication in large scale setup with multi-IRS and multi-BS when the user is connected with a BS through nearest IRS and the direct link to the nearest BS is blocked.

Also, it is noteworthy that combining the signals coming from the direct and indi-

rect IRS-assisted path may suffer from incoherent multi-path delays and it may necessitate sophisticated synchronization, detection, and co-phasing techniques resulting in complex hardware/software design. Therefore, developing the large scale IRS-assisted network to understand the performance gain associated to IRS is crucial specially before designing the complicated hardware in addition to the interference management.

1.3.6 Motivation

The main motivations of the work presented under the scope of the thesis is to tackle few of the fundamental challenges for the future networks which are given as follows.

- Since the significance of aerial 3D-communication and the relevant challenges for 5G and B5G is realized, as shown in previous sections. Which include modeling of the aerial channel, propagation modeling in 3D by taking environmental factors in to account, integration of both aerial and terrestrial network etc. The above challenge (1.2.i) motivates me to study the deployment of unmanned aerial vehicle (UAV) as a flying BS, characterize aerial and ground channel modeling and evaluate the mathematically tractable analysis and optimization for the delay tolerant application. Besides this, the need of providing coverage to remote and hard-to-reach areas for the future network provide me motivation to utilize UAVs as a data-ferry that can load the data from the transmitting end, carry it towards the destination, and deliver it on reaching to the destination as a potential solution to (challenge (1.2.ii)).

- The integration of IRS in the future wireless network brings new challenges as mentioned in (1.2.iii). The fundamental questions such as the IRS functionality, and understanding the scenarios where IRSs can significantly enhance the communication performance, and how to utilize IRS to provide energy efficient solution etc.

  Moreover, one of the emerging trend of the 6G is coexisitng enabling technology as

discussed in previous section, in which the smart user/devices can choose the optimal communication link based on some predefined criteria. Therefore, it is required to design an association criteria based on the channel statistics which is also energy efficient. This idea motivated us to design an airborne communication system in which IRS is mounted on the UAV and terrestrial users are capable to choose the optimal communication link which can be UAV-only, IRS-only and integrated UAV-IRS mode (challenge (1.2.iv)).

- The motivation for the chapter 4 of the thesis is to combine the IRS related challenges to a large scale setup as per 5G and B5G requirement, with the multiple type of communication devices existing together and forming a large scale network. In addition, the motivation is to provide the insight depending on fraction of users assisted the coexisitng IRS-assisted BSs and cellular BSs and blocking objects effects. This chapter answers the outlines challenges in (1.2.iii), (1.2.iv) and (1.2.v).

In general, in this work, the common motivation of all the chapters in the thesis is that the above defined communication setup are not well studied in the literature. That motivates me to obtain the performance analysis in closed form and/or deriving the closed form approximation for simplicity when close form solution is hard to achieve. Moreover, the utilization of the obtained simpler closed form expression to transform the computationally intensive non-convex optimization to convex optimization.

1.4 Objective and Contribution of the Thesis

1.4.1 Objective

The main goal of the thesis is to design a mathematically tractable and accurate communication framework for future wireless networks. In particular, I study various system models

consisting of aerial communication, IRS-enabled communication in both small and large scale setups under different objectives. I aim to analyze and optimize the studied system model for future networks.

To achieve the objective, I use existing approximations, proposed new approximations, designed algorithms, and used tools of fractional programming and stochastic geometry throughout the thesis. The other objectives of the thesis are noted below.

- To tackle the coverage providing issue to remote and hard-to-reach areas, an UAV-assisted data ferrying communication scheme is proposed. In the proposed scheme UAV act as flying BS and can be flexibly sent to any desired geographical region to provide coverage. This scheme provides energy efficient solution by optimizing UAV travelling distance under outage constraint and provide transmission efficient solution by optimizing UAV traveling distance that provide minimum outage within the limited energy consumption budget.

- To overcome the lack in understanding, characterization and modeling of IRSs combined with 3D communication, I propose an IRS-assisted airborne communication scheme. This schemes combats the challenges offered due to LoS and NLoS in 3D aerial communication. In addition, the proposed framework provides useful insight on co-existing enabling technologies for 6G by integrating IRS and UAV together. Also, the scheme develops the understanding regarding the role of integrated IRSs and UAV in end-to-end communication performance measures. The scheme also provides energy efficient solution by taking important IRS and UAV communication factor such as number of IRS elements, the IRS associated power consumption, height of a UAV and by developing the analytical criteria to maximize SE.

- Since 6G is expected to have massive devices and various types of users connected through different transmissions (e.g., users served by direct BS transmissions and indi-

rect IRS-assisted transmissions), characterizing the different types of interference experienced by users in a cellular network with multiple BSs and IRSs becomes crucial. Also, there is a need for comprehensive study, modeling of IRS-assisted communication on large scale for ground users. To tackle these research problems, I propose a comprehensive large scale framework consisting of multiple BSs, IRSs, and various types of users using tools of stochastic geometry. The proposed approach captures the impact of channel fading, locations of BSs and IRSs, arbitrary phase-shifts, and different interference experienced by a typical user in the form of downlink achievable rate, coverage probability, and energy efficiency (EE) of different users.

- To overcome the computationally intensive typical instantaneous optimization frameworks even with the single optimization variable, I proposed the unique solutions for different types of optimization problem that uses closed-form analytical expressions for the end-to-end performance matrices under Rician and Rayleigh fading channels, followed by derived novel approximations and transformations to formulate a convex problem.

1.4.2 Contributions of the Thesis

In this thesis, I develop performance modeling and optimization of UAV-assisted communication systems and IRS-assisted systems for both aerial and ground communication to address their associated challenges. A brief list of contributions is presented next:

1. *End-to-end Performance modeling and optimization a UAV-assisted data ferrying*:

- The proposed UAV-assisted data ferrying characterizes different stages of data ferrying (data loading and delivering links) by considering both the LoS and NLoS transmissions, and specific energy consumption model for rotary wing UAV.

- The novel closed-form expressions of network reliability, bit-error probability (BEP)

and energy efficiency (EE) of the considered network are derived. Also, EE is derived as a function of the SNR outage probability using novel tractable approximations for the derived SNR outage.

- Two different optimization problems are formulated and solved for the optimal ferrying distance under different system constraints providing 95% accuracy from exhaustive search after convexification or in closed-form. A multi objective optimization with the objective of minimizing energy consumption and SNR outage of proposed data ferrying is reformulated as a difference of convex functions (DC) function and solved using a DC algorithm.

2. *End-to-end Performance modeling and optimization UAV-borne reflecting surfaces (i.e., integrated UAV-IRS system):*

- I develop a comprehensive mathematical framework to characterize an integrated UAV-IRS system considering various operation modes, where both UAV and IRS can work in standalone fashion or the Integrated UAV-IRS mode, where receiver has freedom to choose from the best of the both UAV-only and IRS-only link. The proposed modeling captures the LoS air-to-ground (AtG) Rician fading channels and power consumption of UAV and IRS.

- I obtain closed form expressions of outage probability, spectral and energy efficiency and also provide approximate expressions to increase the mathematical tractability.

- I provide optimal solutions using tool from fractional programming. The proposed optimization maximize the spectral and energy efficiency by apprehending critical network parameters such as the number of IRS elements and UAV altitude.

- I derive an analytic criterion to optimally select the UAV-only and IRS-only transmission modes to maximize the capacity and EE for a given number of IRS elements. In

general, the channel state information (CSI) may not be available at the receiver and/or difficult to obtain, therefore the optimization solution I attain is based of average CSI.

3. *Performance modeling and analysis of IRS-assisted downlink cellular networks*:

- I propose a mathematical framework to study the two types of user coexisting in a realistic large-scale multi-BS, multi-IRS scenario, the user performing direct transmission and the user performing IRS-assisted transmission. The proposed framework capture the impact of IRS phase-shifts and the aggregate interference from all IRSs on both kinds of users.

- For the IRS-assisted user, I characterize the desired signal power from the nearest IRS as a sum of scaled generalized gamma (GG) random variables with the parameters of the IRS phase shifts. For the very user, I also compare the signal power for optimized and randomized phase-shifts of the nearest IRS.

- I approximate and validate the aggregate interference from multiple IRSs in a multiple BS scenario as the sum of normal random variables.

- I analyze the coverage probability, spectral and energy-efficiency of both user types using Laplace transform (LT) method.

- I derive the overall coverage probability, spectral and energy efficiency based on the fraction of direct and IRS-assisted users in the network. The analysis captures the effect of IRS deployment intensity as well as direct transmission link blockage probability.

- Through numerical results, I provide useful insights on IRS-assisted as well as direct transmissions that capture impact of IRS interference in a large-scale network as a function of the number of IRS elements, intensity of IRSs and BSs, and the transmit power of BSs.

The detailed discussions on the contributions will be provided in the later chapters of the thesis.

1.5 Organization of the Thesis

The organisation of the thesis is as follows:

Chapter Two: In this chapter, performance analysis and optimization of propose data ferrying approach is provided. Also, insights on porpoised scheme is provided through numerical results considering analysis, approximations and optimization.

Chapter Three: In this chapter, integrated UAV-IRS scheme is proposed. Performance analysis and optimization are also presented considering the impact of main IRS and UAV factors in to account.

Chapter Four: In this chapter, I propose IRS-assisted downlink communication for the large scale setup with two types of user, the user associated to BS through IRS and the user associated to the BS directly. Performance analysis and numerical results provide interesting insights on the IRS-assisted large-scale communication.

Chapter Five: In this chapter, I summarize and conclude the research presented in the thesis followed by few possible extensions and future directions.

Note: The materials presented in chapter 2, chapter 3 and chapter 4 are reproduced from the published paper provided in Section 5.2.

Chapter Two

End-to-End Energy Efficiency and Reliability of UAV-Assisted Wireless Data Ferrying

This chapter characterize and design the system model for the UAV assisted data ferrying. The framework for performance analysis in terms of reliability and end to end energy efficiency is provided in this chapter. This chapter also presents approximate and exact performance performance analysis. I also formulate three different variants of optimization and the solution approach. In this chapter, first I present the introduction followed by the description of the system model in Section 2.3. In Section 2.4, I characterize the reliability and BEP for the considered network. In Section 2.5, I derive the end-to-end energy efficiency and the SNR outage probability for the considered network followed by approximations. Various optimization problems are formulated in Section 2.6. Then, I present the numerical results in Section 2.7 before summary of observations in Section 2.8. A list of important variables is in **Table 2.1**.

2.1 Introduction

Unmanned aerial vehicle (UAV)-assisted data ferrying is a key enabling technology for wireless backhauling and multicasting in beyond 5G wireless networks. Different from conventional relaying, where a UAV establishes a communication link between the ground source and destination simultaneously, data ferrying allows a UAV to load the data from a source, carry, and then deliver data to the destination when reaching sufficiently close to it [15]. This approach is known as *load carry and deliver (LCAD)* for fixed wing UAVs. Data ferrying is beneficial for delay-tolerant applications where the source and the destination do not have a direct communication link. However, the energy consumption of UAV-assisted data ferrying is crucial since the UAVs have limited on-board energy and the UAVs do not only consume communication energy but also significant propulsion energy to remain aloft or maintain their movement [13, 14]. The propulsion energy is directly proportional to the size of the UAV and the distance the UAV travels to ferry the data, whereas the communication energy depends on the channel fading and the path-loss factors etc. Accurate performance modeling and optimization of UAV-assisted data ferrying networks require precise energy consumption model, aerial path-loss and channel fading models.

2.1.1 Background Work

A series of research works [30–35] considered signal-to-noise ratio (SNR) outage characterization of UAV-assisted communications assuming either line-of-sight (LoS) Rician or non-LoS (NLoS) Nakagami-m faded aerial channels. However, in practice LoS and NLoS exists together, therefore, it is crucial to consider both types of links. The impact of having a certain LoS and NLoS probability was ignored in [30–35]. Also, the derived expressions are generally in the form of complicated mathematical functions that cannot be directly used for network planning and optimization purposes. For instance, [30, 31] provided closed-form expressions

for the SNR outage probability assuming Nakagami-m fading aerial channels with no notion of LoS and NLoS transmissions. The bit error rate (BER) has also been analyzed in [30] considering Nakagami-m fading channels. In addition, [32, 33] assumed Rician faded LoS aerial channels and derived the SNR outage in the form of Marcum Q-function. In [34], the SNR outage probability was analyzed for Rician and Rayleigh fading channels for LoS and NLoS channels, respectively. However, the final closed-form expressions in [34] are in the form of Marcum Q-function and Bessel function. The expressions derived in [30–34] are generally either in the form of special functions (such as Q-function or Hypergeometric function) or are represented using integrals. As such, their application to the optimization of network parameters is a fundamental challenge.

None of the aforementioned research works considered the performance characterization or optimization of UAV-assisted wireless data ferrying. The idea of UAV-assisted data ferrying (referred to as LCAD) was proposed in [15] assuming fixed wing UAV. Both the data loading and delivering links were considered. Similarly, [36] analyzed the throughput and delay trade-off of a similar data ferrying system where coverage to multiple ground nodes is provided by the UAV, i.e. UAV delivers data to a node when reaching sufficiently close to it. Different from fixed-wing UAVs (where hovering is not possible), [21] proposed fly hover and communicate (FHC) protocol for rotary wing UAVs where multiple ground nodes are served with a single UAV. That is, UAV flies to each user and communicate using optimal hovering location to minimize energy consumption and mission completion time. Successive iterative algorithms are solved at each location to find next optimal hovering location to serve each ground node. Note that the energy consumption of a rotary-wing UAV is fairly different from fixed-wing UAVs. In [37], the performance of a UAV was optimized when the UAV multicasts a data file to multiple ground receivers by designing the optimal trajectory that minimizes the mission time under a predefined quality of service (QoS) constraint. To minimize the mission completion time, the authors formulated a traveling salesman (TSM) problem for

a UAV to communicate with each ground node individually and proposed random linear network coding (RLNC) to multicast the data [37]. Nonetheless, both [21, 36] considered only data transmission links and ignored the performance limitation caused by the data loading links.

2.1.2 Contributions

I consider the performance modeling and optimization of a UAV-assisted data ferrying network with Rician and Rayleigh fading for LoS and NLoS scenarios, respectively. Our contributions are as follows:

- I characterize the end-to-end performance of a UAV-assisted data ferrying considering (i) both the data loading and delivering links, (ii) both the LoS and NLoS transmissions in the data loading and delivering links, (iii) Rician fading model for LoS and Rayleigh fading model for NLoS transmissions, and (iv) specific energy consumption model for the rotary wing UAV.

- I derive novel closed-form expressions for end-to-end network reliability[1] and bit-error probability (BEP) of the considered UAV-assisted data ferrying network. I characterize the reliability both with and without packet retransmission technique called automatic repeat request (ARQ). The derived expressions are novel compared to the expressions derived in conventional decode-and-forward (DF) relaying literature with Rician fading. Typically, they used single hop equivalent expression for BEP and does not consider averaging over the Rician fading channel [44].

- I derive end-to-end energy efficiency (a function of the SNR outage probability) and develop novel tractable approximations for the derived SNR outage. I demonstrate the

---

[1]To date, reliability has been derived either based on the throughput [38], transmission outage probability [39], bit-error probability (BEP) or packet error probability (PEP) [40–43].

use of approximations in optimizing the distance that a UAV should travel to balance the energy-rate trade-offs.

- I formulate two different optimization problems and solve for the optimal ferrying distance, i.e. (i) outage-constrained energy minimization and (ii) energy-constrained SNR outage minimization. In the first problem, I convexify the problem and demonstrate that the obtained solution is 95% close to the solution from exhaustive search. To convexify the problem, I propose a modified approximation of the error function approximation presented in [45]. I provide a comparison to [45] and demonstrate that the proposed approximation is more accurate with polarity consistency. Closed-form optimal solutions are obtained for the second problem.

- I formulate a bi-objective optimization problem with the objectives to minimize the SNR outage and energy consumption with desired SNR outage probability constraints. The objective function is then reformulated using difference of convex functions (DC) and solved using a DC algorithm.

Numerical results are presented to validate the derived expressions. Insights are extracted related to the impact of LoS Rician and NLoS Rayleigh fading channels on a variety of performance metrics as well as the optimal ferrying distance considering a variety of objective functions.

2.2 Mathematical Preliminaries

- **Signal-to-Interference-Plus-Noise Ratio (SINR)**:

  The received signal power of the typical user from the serving BS given the transmission mode/channel is expressed as:

$$S_{(.)} = P d_{(.)}^{-\alpha} X_{(.)}, \tag{2.1}$$

28

Where P is transmission power of the BS, $d_{(.)}$ represents the distance between typical user and BS, $\alpha_{(.)}$ represents pathloss exponent and $X_{(.)}$ represents the channel fading.

For two tier network transmitting in same bandwidth, the aggregate interference is sum of interference of tier-1 and tier-2, which can be written as:

$$I_{(.)} = I_{(.)}^1 + I_{(.)}^2, \tag{2.2}$$

Where $I_{(.)}^i$ represents the total interference faced by typical user from the $i-$th tier. The total SINR $\gamma_{(i)}$ is given from (2.1) and (2.2) as

$$\gamma_{(.)} = \frac{S_{(.)}}{I_{(.)} + N_0}. \tag{2.3}$$

However, the given SINR equation simplifies to signal-to-noise ratio for the signal source, single destination and single BS scenario.

- **Outage Probability**:

  The outage probability of a typical user given a wireless communication link/mode is defined as $O_{(.)} = \Pr(\gamma(.) < \gamma_{th})$, where $\gamma(.)$ and γ_{th} represents link SINR and minimum receiver SINR requirement respectively, $O_{(.)}$ is given as:

  $$O_{(.)} = \int_0^{\gamma_{th}} f_{\gamma_{(.)}}(\gamma)d\gamma.$$

  where $f_\gamma(\gamma)$ is the probability density function of the instantaneous SNR. Furthermore, the coverage probability is given as $C_{(.)} = 1 - O_{(.)}$.

- **Bit Error Probability (BEP)**:

  By conditioning on fading channel SNR, the BEP of Gaussian noise is given as:

  $$P_{b_{(.)}} = \int_0^\infty Q(\sqrt{2\gamma})f_{\gamma_{(.)}}(\gamma)d\gamma.$$

- **Ergodic Capacity**:

  The achievable ergodic capacity of a typical user $R_{(.)}$ is given as follows: [46]

  $$R_{(.)} = \mathbb{E}[\log_2(1 + \gamma_{(.)})]$$

- **Energy Efficiency (EE)**:

  The $EE_{(.)}$ of a typical user is given as follows:

  $$EE_{(.)} = \frac{R_0}{BE_{tot}} (1 - O_{(.)}),$$

  where R_0 and B are the desired rate and channel bandwidth, respectively. Energy consumption E_{tot} of the overall system and $O_{(.)}$ is the SNR outage.

- **Moment Generating Function (MGF)-Based Approach for Ergodic Capacity**:

  The achievable ergodic capacity of a typical user can be given by using the coverage probability expressions as shown below [46]:

  $$\mathbb{E}[\log_2(1 + SINR)] = \frac{1}{\ln(2)} \int_0^\infty \frac{P(SINR > t)}{t} \, dt.$$

  However, the aforementioned evaluation adds one more layer of integration on top of the coverage probability. Therefore, I use an alternative LT-based approach to evaluate ergodic capacity by leveraging on Hamdi's lemma [47] given as follows:

  $$\mathbb{E}\left[\ln\left(1 + \frac{X}{Y + N_0}\right)\right] = \int_0^\infty \frac{\mathcal{L}_Y(s) - \mathcal{L}_{X,Y}(s)}{s} \exp(-N_0 s) ds,$$

  where $\mathcal{L}_Y(s)$ and $\mathcal{L}_{X,Y}(s)$ represent the LT of Y and joint LT of X and Y, respectively.

- **Rayleigh Fading**: Rayleigh fading is considered reasonable when radio signal scatters from many objects in the environment and cause multipath. The distribution of the Rayleigh fading channel h is given as follows:

$$p_h(x) = \frac{2x}{\Omega} e^{-x^2/\Omega}, \;\; x \geq 0,$$

Where Ω denotes the power of the channel h.

- **Rician Fading**: Rician fading is considered reasonable when the radio signal received at the receiver has a dominant line of sight component along with several multipath. The probability distribution function of a fading channel h

$$f_h(x) = \frac{(K+1)}{\lambda} \exp\left(-K - \frac{(K+1)x}{\lambda}\right) I_0\left(2\sqrt{\frac{K(K+1)}{\lambda}} x\right),$$

Where where λ is the mean value of RV h, K is the Rician K-factor defined as the ratio of the power of the line-of-sight (LOS) component to the separate components and $I_0(.)$ is zeroth order modified Bessel function of the first kind.

Next, the system model is discussed.

2.3 System Model and Assumptions

2.3.1 UAV-Assisted Data Ferrying Model

I consider a UAV-assisted data ferrying network in which a rotary-wing UAV is responsible to ferry and transmit the data taken from a source BS BS_s to $\mathcal{K}$ destined RXs. The communication is established from BS_s located at $\mathbf{S}(x_s, y_s, 0)$ to UAV and then UAV to k-th ground receiver RX_k located at $(x_k, y_k, 0)$ or (r_k, ϕ_k). There is no direct connection available between the source BS and destination RXs. Each RX_k is uniformly distributed in a circular region of radius R around the cell center $\mathbf{C}(x_c, y_c, 0)$. Since the destination RXs are uniformly distributed, the distribution of their respective distances from $\mathbf{C}$ is given as $f_r(r_k) = \frac{2r_k}{R^2}, \quad 0 \leq r_k \leq R.$
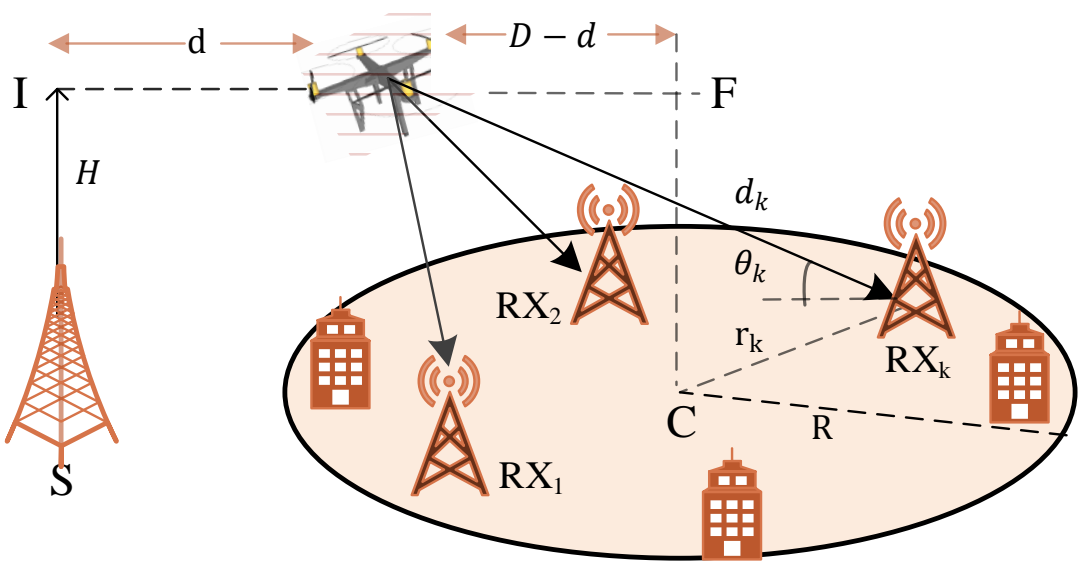
Figure 2.1 UAV-assisted data ferrying for multicasting and serving K terrestrial receivers.

The UAV loads the data from the source BS_s which is at distance $d_u = H$ from the UAV and carries it to a distance d from **I** prior to the downlink transmission. The initial and final locations of the UAV flight, i.e. $\mathbf{I}(x_s, y_s, H)$ and $\mathbf{F}(x_c, y_c, H)$ are located right above **S** and **C**, respectively. Here, $d = 0$ corresponds to the situation when the UAV decides to transmit from **I** and minimizes its energy consumption due to flight and $d = D$ corresponds to the situation when UAV decides to transmit from **F** and minimizes the communication outage probability. Note that, $0 \leq d \leq D$ and $D = \sqrt{(x_s - x_c)^2 + (y_s - y_c)^2}$.

The uplink (data loading) and downlink (data delivering) transmissions use the same frequency channel but occur at different time slots. In the downlink, the UAV transmits the same data to each of the $\mathcal{K}$ RXs simultaneously (i.e. I consider a **multicasting** scenario). Each of the $\mathcal{K}$ RXs has a fixed data rate requirement R_0 defined as $R_0 = B \log_2(1 + \Gamma_0)$, where Γ_0 represents the minimum end-to-end SNR threshold to achieve R_0, i.e. $\Gamma_0 = 2^{\frac{R_0}{B}} - 1$. Here, B represents the transmission bandwidth. Note that the UAV can travel up to a maximum distance D from **I**, however, the UAV may stop in between **I** and **F** when the desired data

rate is met (Figure 2.1). A list of important variables is in **Table 1**.

Table 2.1 Chapter 2: Summary of the main symbols and their definitions

Notation	Description
γ_u, γ_k	UL SNR, DL SNR of k-th RX
Γ_0	End-to-end SNR threshold
$p_u; p_d$	UL and DL power consumption
P_h	power consumption in hovering state
R_0	Data rate requirement
$P(V)$	power consumption of UAV flying with constant velocity
h_u, h_k	UL and DL small-scale fading gain
X_u, X_k	$|h_u|^2, |h_k|^2$
θ_u, θ_k	UL and DL elevation angle
H	Height of UAV
d_k	Distance between UAV at $\mathbf{d}$ to k-th RX
$d; D$	Distance travelled by UAV;Distance between I & F
$\mathcal{K}$	Number of RXs in downlink side
$K(\theta_u); K(\theta_k)$	Rician fading channel K-factor for UL and DL
$K_u; K_k$	Short representation of $K(\theta_u)$ & $K(\theta_k)$
d_0	Distance between UAV at distance d & $\mathbf{C}$
$\alpha(\theta_u); \alpha(\theta_k)$	Path-loss exponent for UL & DL
$\alpha_u; \alpha_k$	short representation of $\alpha(\theta_u)$ & $\alpha(\theta_k)$
k	RX index at downlink
N_0	Noise power spectral density
R	Downlink cell radius
T_u	Hovering time in UL

Continued on next page

Table 2.1 – *Continued from previous page*

Notation	Description
T_d	Hovering time of UAV in downlink
T_c	Transmission time of UAV
$p_L(\theta_u); p_N(\theta_u)$	Probability of LoS & NLoS in UL
$p_L(\theta_k), p_N(\theta_k)$	Probability of LoS & NLoS of k-th RX in DL
υ_i	Event based on UL & DL LoS probability
L	Packet length
$P_b^k(\upsilon_i, d_k)$	End-to-end conditional bit error probability
$\mathbb{P}_\epsilon^k(\upsilon_i, d_k)$	End-to-end packet error probability
$P_b^{u,L}; P_b^{u,N}$	Bit error probability in UL LoS & UL NLoS
$P_\epsilon^{k,L}; P_\epsilon^{k,N}$	PEP DL LoS & DL NLoS for BS$_k$ conditioned on d_k & υ_i
$P_b{}^k(d_k)$	End-to-end bit error probability conditioned on d_k only
(r_k, ϕ_k)	Coordinates of BS$_k$ w.r.t., cell center C
τ_R, τ	Threshold on reliability; threshold on outage probability
$\Omega_u; \Omega_k$	Mean local power of UL and DL of BS$_k$
$\mathbb{P}(\upsilon_i)$	Probability of occurrence of event υ_i
$F_{X_u}^L; F_{X_u}^N$	UL CDF for LoS and NLoS

2.3.2   Aerial Channel Model

Depending on the elevation angle between the UAV and ground nodes (or altitude of the UAV) and the environment (e.g. the intensity and heights of buildings), the transmission to the ground users may have LoS or non-LoS channel. The elevation angle (in rad) between

34

the UAV and BS_k is given as follows:

$$\theta_k = \arctan\left(\frac{H}{\sqrt{(x_k - d)^2 + y_k^2}}\right)$$
$$= \arctan\left(\frac{H}{\sqrt{(r_k \cos(\phi_k) - d)^2 + r_k^2 \sin(\phi_k)^2}}\right). \tag{2.4}$$

Similarly, the elevation angle between the UAV and BS_s is $\theta_u = \pi/2$ rad. The probability of LoS in the uplink and downlink is a function of θ_u and θ_k, respectively, i.e.

$$p_L(\theta_u) = (e_u \exp(-g_u(\theta_u - e_u)) + 1)^{-1}, \tag{2.5}$$

$$p_L(\theta_k) = (e_k \exp(-g_k(\theta_k - e_k)) + 1)^{-1}, \tag{2.6}$$

where e_u, e_k, g_u, and g_k are the environment parameters obtained from the curve fitting using Damped Least-Squares (DLS) method [48]. I model the LoS and NLoS transmissions with Rician and Rayleigh fast fading channels, respectively. For LoS Rician fading, the probability density function (PDF) of the fading channel power X_L is given as:

$$f_{X_L}(x) = \frac{K+1}{\Omega} e^{-K - \frac{(K+1)x}{\Omega}} I_0\left(2\sqrt{\frac{K(K+1)x}{\Omega}}\right)$$
$$= \sum_{\ell=0}^{\infty} \frac{b(bK)^\ell}{(\ell!)^2} x^\ell e^{-bx-K}, \tag{2.7}$$

in which K is the Rician factor and I_0 is a modified Bessel function of the first kind and $b = \frac{K+1}{\Omega}$ [49]. The PDF of NLoS Rayleigh fading channel power is obtained by substituting $K = 0$ in (2.7) as follows:

$$f_{X_N}(x) = \frac{1}{\Omega} \exp\left(-\frac{x}{\Omega}\right), \tag{2.8}$$

where Ω is the mean local power of the fading channel. The path-loss exponent α and K-factor for the Rician uplink channel are a function of the elevation angle, i.e. [50]

$$\alpha(\theta_u) = p_L(\theta_u)q_u + v_u, \qquad K(\theta_u) = w_u \exp(z_u \theta_u). \tag{2.9}$$

Here q_u,v_u,w_u, and z_u are constants depending on the uplink environment [48]. Similar to (2.9), for the downlink I can write

$$\alpha(\theta_k) = p_L(\theta_k)q_d + v_d, \qquad K(\theta_k) = w_d \exp(z_d\theta_k). \tag{2.10}$$

respectively. Again, q_d,v_d,w_d, and z_d are constants depending on the downlink environment [48].

2.3.3   Uplink and Downlink Transmission Model

The uplink received signal at the UAV can be defined as

$$y_u = \sqrt{\hat{A}p_u\eta_u^{-1} d_u^{-\alpha(\theta_u)}} \ h_u \ s + w_u, \tag{2.11}$$

where s is the binary phase shift keying (BPSK) signal transmitted from BS_s to the UAV, η_u denotes the excess aerial path-loss, p_u is the uplink transmission power of BS_s, d_u is the distance between the BS_s and the UAV located at $\mathbf{I}$, i.e. $d_u = H$ (Figure. 2.1), $\hat{A}$ reflects system parameters (e.g. operating frequency and antenna gain), w_u is the noise which follows zero-mean Gaussian distribution with power spectral density N_0, and h_u is the channel fading gain. The uplink signal-to-noise-ratio (SNR) using (2.11) is formulated as:

$$\gamma_u = \frac{\hat{A}p_u\eta_u^{-1} \ H^{-\alpha(\theta_u)} \ X_u}{N_0}, \tag{2.12}$$

where $X_u = |h_u|^2$. The distribution of X_u follows from a non-central chi-square distribution given in (2.7) for LoS and exponential distribution given in (2.8) for NLoS.

In the downlink, the UAV communicates to $\mathcal{K}$ RXs. The distance between the UAV at d and the k-th ground RX is represented by $d_k, \forall k$ (Figure.2.1). The received signal y_k at k-th RX is $y_k = \sqrt{\hat{A}p_d\eta_d^{-1} d_k^{-\alpha(\theta_k)}} \ h_k \ y_u + w_k$, where η_d and p_d denote the excess aerial path-loss and downlink transmission power of UAV, respectively. The SNR received at k-th RX in the downlink can then be expressed as:

$$\gamma_k = \frac{\hat{A}p_d\eta_d^{-1} \ d_k^{-\alpha(\theta_k)} \ X_k}{N_0}, \tag{2.13}$$

where $X_k = |h_k|^2$. The distribution of X_k follows from a non-central chi-square distribution and exponential distribution given in (2.7) for LoS and (2.8) for NLoS, respectively. The distance between the UAV and RX k is given as $d_k = \sqrt{(D - d - r_k \cos(\phi_k))^2 + (r_k \sin(\phi_k))^2 + H^2}$. **Note that from this point onward I will use K_u as a short notation for $K(\theta_u)$, K_k as a short notation for $K(\theta_k)$, α_u and α_k as $\alpha(\theta_u)$ and $\alpha(\theta_k)$ for brevity, respectively.**

2.3.4 Energy Consumption Model

The total energy consumption of a UAV comprises of (i) propulsion energy which is the energy consumed by UAV in traveling from one location to the other location (plus hovering energy in case of rotary wing UAVs), and (ii) transmission energy is the energy consumed by UAV for communication purposes. The propulsion energy (typically in the order of hundreds of watts [51]) is required to keep the UAV aloft and fly forward/vertically. The communication energy of UAV is in the order of tens of watts [52]. A trade-off exists between the communication and propulsion energy as a function of the distance that UAV travels while ferrying the data. The consumed energy for the data loading phase, UAV travelling phase, and downlink transmission phase are given in the following.

Uplink Data Loading Phase

The UAV hovers at **I** for a predefined duration T_u (Figure 2.1)[2]. The energy consumption due to hovering of UAV and communication of the source BS in the uplink [21] is given as:

$$E^u = (P_h + p_u)T_u, \tag{2.14}$$

---

[2]I assume that transmission time T_u is the time data takes to reach to the UAV which is at location **I** (e.g. $T_u = \frac{H}{c}$). To assure that complete data is uploaded to UAV from BS_s, I can add an extra delay to the transmission time.

where p_u is the uplink power consumption of BS_s and P_h is the propulsion power consumption of UAV in the hovering state given as follows (Eq 12.13 of [53]):

$$P_h = P_0 + P_i = \frac{\delta}{8}\rho s A \xi^3 r^3 + (1 + \kappa)\sqrt{\frac{(mg)^3}{2\rho A}}, \tag{2.15}$$

where ρ, A, ξ, r, s, δ, and κ denote the air density (in kg/m^3), rotor disc area (in m^2), blade angular velocity (in rad/sec), rotor radius (in m), rotor solidity, profile drag coefficient of the blade, and incremental correction factor of induced power, respectively. The total weight W of the UAV is approximately equal to the gravitational force, i.e. $W = mg$ (in Newton), where m is the UAV mass (in kg) and g denotes earth gravity (in m/s^2).

UAV Travelling Phase

The energy consumption during the travelling time is solely due to the propulsion energy as the UAV is not communicating during the flight. When the UAV moves with the constant velocity V and carries the data to a distance d before delivering to downlink BS_s, the energy consumption can be modeled as follows:

$$E^t(d) = P(V)d/V, \tag{2.16}$$

where $P(V)$ is the power consumed by the blade profile, induced power, and parasitic power of the UAV (Eq 7 of [21]), i.e.

$$P(V) = P_0\left(1 + \frac{3V^2}{U_{\text{tip}}^2}\right) + P_i\left(\sqrt{1 + \frac{V^4}{4v_0^4}} - \frac{V^2}{2v_0^2}\right)^{\frac{1}{2}} + \frac{1}{2}\hat{d}_0\rho s A V^3, \tag{2.17}$$

where U_{tip} denotes the tip speed of the rotor blade, v_0 is the mean rotor induced velocity, and $\hat{d}_0$ is the fuselage drag ratio. By substituting $V = 0$ in the aforementioned equation, I get the hovering power as given in (2.15). Note that $E^t(d)$ is directly proportional to the distance traveled by the UAV d.

Downlink Transmission Phase

In the downlink, the UAV experiences energy consumption due to communication and hovering. I consider that the serving region (i.e. the cell radius R) in which all receivers are located is very small compared to the traveling distance of UAV $r_k = 0$, i.e. $d_k = d_0 = \sqrt{(D-d)^2 + H^2}$ for simplicity. Under this assumption, the farthest or nearest receiver becomes approximately the same as the receiver who is located at the cell-center (see Figure 2.2). As such, I consider the outage probability, with respect to the cell-center, as
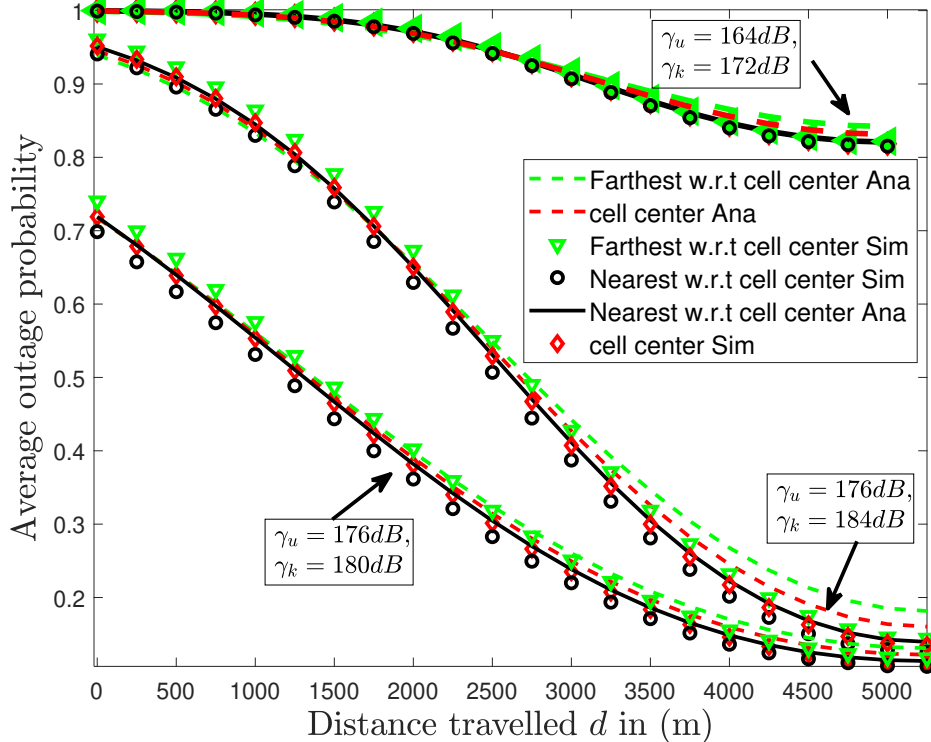
Figure 2.2 Outage of receivers that are located nearest and farthest from the cell-center as well as the receiver located at the cell-center, considering Rayleigh/Exp distribution $\alpha = 2.5$ as a function of d.

an approximate performance measure of all users in the serving region. The UAV hovering time T_d is assumed to be at least equal to the time in which a user located at the cell center receives data from UAV, where T_c is the transmission time of the UAV. It is important to

note that the UAV can transmit at any specific distance d, from the initial point on the trajectory, if the QoS criterion is met. Therefore, the traveling time of UAV to location d is separate from the transmission time in the downlink T_c. The downlink energy consumption at UAV can thus be modeled as follows:

$$E^d(d) = P_h T_d + p_d T_c = P_h \frac{d_0}{c} + p_d T_c, \qquad (2.18)$$

where $d_0 = \sqrt{(D-d)^2 + H^2}$, c is the speed of light, and T_d is the hovering time of UAV. Since the UAV will be transmitting for the entire hovering duration, I assume that $T_d = T_c$.

End-to-End Energy Consumption

The overall energy consumption can be obtained by adding (2.14), (2.16), and (2.18) as follows:

$$E_{tot}(d) = \frac{(P_h + p_d)\sqrt{(D-d)^2 + H^2}}{c} + \frac{P(V)d}{V} + C, \qquad (2.19)$$

where $C = p_u T_u + P_h T_u$. I assume that sufficiently large memory is available at the UAV to store the complete data for one trip.

2.4 End-to-End Reliability and Bit Error Probability Analysis

In this section, I derive the end-to-end reliability with and without ARQ and BEP (the ratio of the number of bits in error to the total number of transmitted bits) of the considered network. The end-to-end BEP and PEP for the k-th RX are conditioned on the following events, i.e.

(i) **Event v_1:** when both the uplink and downlink incur LoS Rician fading, i.e.

$\{p_L(\theta_u) > p_N(\theta_u), p_L(\theta_k) > p_N(\theta_k)\}$, where $p_N(\cdot)$ depicts the NLoS probability,

(ii) **Event v_2:** when the uplink experiences LoS Rician fading and the downlink experiences NLoS Rayleigh fading, i.e. $\{p_L(\theta_u) > p_N(\theta_u), p_L(\theta_k) < p_N(\theta_k)\}$,

(iii) **Event v_3:** when the uplink experiences NLoS Rayleigh fading and the downlink experiences LoS Rician fading, i.e. $\{p_L(\theta_u) < p_N(\theta_u), p_L(\theta_k) > p_N(\theta_k)\}$, and

(iv) **Event v_4:** when the uplink and downlink experience NLoS and NLoS Rayleigh fading, i.e. $\{p_L(\theta_u) < p_N(\theta_u), p_L(\theta_k) < p_N(\theta_k)\}$.

Conditioned on v_i, d_k and using the definition of reliability from [41], the end-to-end PEP of k-th RX $\mathbb{P}_\epsilon^k(v_i, d_k)$ should meet the reliability threshold (or packet error threshold) τ_R [41]. I model the reliability constraint without ARQ as:

$$\mathbb{P}_\epsilon^k(v_i, d_k) \leq \tau_R, \tag{2.20}$$

where a packet is assumed to be in error even if a single bit is in error and I assumed that the bit errors are independent (e.g. due to large interleaver size, fast fading and uncoded transmission); therefore, I have

$$\mathbb{P}_\epsilon^k(v_i, d_k) = 1 - \left(1 - P_b^k(v_i, d_k)\right)^L, \tag{2.21}$$

where L is the number of bits per packet with the assumption that cyclic redundancy check (CRC) is not available at the UAV in uplink, and $P_b^k(v_i, d_k)$ is the conditional BEP given as $P_b^k(v_i, d_k) \leq 1 - (1 - \tau_R)^{\frac{1}{L}}$.

Remark: The end-to-end PEP with ARQ and n retransmissions $\mathbb{P}_\epsilon^k(n, v_i, d_k)$ can be obtained from the BEP under the assumption of i.i.d. channels [54] in each retransmission (e.g. due to large interleaver size, fast fading and uncoded retransmissions); for both uplink and downlink as

$$\mathbb{P}_\epsilon^k(n, v_i, d_k) = 1 - (1 - P_\epsilon^u(n))(1 - P_\epsilon^k(n)), \tag{2.22}$$

where $n = 0, 1, \cdots, \mu$ and μ is the maximum number of retransmissions, The PEP of both uplink and downlink are $P_\epsilon^u(n) = (1 - (1 - P_b^u)^L)^{n+1}$ and $P_\epsilon^k(n) = (1 - (1 - P_b^k)^L)^{n+1}$,

respectively. It is assumed that both UAV and downlink receivers have single bit feedback associated to it. The reliability constraint in (2.20) can be rewritten by considering ARQ as $\mathbb{P}_\epsilon^k(n, v_i, d_k) \leq \tau_R$. For $n = 0$ and no CRC in the uplink (i.e. $P_\epsilon^u(n) = 0$, $P_\epsilon^k(n) = \mathbb{P}_\epsilon^k(v_i, d_k)$), $\mathbb{P}_\epsilon^k(n, v_i, d_k)$ converges to (2.21).

2.4.1 Methodology of Analysis

To derive the reliability and $\mathbb{P}_b^k(v_i, d_k)$, the steps are as follows:

1. Derive the uplink BEP $P_b^{u,L}$ and $P_b^{u,N}$ for LoS (Rician) and NLoS (Rayleigh) fading channels, respectively.

2. Derive the downlink BEP $P_b^{k,L}$ and $P_b^{k,N}$ for LoS (Rician) and NLoS (Rayleigh) fading for BS_k, respectively.

3. The bit error can occur in two scenarios [55]: (i) when the uplink transmission is in error but the downlink transmission is successful (ii) when the uplink transmission is successful but the downlink transmission is in error. Conditioned on d_k and v_i, the end-to-end BEP of k-th BS is given as follows [44, 55]:

$$P_b^k(v_i, d_k) = (1 - P_b^u) P_b^k + P_b^u (1 - P_b^k), \tag{2.23}$$

where P_b^u and P_b^k are the uplink and downlink conditional BEPs for k-th link, respectively, given v_i and d_k.

For events v_1, v_2, v_3, and v_4, (2.23) can be rewritten as:

$$
\begin{aligned}
P_b^k(v_1, d_k) &= \left(1 - P_b^{u,L}\right) P_b^{k,L} + P_b^{u,L} \left(1 - P_b^{k,L}\right), \\
P_b^k(v_2, d_k) &= \left(1 - P_b^{u,L}\right) P_b^{k,N} + P_b^{u,L} \left(1 - P_b^{k,N}\right), \\
P_b^k(v_3, d_k) &= \left(1 - P_b^{u,N}\right) P_b^{k,L} + P_b^{u,N} \left(1 - P_b^{k,L}\right), \\
P_b^k(v_4, d_k) &= \left(1 - P_b^{u,N}\right) P_b^{k,N} + P_b^{u,N} \left(1 - P_b^{k,N}\right).
\end{aligned}
\tag{2.24}
$$

4. Derive the BEP of multicasting system ($P_b^{\mathrm{MC}}(d_k)$).

5. The unconditioned BEP (after averaging over υ_i and d_k) for any arbitrary BS can then be given as follows:

$$P_b = \sum_{i=1}^{4} \mathbb{P}(\upsilon_i)\mathbb{E}_{d_k}[P_b^k(\upsilon_i, d_k)], \tag{2.25}$$

where $\mathbb{P}(\upsilon_i)$ is the probability of event υ_i.

2.4.2   Characterization of Uplink BEP - ($P_b^{u,L}$ and $P_b^{u,N}$)

Proposition 1 (BEP $P_b^{u,L}$ - LoS Rician Fading). *The BEP in the uplink LoS transmission channel (i.e. Rician fading) can be derived as follows:*

$$P_b^{u,L} = \sum_{\ell=0}^{\infty} q_u(\ell)\left(\beta_1^{-\ell-1} + 3\beta_2^{-\ell-1}\right), \tag{2.26}$$

where $q_u(\ell) = \frac{b_u e^{-K_u}(b_u K_u)^{\ell}}{12\ell!}$, $\beta_1 = \frac{\hat{A}p_u \eta_u^{-1}}{2H^{\alpha_u}N_0} + b_u$, $\beta_2 = \frac{2\hat{A}p_u \eta_u^{-1}}{3H^{\alpha_u}N_0} + b_u$, *and* $b_u = \frac{K_u+1}{\Omega_u}$.

Proof. By conditioning on $X_u = |h_u|^2$, the BEP in the uplink can be written using the BEP of Gaussian noise as:

$$P_b^{u,L} = \mathbb{E}_{X_u}\left[Q\left(\sqrt{2(\beta_1 - b_u)\,X_u}\right)\right]. \tag{2.27}$$

Using the exponential approximation for Q-function [56], i.e. $Q(x) = \frac{1}{12}e^{-\frac{x^2}{2}} + \frac{1}{4}e^{-\frac{2x^2}{3}}$, I simplify (2.27) as follows:

$$P_b^{u,L} = \mathbb{E}_{X_u}\left[\frac{1}{12}e^{-(\beta_1-b_u)X_u} + \frac{1}{4}e^{-(\beta_2-b_u)X_u}\right]. \tag{2.28}$$

The first expectation over X_u in (2.28) can be solved by averaging over the PDF of non-central chi-square distribution given in (2.7) and by substituting z with X_u and b with b_u. The first term of (2.28) can be solved as follows:

$$\frac{1}{12}\mathbb{E}_{X_u}\left[e^{-(\beta_1-b_u)X_u}\right] = \sum_{\ell=0}^{\infty} q_u(\ell)\beta_1^{-\ell-1}, \tag{2.29}$$

43

where the closed-form is calculated using the definition of Gamma function in (2.29), i.e. $\int_0^\infty e^{-\beta_1 x} x^\ell dx = \beta_1^{-\ell-1} \Gamma(\ell+1)$. Following the same steps, I solve the second expectation in (2.28) as:

$$\mathbb{E}_{X_u}\left[\frac{1}{4}e^{-(\beta_2 - b_u)X_u}\right] = \sum_{\ell=0}^{\infty} q_u(\ell)\beta_2^{-\ell-1}. \tag{2.30}$$

Substituting (2.29) and (2.30) in (2.28), I get **Proposition 1**. $\blacksquare$

Corollary 1 (BEP $P_b^{u,N}$ - NLoS Rayleigh Fading). *Substituting $K_u = 0$ in Proposition 1, the BEP in the NLoS Rayleigh fading channel (2.26) is given as follows:*

$$P_b^{u,N} = \frac{1}{12\Omega_u}\left(\beta_1^{-1} + 3\beta_2^{-1}\right), \tag{2.31}$$

*where β_1 and β_2 are given as in **Proposition 1**.*

2.4.3 Characterization of Downlink BEP - ($P_b^{k,L}$ and $P_b^{k,N}$)

Proposition 2 (BEP $P_b^{k,L}$ - LoS Rician Fading). *The BEP P_b^k in the downlink for k-th RX can be derived as follows:*

$$P_b^{k,L} = \sum_{\ell=0}^{\infty} q_d(\ell)\left(\left(\frac{\beta_1'}{d_k^{\alpha_k}} + b_k\right)^{-\ell-1} + 3\left(\frac{\beta_2'}{d_k^{\alpha_k}} + b_k\right)^{-\ell-1}\right), \tag{2.32}$$

where $q_d(\ell) = \frac{b_d^{\ell+1} e^{-K_k} K_k^\ell}{12(\ell!)}$, $\beta_1' = \frac{\hat{A}p_d \eta_k^{-1}}{2N_0}$, $\beta_2' = \frac{2\hat{A}p_d \eta_k^{-1}}{3N_0}$ and $b_k = \frac{K_k+1}{\Omega_d}$.

Proof. The proof can be done following similar steps as in the proof of **Proposition 1**. $\blacksquare$

Corollary 2 (BEP $P_b^{k,N}$ - NLoS Rayleigh Fading). *: The BEP $P_b^{k,N}$ in the downlink NLoS transmission link can be given by substituting $K_k = 0$ in (2.32) as follows:*

$$P_b^{k,N} = \frac{1}{12\Omega_d}\left(\left(\frac{\beta_1'}{d_k^{\alpha_k}} + \frac{1}{\Omega_d}\right)^{-1} + 3\left(\frac{\beta_2'}{d_k^{\alpha_k}} + \frac{1}{\Omega_d}\right)^{-1}\right), \tag{2.33}$$

*where β_1' and β_2' are given as in **Proposition 2**.*

2.4.4   End-to-End BEP of RX k, $P_b^k(d_k)$

Conditioned on d_k, the end-to-end BEP $P_b^k(d_k)$ can be derived as follows:

$$P_b^k(d_k) = \sum_{i=1}^{4} \mathbb{P}(v_i) P_b^k(v_i, d_k), \qquad (2.34)$$

where $\mathbb{P}(v_i)$ represents the probability of event v_i. The occurrence of each event can be written as the product of two individual events, i.e. $\mathbb{P}(v_1) = p_L(\theta_u) p_L(\theta_k)$, $\mathbb{P}(v_2) = p_L(\theta_u) p_N(\theta_k)$, $\mathbb{P}(v_3) = p_N(\theta_u) p_L(\theta_k)$, $\mathbb{P}(v_4) = p_N(\theta_u) p_N(\theta_k)$. Note that $p_N(\cdot) = 1 - p_L(\cdot)$.

Also, $P_b^k(v_1, d_k)$ is given by using (2.26) and (2.32) in (2.23). $P_b^k(v_2, d_k)$ is given by using (2.26) and (2.33) in (2.23). $P_b^k(v_3, d_k)$ is given by substituting (2.31) and (2.32) in (2.23). $P_b^k(v_4, d_k)$ is obtained by using (2.31) and (2.33) in (2.23).

2.4.5   Overall BEP of the MultiCasting System, $P_b^{\mathrm{MC}}(d_k)$

Conditioned on d_k, the overall BEP of the considered multicasting network can be expressed as follows:

$$P_b^{\mathrm{MC}}(d_k) = \sum_{k=1}^{2^{\mathcal{K}}-1} \frac{1}{2^{\mathcal{K}} - 1} \prod_{k=1}^{\mathcal{K}} (1 - P_b^k(d_k))^{1-s_k} (P_b^k(d_k))^{s_k}. \qquad (2.35)$$

To elaborate the above expression, let us consider a simple example of two RXs $\mathcal{K} = 2$. Each RX $k \in \mathcal{K}$ can experience successful or erroneous transmission denoted by $s_k = 0$ and $s_k = 1$, respectively. $\mathbf{S}$ represents the set containing all possible combinations (i.e. $2^{\mathcal{K}}$ combinations). For two RXs, I have $\mathbf{S} = \{00, 01, 10, 11\}$ where each combination is $\mathbf{s} \in \mathbf{S}$. The first combination $\mathbf{s} = \{00\}$ corresponds to both RXs having no errors so need not be considered in the overall BEP. Then, $\mathbf{s} = \{01\}$ corresponds to the event when first RX in success while the second RX is in error with BEP given by $(1 - P_b^1(d_1)) P_b^2(d_2)$. Similarly for $\mathbf{s} = \{10\}$ and $\mathbf{s} = \{11\}$, the corresponding BEPs are $P_b^1(d_1)(1 - P_b^2(d_2))$ and $P_b^1(d_1) P_b^2(d_2)$, respectively. Averaging over all combinations with at least one error, I obtain (2.35).

On the other hand, when $\mathbf{s}_k$ is known *a priori* for each RX k based on certain QoS

constraints, the overall BEP can be expressed as follows:

$$P_{b_{s_k}}^{\text{MC}}(d_k) = \prod_{k=1}^{\mathcal{K}} (P_b{}^k(d_k))^{s_k} (1 - P_b{}^k(d_k))^{1-s_k}, \tag{2.36}$$

where

$$s_k = \begin{cases} 1 & P_b{}^k(v_i, d_k) > 1 - (1 - \tau_R)^{1/L} \\ 0 & P_b{}^k(v_i, d_k) \leq 1 - (1 - \tau_R)^{1/L} \end{cases}. \tag{2.37}$$

That is, s_k obtained by solving (2.20) and (2.21).

2.4.6   BEP of Any Arbitrary BS

Finally, deconditioning over d_k (which in turn implies averaging over r_k and ϕ_k) yields the BEP $P_b{}^k$ as:

$$\begin{aligned} P_b &= 1 - \int_0^R \int_0^{2\pi} P_b{}^k(d_k) \frac{r_k}{\pi R^2} dr_k d\phi_k \\ &= 1 - \sum_{i=1}^4 \int_0^R \int_0^{2\pi} \mathbb{P}(v_i) P_b{}^k(v_i, d_k) \frac{r_k}{\pi R^2} dr_k d\phi_k. \end{aligned} \tag{2.38}$$

The integrals can be solved using standard mathematical software such as `MATLAB` and `MATHEMATICA`.

It is important to note that our analysis can be extended for the nearest (farthest) user by replacing the probability density function (PDF) of the distance of the k-th user from cell-center with the PDF of the user who is located at the minimum (maximum) distance from the cell-center using order statistics.

2.5   End-to-End Energy-Efficiency and SNR Outage Probability

In this section, I characterize the network energy-efficiency and SNR outage probability of the considered multicasting network. Energy-efficiency (EE) is defined as the ratio of the number

of successfully delivered bits and the total network energy consumption (in bits/Joule) [57]. The analytical methodology to derive EE is as follows:

1. Conditioned on v_i and d_k, characterize the end-to-end EE of k-th RX as follows:

$$\text{EE}(v_i, d_k) = \frac{R_0}{BE_{tot}(d)}(1 - O_k(d_k)),\tag{2.39}$$

   where R_0 and B are the desired rate and channel bandwidth, respectively. Energy consumption $E_{tot}(d)$ is given in (2.19) and $O_k(d_k)$ is the SNR outage of k-th BS.

2. Characterize the SNR outage $O_k(d_k)$ of the k-th BS.

3. Characterize the overall SNR outage $O_k^{\text{MC}}(d_k)$ of the multicasting system.

4. Characterize the unconditioned end-to-end outage probability of any arbitrary RX as follows:

$$O = \sum_{i=1}^{4}\mathbb{E}_{d_k}[\mathbb{P}(v_i)O_k(v_i, d_k)].\tag{2.40}$$

5. Characterize the overall EE^{MC} of the network.

2.5.1   End-to-End Outage Probability of RX k, $O_k(d_k)$

Assuming that the UAV can perform decoding and storing of the data during flight, the end-to-end SNR Γ_k for k-th RX can be modeled as [58]:

$$\Gamma_k = \min\{\gamma_u, \gamma_k\}.\tag{2.41}$$

Conditioned on d_k and v_i, the end-to-end transmission outage probability of k-th RX is defined as:

$$\begin{aligned}O_k(v_i, d_k) =&\mathbb{P}(\Gamma_k < \Gamma_0|v_i) = \mathbb{P}[\min(\gamma_u, \gamma_k) < \Gamma_0|v_i]\\ =&1 - (1 - F_{\gamma_u}(\Gamma_0))(1 - F_{\gamma_k}(\Gamma_0)),\end{aligned}\tag{2.42}$$

where $F_{\gamma_u}(\Gamma_0)$ and $F_{\gamma_k}(\Gamma_0)$ represent the CDF of uplink and downlink SNR evaluated at Γ_0 (i.e. uplink and downlink conditional SNR outage), respectively, for the k-th BS.

For events v_1, v_2, v_3, and v_4, (2.42) can be rewritten as:

$$
\begin{aligned}
O_k(v_1, d_k) &= 1 - \left(1 - F_{\gamma_u}^L(\Gamma_0)\right)\left(1 - F_{\gamma_k}^L(\Gamma_0)\right), \\
O_k(v_2, d_k) &= 1 - \left(1 - F_{\gamma_u}^L(\Gamma_0)\right)\left(1 - F_{\gamma_k}^N(\Gamma_0)\right), \\
O_k(v_3, d_k) &= 1 - \left(1 - F_{\gamma_u}^N(\Gamma_0)\right)\left(1 - F_{\gamma_k}^L(\Gamma_0)\right), \\
O_k(v_4, d_k) &= 1 - \left(1 - F_{\gamma_u}^N(\Gamma_0)\right)\left(1 - F_{\gamma_k}^N(\Gamma_0)\right).
\end{aligned}
\tag{2.43}
$$

To evaluate (2.43), I characterize $F_{\gamma_u}^L(\Gamma_0)$, $F_{\gamma_u}^N(\Gamma_0)$, $F_{\gamma_k}^L(\Gamma_0)$ and $F_{\gamma_k}^N(\Gamma_0)$, respectively, in the following.

Characterization of $F_{\gamma_u}^L(\Gamma_0)$ and $F_{\gamma_u}^N(\Gamma_0)$

Using (2.12), the uplink SNR outage can be given as follows:

$$
F_{\gamma_u}(\Gamma_0) = \mathbb{P}\left(\gamma_u \leq \Gamma_0\right) = \mathbb{P}\left(X_u \leq \Gamma_u'\right) = F_{X_u}(\Gamma_u'),
\tag{2.44}
$$

where $X_u = |h_u|^2$ represents non-central chi square distribution and $\Gamma_u' = \frac{N_0 \Gamma_0}{\hat{A} p_u \eta_u^{-1} H^{-\alpha_u}}$. Using the alternate exact expression for PDF in (2.7), the CDF of non-central chi-square distribution can be given as follows [49, 59, 60]:

$$
F_X(x) = 1 - \sum_{\ell=0}^{\infty} \sum_{m=0}^{\ell} f(m, l) x^m e^{-bx},
\tag{2.45}
$$

where $f(m, \ell) = e^{-K} \frac{K^\ell b^m}{\ell! m!}$, $b = \frac{K+1}{\Omega}$, Ω is the mean local power of the Rician channel, and K is the Rician factor.

After substituting $x = \Gamma_u'$ in (2.45), $F_{\gamma_u}^L(\Gamma_0) = F_{X_u}^L(\Gamma_u')$ for LoS fading can be evaluated as follows:

$$
F_{X_u}^L(\Gamma_u') = 1 - \sum_{\ell=0}^{\infty} \sum_{m=0}^{\ell} f_u(m, l)\left(\Gamma_u'\right)^m \exp\left(-b_u \Gamma_u'\right),
\tag{2.46}
$$

where $b_u = \frac{K_u+1}{\Omega_u}$, $f_u(m,\ell) = e^{-K_u} \frac{K_u^\ell b_u^m}{\ell! m!}$, and Ω_u is the mean local power of the Rician channel in uplink.

Substituting $K_u = 0$ in (2.46), $F_{X_u}^N(\Gamma'_u)$ for NLoS Rayleigh fading can be expressed as follows:

$$F_{X_u}^N(\Gamma'_u) = 1 - e^{-\Gamma'_u/\Omega_u}, \tag{2.47}$$

where Γ'_u is defined as in (2.44).

Characterization of $F_{\gamma_k}^L(\Gamma_0)$ and $F_{\gamma_k}^N(\Gamma_0)$

Using (2.13), the downlink SNR outage of k-th RX can be given as follows:

$$F_{\gamma_k}^L(\Gamma_0|d_k) = \mathbb{P}\left(\frac{\hat{A} p_d \eta_d^{-1} d_k^{-\alpha_k} X_k}{N_0} \leq \Gamma_0\right) = F_{X_k}^L(\Gamma'_k|d_k)$$

$$\overset{(a)}{=} 1 - \sum_{\ell=0}^{\infty} \sum_{m=0}^{\ell} f_d(m,l) (\Gamma'_k d_k^{\alpha_k})^{m_2} \exp\left(-b_k \Gamma'_k d_k^{\alpha_k}\right), \tag{2.48}$$

where $d_k = \sqrt{(D - d - r_k \cos(\phi_k))^2 + (r_k \sin(\phi_k))^2 + H^2}$, $\Gamma'_k = \frac{N_0 \Gamma_0}{\hat{A} p_d \eta_d^{-1}}$, and (a) follows by taking $x = \Gamma'_k d_k^{\alpha_k}$ in (2.45). Also, $b_k = \frac{K_k+1}{\Omega_d}$, $f_d(m,\ell) = e^{-K_k} \frac{K_k^\ell b_k^m}{\ell! m!}$, and Ω_d is the mean local power of the downlink Rician channel.

Substituting $K_k = 0$ in (2.48), $F_{X_k}(\Gamma'_k)$ for NLoS Rayleigh fading can be expressed as follows:

$$F_{X_k}^N(\Gamma'_k|d_k) = 1 - e^{-\frac{\Gamma'_k}{\Omega_d} d_k^{\alpha_k}}. \tag{2.49}$$

End-to-End SNR Outage, $O_k(d_k)$

Conditioned on d_k, I write $O_k(d_k)$ as follows:

$$O_k(d_k) = \sum_{i=1}^{4} \mathbb{P}(v_i) O_k(v_i, d_k), \tag{2.50}$$

where $\mathbb{P}(v_i)$ represents the probability of event v_i. That is, $\mathbb{P}(v_1) = p_L(\theta_u)p_L(\theta_k)$, $\mathbb{P}(v_2) = p_L(\theta_u)p_N(\theta_k)$, $\mathbb{P}(v_3) = p_N(\theta_u)p_L(\theta_k)$, $\mathbb{P}(v_4) = p_N(\theta_u)p_N(\theta_k)$.

For each event v_i, $O_k(v_i, d_k)$ can be derived as in the following:

(a) Event v_1: Using (2.46) and (2.48) in (2.42), I have

$$
\begin{aligned}
O_k(v_1, d_k) = 1 - & \left(\sum_{\ell=0}^{\infty} \sum_{m=0}^{\ell} f_u(m, l) \, (\Gamma'_u)^m \, e^{-b_u \Gamma'_u} \right) \\
& \times \left(\sum_{\ell=0}^{\infty} \sum_{m=0}^{\ell} f_d(m, l) \, (\Gamma'_k d_k^{\alpha_k})^{m_2} \exp\left(-b_k \Gamma'_k d_k^{\alpha_k}\right) \right).
\end{aligned}
\tag{2.51}
$$

(b) Event v_2: Similarly, I obtain $O_k(v_2, d_k)$ using (2.46) and (2.49) in (2.42). **(c) Event v_3:** $O_k(v_3, d_k)$ using (2.47) and (2.48) in (2.42). **(d) Event v_4:** $O_k(v_4, d_k)$ using (2.47) and (2.49) in (2.42).

2.5.2 Overall SNR Outage of the MultiCasting System, $O^{\mathrm{MC}}(d_k)$

Conditioned on d_k, the overall network outage of the considered multicasting network (similar to overall BEP) can be expressed as follows:

$$
O^{\mathrm{MC}}(d_k) = \sum_{k=1}^{2^{\mathcal{K}}-1} \frac{1}{2^{\mathcal{K}} - 1} \prod_{k=1}^{\mathcal{K}} (1 - O_k(d_k))^{1-s_k} (O_k(d_k))^{s_k},
\tag{2.52}
$$

where $s_k = 1$ when the transmission fails for the k-th RX and $s_k = 0$ when the transmission is successful. When $\mathbf{s}_k$ is known *a priori* for each RX k based on certain QoS constraints, the overall network outage can be expressed as follows:

$$
O_{s_k}^{\mathrm{MC}}(d_k) = \prod_{k=1}^{\mathcal{K}} (O_k(d_k))^{s_k} (1 - O_k(d_k))^{1-s_k},
\tag{2.53}
$$

where

$$
s_k = \begin{cases} 1 & O_k(v_i, d_k) > \tau'_R \\ 0 & O_k(v_i, d_k) \leq \tau'_R \end{cases},
\tag{2.54}
$$

where τ'_R is an arbitrary constraint on outage probability.

2.5.3 SNR Outage of an Arbitrary BS

Deconditioning over d_k (which in turn implies averaging over r_k and ϕ_k) yields the outage O as follows:

$$
\begin{aligned}
O &= 1 - \int_0^R \int_0^{2\pi} O_k(d_k) \frac{r_k}{\pi R^2} dr_k d\phi_k \\
&= 1 - \sum_{i=1}^4 \int_0^R \int_0^{2\pi} \mathbb{P}(v_i) O_k(v_i, d_k) \frac{r_k}{\pi R^2} dr_k d\phi_k.
\end{aligned}
\tag{2.55}
$$

2.5.4 Overall Energy-Efficiency

Conditioned on d_k, the energy-efficiency of the considered multicasting system can be derived as follows:

$$
\mathrm{EE}^{\mathrm{MC}}(d_k) = \sum_{\mathbf{s} \in \mathbf{S}} \frac{R_0 \left(\mathcal{K} - \sum_{k=1}^{\mathcal{K}} s_k \right)}{(2^{\mathcal{K}} - 1) B E_{tot}(d)} O_{s_k}^{\mathrm{MC}}(d_k),
\tag{2.56}
$$

where R_0 depicts bits/sec for each individual link, B is in Hz, $s_k = 1$ when the transmission fails for the k-th RX and $s_k = 0$ when the transmission is successful. Note that the term $\frac{R_0 \left(\mathcal{K} - \sum_{k=1}^{\mathcal{K}} s_k \right)}{B}$ represents the total number of successfully received bits of the overall network. On the other hand, when $\mathbf{s}_k$ is known *a priori* for each RX k based on certain QoS constraints, the overall network energy-efficiency can be expressed as follows:

$$
\mathrm{EE}^{\mathrm{MC}}(d_k) = \frac{R_0 \left(\mathcal{K} - \sum_{k=1}^{\mathcal{K}} s_k \right)}{B E_{tot}(d)} O_{s_k}^{\mathrm{MC}}(d_k),
\tag{2.57}
$$

where s_k is defined in (2.54).

2.5.5 Approximations for Rician Fading Channels

The exact end-to-end outage for Rician fading can be simplified by approximating the Bessel function of first kind in (2.7) using sum of pure finite real exponent series approximation

$I_0(x) = \sum_{i=1}^{4} S_i \exp(T_i x)$. The PDF of the non-central chi square distribution can thus be simplified as follows [61]:

$$f_X(x) = \frac{K+1}{\Omega} e^{-K - \frac{(K+1)x}{\Omega}} \sum_{i=1}^{4} S_i e^{T_i\left(2\sqrt{\frac{K(K+1)x}{\Omega}}\right)}. \tag{2.58}$$

Subsequently, I derive the approximate CDF as follows.

Proposition 3 (Approximate CDF). *Integrating (2.58) yields the approximate CDF of the non-central chi square distribution as:*

$$F_X(\Gamma) \approx \sum_{i=1}^{4} S_i \left(1 - e^{-b\Gamma + 2\sqrt{b\Gamma}\eta_{2i}} + \xi_i + \psi_i \operatorname{erf}[\sqrt{b\Gamma} - \eta_{2i}]\right) e^{-K},$$

where $\psi_i = e^{\eta_{2i}^2}\sqrt{\pi}\eta_{2i}$, $\xi_i = \psi_i \operatorname{erf}(\eta_{2i})$, *and* $\eta_{2i} = \sqrt{K}T_i$.

Subsequently, using **Proposition 3**, I obtain $F_{X_u}^L(\Gamma'_u)$ by substituting b with b_u, K with K_u, and Γ with Γ'_u. Also, I approximate $F_{X_k}(\Gamma'_k|d_k)$ by substituting b with b_k and K with K_k and Γ with $\Gamma'_k d_k^{\alpha_k}$, respectively, as follows:

$$F_{X_u}^L(\Gamma'_u) \approx \sum_{i=1}^{4} S_i e^{-K_u} \left(1 - e^{(-b_u\Gamma'_u + 2\sqrt{b_u\Gamma'_u}\eta_{2i})} + \xi_i + \psi_i \operatorname{erf}\left(\sqrt{b_u\Gamma'_u} - \eta_{2i}\right)\right), \tag{2.59}$$

$$F_{X_k}^L(\Gamma'_k|d_k) \approx \sum_{i=1}^{4} S_i e^{-K_k} \left(1 - e^{(-\eta_1^2 d_k^{\alpha_k} + G_i d_k^{\alpha_k/2})} + \xi_i + \psi_i \operatorname{erf}\left(\eta_1 d_k^{\alpha_k/2} - \eta_{2i}\right)\right), \tag{2.60}$$

where $\psi_i = e^{\eta_{2i}^2}\sqrt{\pi}\eta_{2i}$, $\xi_i = \psi_i \operatorname{erf}(\eta_{2i})$, and $\eta_{2i} = \sqrt{K_u}T_i$, $\eta_1 = \sqrt{b_d\Gamma'_k}$ and $G_i = 2\eta_{2i}\eta_1$. Also S_i and T_i are in vector form. Where **S** ad **T** are given as **S** = [0.1682, 0.1472, 0.445, 0.2382] and **T** = [0.7536, 0.9739, −0.715, 0.2343], respectively. Next, I approximate (2.60) as shown in (2.61) where (2.61)(a) follows from the approximate CDF in (2.60) referred to as *Four-Node Approximation*, (2.61)(b) follows from the proposed approximation of erf(x) as:

$$\operatorname{erf}(x) = 1 - a_1 e^{-b'x^2} - a_2 e^{-2b'x}, \tag{2.62}$$

where $E_1 = e^{-K_k} \sum_{i=1}^{4} S_i(1 + \xi_i + \psi_i)$ and **a** = [**0.3017 0.4389**]$^\mathbf{T}$, and $b' = 1.051$. I refer this approximation as *Four-Node with Error Function Approximation*. Note that (2.62) is

$$F^L_{X_k}(\Gamma'_k|d_k) \overset{(a)}{=} \sum_{i=1}^{4} S_i e^{-K_k} \left(1 - e^{(-\eta_1^2 d_k^{\alpha_k} + G_i d_k^{\alpha_k/2})} + \xi_i + \psi_i \, \mathrm{erf}\left(\eta_1 d_k^{\alpha_k/2} - \eta_{2i}\right)\right)$$

$$\overset{(b)}{=} 1 - E_1 + e^{-K_k} \sum_{i=1}^{4} S_i \left\{ e^{(-\eta_1^2 d_k^{\alpha_k} + G_i d_k^{\alpha_k/2})} + a_1 \psi_i e^{-b'(\eta_1 d_k^{\alpha_k/2} - \eta_{2i})^2} + a_2 \psi_i e^{-2b'(\eta_1 d_k^{\alpha_k/2} - \eta_{2i})} \right\}$$

$$\overset{(c)}{=} 1 - E_1 + e^{-K_k} \sum_{i=1}^{2} S_i \left\{ e^{(-\eta_1^2 d_k^{\alpha_k} + G_i d_k^{\alpha_k/2})} + a_1 \psi_i e^{-b'(\eta_1 d_k^{\alpha_k/2} - \eta_{2i})^2} + a_2 \psi_i e^{-2b'(\eta_1 d_k^{\alpha_k/2} - \eta_{2i})} \right\}.$$

$$(2.61)$$

different from the approximation in [45], i.e.

$$\mathrm{erf}(x) \approx 1 - \sum_{n=1}^{N=2} a_n e^{-nb'x^2} \approx 1 - a_1 e^{-b'x^2} - a_2 e^{-2b'x^2}. \qquad (2.63)$$

Then, (2.61)(c) follows from truncating the last two terms of the *Four-Node approximation*. I refer this approximation as *Two-Node with Error Function Approximation*. Note that this is different from finding the two-node approximation of the Bessel function to find the density function. *The applications of these approximations are discussed in the following Remark and in the next section.*

Remark: The proposed approximations of the Rician CDF listed in (2.61)(a), (2.61)(b), and (2.61)(c) can be directly used to compute the end-to-end outage probability expressions derived in Section 2.5. Figure 2.3(a) validates the proposed approximations in (2.61) for the exact $\mathrm{erf}(x)$. The existing approximation in (2.63) provides tighter bound to $\mathrm{erf}(x)$ for $x \geq 0$. However, the proposed approximation in (2.61) provides a slightly loose bound which is remarkably valid for a wider region (polarity of the approximation remains the same as $\mathrm{erf}(x)$ function). Figure 2.3(b) compares the SNR outage using *Four-Node approximation*, *Two-Node approximation*, and simulation results. The results depict that the two-node approximation is less precise compared to the four-node approximation; however, it has significant analytical tractability.
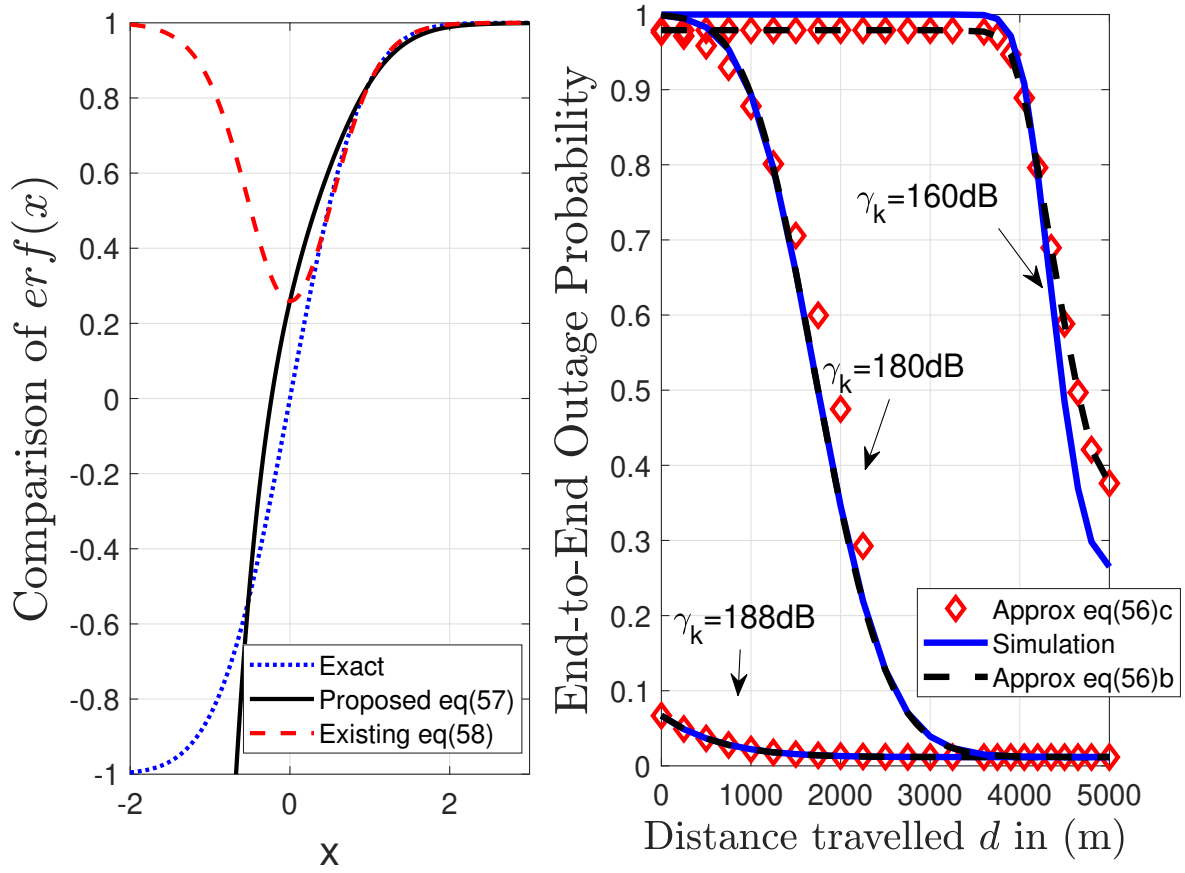
Figure 2.3 Validation of (a) erf(x) and (b) outage probability of RX k with Rician K-factor $K = 10$, $\bar{\gamma}_u = 172$ dB with $\tau = 0.3$.

2.6   Optimization Problems

In this section, I consider two different optimization problems to minimize the end-to-end energy consumption and outage probability of RX k located at cell-center. The objectives of the problems are (i) energy-constrained SNR outage minimization and (ii) outage-constrained energy consumption minimization. Note that $d_k = \sqrt{(D - d - r_k \cos(\theta'_k))^2 + (r_k \sin(\theta'_k))^2 + H^2}$. However, in this section, I consider that serving region (i.e. the cell radius R) in which all receivers are located is very small compared to the traveling distance of UAV $r_k = 0$, i.e. $d_k = d_0 = \sqrt{(D - d)^2 + H^2}$ for simplicity. Under this assumption, the farthest or nearest receiver becomes approximately the same as the receiver who is located at the cell-center. This assumption is valid for the scenarios such as when UAV starts from the city center and delivers data to remote area far away as described in Section 1.3.2. Also, I consider K and α as independent of elevation angles. I demonstrate in the results section that the variation in elevation angle during the UAV travel does not significantly impact α and K.

2.6.1   Outage-Constrained Energy Minimization

I minimize energy consumption $E_{tot}(d)$ in (2.19) under the SNR outage constraints as formulated in the following:

$$\mathbf{P1} : \min_{d} \; E_{tot}(d)$$

$$\text{s.t. } \mathbf{C1} : O_k(v_i, d_0) \leq \tau,$$

$$\mathbf{C2} : d \leq D, \quad d \geq 0,$$

where $E_{tot}(d) = \frac{(P_h + p_d)\sqrt{(D-d)^2 + H^2}}{c} + \frac{P(V)d}{V} + C$ is convex. The convexity is verified by noting that the second derivative $E''_{tot}(d) \geq 0$ is non-negative with respect to optimization variable d, hence $E_{tot}(d)$ is a convex function. However, the outage constraint based on the four event i not linear. Hence the problem is non-convex. To solve the optimization problem, we convexify the problem using the simplifications of the expression with the help of the

approximation proposed in previous sections. The convexification provides sub optimal result without running time consuming and computationally expensive simulations. The steps are provided next.

Optimization for Events υ_1 and υ_3: First I solve **P1** considering downlink LoS Rician fading channel. This solution approach will be applicable for the events υ_1, υ_3 for which

$$O_k(\upsilon_i, d_0) = 1 - U \sum_{\ell=0}^{\infty} \sum_{m=0}^{\ell} f_d(m, l) \left(\Gamma'_k d_0^\alpha\right)^{m_2} e^{\left(-b_d \Gamma'_0 d_0^\alpha\right)}. \tag{2.64}$$

For event υ_1, $U = \left(1 - F_{\gamma_u}^L(\Gamma_0)\right)$ can be calculated from (2.46). For event υ_3, $U = \left(1 - F_{\gamma_u}^N(\Gamma_0)\right)$ can be calculated from (2.47). The outage probability constraint **C1** is complicated because of the infinite double summations. To simplify **C1**, I use (2.60) since the approximation is analytically tractable. However, **(i)** the approximation still has the error function $\operatorname{erf}(\cdot)$ with the optimization variable d inside it, and **(ii)** the weights T_i in (2.60) are mixed (both positive and negative) and I know that "non negative weighted sum of convex function is convex". As such, obtaining a convex function is a problem due to T_3.

To resolve **(i)** and **(ii)**, I use (2.61)(b) and (2.61)(c) approximations, respectively. The modified problem **P1** be given by substituting $O_k(\upsilon_i, d_k)$ in **C1** as follows:

$$\begin{aligned} O_k(\upsilon_i, d_0) = & 1 - U \left(1 - E_1 + e^{-K} \sum_{i=1}^{2} S_i \left\{ e^{(-\eta_1^2 d_0^\alpha + G_i d_0^{\alpha/2})} \right. \right. \\ & \left. \left. + a_1 \psi_i e^{-b'(\eta_1 d_0^{\alpha/2} - \eta_{2i})^2} + a_2 \psi_i e^{-2b'(\eta_1 d_0^{\alpha/2} - \eta_{2i})} \right\} \right). \end{aligned}$$

Then, I transform the optimization variable $z = d_0^{\alpha/2} = ((D - d)^2 + H^2)^{\alpha/4}$ to simplify **C1** as follows:

$$O_k(\upsilon_i, z) = 1 - U \left(1 - E_1 + e^{-K} \sum_{i=1}^{2} s_i \left\{ e^{(-\eta_1^2 z^2 + G_i z)} + a_1 \psi_i e^{-b'(\eta_1 z - \eta_{2i})^2} + a_2 \psi_i e^{-2b'(\eta_1 z - \eta_{2i})} \right\} \right).$$

Subsequently, **P1** can be reformulated as follows:

$$\textbf{P2}: \min_{z} \ E_{tot}(z)$$

$$\text{s.t. } \textbf{C1}: O_k(v_i, z) \le \tau \tag{2.65}$$

$$\textbf{C2}: z \le (H^2 + D^2)^{\alpha/4}, z \ge H^{\alpha/2},$$

where

$$E_{tot}(z) = \frac{(P_h + p_d)z^{2/\alpha}}{c} + \frac{P(V)(D - \sqrt{z^{4/\alpha} - H^2})}{V} + C$$

is monotonically decreasing function hence quasi-convex (for proof please see **Appendix B**). Therefore, I replace $E_{tot}(z)$ in **P2** with z in **P3**. The obtained outage expression is the sum of log-concave (concave function in the argument of first and second exponents) and log-affine (due to linear argument of third exponent) functions which is non-convex. To write the function in the form of log of sum of exponential functions, I use the binomial approximation $(1 + x)^n \approx 1 + nx$ after completing squares in the argument of first exponential. This step linearizes the arguments of the three exponents which makes **C1** log-affine. **P3** can thus be written as follows:

$$\textbf{P3}: \min_{z} \ z$$

$$\text{s.t. } \textbf{C1}: \sum_{i=1}^{2} S_i \left(e^{\eta_1^2(2z - \frac{G_i}{2\eta_1^2})} g + a_1 \psi_i e^{-b' \eta_{2i}^2 (\frac{2\eta_1}{\eta_{2i}} z - 1)} + a_2 \psi_i e^{-2b'(\eta_1 z - \eta_{2i})} \right) \ge \tau'$$

$$\textbf{C2}: z \le (H^2 + D^2)^{\alpha/4}, z \ge H^{\alpha/2},$$

where $\tau' = e^K \left(\frac{\tau - 1}{U} + 1 - E_1 \right)$. Note that **P3** is now convex with **C1** in the form of sum of log-affine exponential function [62] which is convex since the weights are positive and argument within exponential functions are linear and can be written as log-sum-exponents. **P3** can thus be solved using standard convex optimization techniques.

Optimization for Events v_2 and v_4: For events with downlink NLoS Rayleigh fading channels, **P3** can be solved by substituting $O_k(v_i, z) = 1 - Ue^{-b_k \Gamma_k' z^2}$ using (2.49). Note that, for event v_2, $U = \left(1 - F_{\gamma_u}^L(\Gamma_0)\right)$ can be calculated from (2.46) and, for event v_4, $U = \left(1 - F_{\gamma_u}^N(\Gamma_0)\right)$ is given from (2.47).

Proposition 4 (Closed-Form Optimal Solution d^* for Rayleigh Fading Downlink Channels).
Since the objective is monotonically decreasing with respect to z, the solution lies at the boundary where the equality of **C1** *of* **P3** *holds. The closed-form optimal solution z^* can be obtained by solving the constraint $O_k(v_i, z) = 1 - Ue^{-b_k\Gamma'_k z^2} = \tau'$. By ignoring the positive root which is infeasible as it results in optimal value out of the range of d, I obtain d^* given as follows:*

$$d^* = D - \sqrt{\left(\frac{\Omega_u}{\Gamma'_u}\log\left(\frac{1-\tau}{U}\right)\right)^{2/\alpha} - H^2}. \tag{2.66}$$

In addition, $d^* = 0$ and $d^* = D$, if the constraint satisfies at $d = 0$ and $d = D$, respectively.

2.6.2 Energy-Constrained SNR Outage Minimization

Here, I minimize SNR outage subject to energy constraints $E_{tot}(z) \leq E_\tau$ such that the total energy consumption remains within minimum energy budget of UAV. I formulate the problem using (2.43) and (2.19) in variable z as follows:

$$\mathbf{P1} : \min_{z} \quad O_k(v_i, z)$$
$$\text{s.t.} \quad \mathbf{C1} : \frac{(P_h + p_d)z^{2/\alpha}}{c} + \frac{P(V)(D - \sqrt{z^{4/\alpha} - H^2})}{V} + C \leq E_\tau,$$
$$\mathbf{C2} : z \leq (H^2 + D^2)^{\alpha/4}, z \geq H^{\alpha/2},$$
$$\mathbf{C3} : \frac{m}{z^2} - b_d\Gamma'_k < 0,$$

where constraint **C3** is the feasibility constraint. Under this feasibility condition, I can replace $O_k(v_i, z)$ with z in the objective function as follows:

$$\mathbf{P2} : \min_{z} \quad z$$
$$\text{s.t.} \mathbf{C1} : \frac{(P_h + p_d)z^{2/\alpha}}{c} + \frac{P(V)(D - \sqrt{z^{4/\alpha} - H^2})}{V} + C \leq E_\tau,$$
$$\mathbf{C2} \; \& \; \mathbf{C3}.$$

Under the feasibility regime, the outage probability $O_k(v_i, d_k) \; \forall i = 1, 2, 3, 4$ is monotonically decreasing function of z (see **Appendix C** for proof). Due to the monotonic nature of the

objective and constraint, the solution to the above problem lies at the boundary where **C1** becomes an equality constraint.

Proposition 5 (Closed-Form Optimal UAV Distance for Energy-Constrained Outage Minimization). *The optimal solution z^* can be obtained by solving $E_{tot}(z) - E_\tau = 0$, taking the solution with positive root and then substituting z^* in $z = d_0^{\alpha/2}$ to obtain d^* by taking the solution with negative root:*

$$d^\star = D - 2\sqrt{\frac{\left(\kappa_3 + F^2 + 2F\sqrt{\kappa_3}\right)}{(\kappa_1^2 - 1)^2} - H^2}, \tag{2.67}$$

where $\kappa_3 = \kappa_1^2(F^2 + \kappa_2^2)$, $\kappa_2^2 = (\kappa_1^2 - 1)H^2$, $\kappa_1 = \frac{cP(V)}{(P_h + p_d)V}$ and $F = \left(E_\tau - C - D\frac{P(V)}{V}\right)\frac{c}{(P_h + p_d)}$. This solution is valid for events v_i, $\forall i = 1, \cdots, 4$.

2.6.3 Multi-Objective Optimization

In this subsection, I simultaneously minimize both the energy consumption and outage probability. I formulate a bi-objective optimization problem with weights λ and $1 - \lambda$ to the energy consumption and outage probability, respectively. The problem is formulated as follows:

$$\textbf{P1} \quad \min_z \ \lambda E_{tot}(z) + (1 - \lambda)O_k(z)$$

$$\text{s.t.} \ \textbf{C1} : O_k(v_i, z) \leq \tau \tag{2.68}$$

$$\textbf{C2} : z \leq (H^2 + D^2)^{\alpha/4}, z \geq H^{\alpha/2}.$$

In (2.68) the unit of $E_{tot}(z)$ is Joules and of the order of thousands, whereas the outage probability is unitless quantity between '0' to '1'. The objective function is implicitly biased towards energy consumption. With the help of normalization of $E_{tot}(z)$ (i.e. shifting and scaling of $E_{tot}(z)$ as $\frac{E_{tot}(z) - E_{\min}}{E_{\max} - E_{\min}}$), (i) I reduce the magnitude of $E_{tot}(z)$ from '0' to '1' which was required to create a balance between the energy consumption and outage probability, and (ii) I make $E_{tot}(z)$ a unitless quantity. Now both the terms are of same order and can be added together. Note that $E_{\max}$ and $E_{\min}$ represent maximum and minimum value of energy

consumption that is obtained by substituting the limits of $z = H^{\alpha/2}$ and $z = (D^2 + H^2)^{\alpha/4}$, respectively, in $E_{\text{tot}}(z)$ defined in Section 2.6.2 problem **P1**. That is, $E_{\max} = \frac{(P_h + p_d)H}{c} + \frac{P(V)}{V}D + C$ and $E_{\min} = \frac{(P_h + p_d)\sqrt{H^2 + D^2}}{c} + C$. The objective of **P1** can thus be rewritten as follows:

$$U(z) = O_k(z) + \bar{\nu}\left(E_{tot}(z) - E_{\min}(z)\right), \tag{2.69}$$

where $\bar{\nu} = \frac{\lambda}{1-\lambda}\frac{1}{E_{\max} - E_{\min}}$ minimizes outage probability when $\frac{\lambda}{1-\lambda} = 0$ and minimizes energy consumption when $\frac{\lambda}{1-\lambda} = \infty$ [63, 64]. The selection of weights is a choice of decision maker. To solve **P1**, I use the fact that the objective function can be formulated as a difference of two convex functions as follows:

$$U(z) = \bar{\nu}\left(E_{tot}(z) - E_{\min}\right) - (-O_k(z)). \tag{2.70}$$

By defining $Q(z) = G(z) - H(z)$ where $G(z)$ and $H(z)$ are convex functions given by $G(z) = \bar{\nu}(E_{tot}(z) - E_{\min}(z))$ and $H(z) = -O_k(z)$, respectively, I formulate **P1** as follows:

$$\textbf{P2} \quad Q(z) = \min_{z} \ G(z) - H(z)$$
$$\text{s.t. } \textbf{C1}: O_k(v_i, z) \leq \tau \tag{2.71}$$
$$\textbf{C2}: z \leq (H^2 + D^2)^{\alpha/4}, z \geq H^{\alpha/2},$$

where

$$G(z) = \bar{\nu}\left(\frac{(P_h + p_d)}{z^{-2/\alpha}c} + \frac{P(V)(D - \sqrt{z^{4/\alpha} - H^2})}{V} + C - E_{\min}(z)\right),$$

$$H(z) = \max\left\{-1 + U\left(1 - E_1 + e^{-K}\sum_{i=1}^{2}S_i\left\{e^{\eta_1^2(2z - \frac{\eta_{2i}}{\eta_1})}g\right.\right.\right.$$
$$\left.\left.\left. + a_1\psi_i e^{-b_n\eta_{2i}^2(\frac{2\eta_1}{\eta_{2i}}z-1)} + a_2\psi_i e^{-2b_n(\eta_1 z - \eta_{2i})}\right\}\right), 0\right\}.$$

It should be noted that the outage probability approximation results in the value beyond [0 1] range therefore to limit the range I use $\max(.,0)$. It is clear from **Appendix A** that $G(z)$ is convex and $H(z)$ is also convex, respectively, with respect to z. However, in

general, (2.71) is not a convex/concave problem. That is, the objective function is a difference of convex functions. DC programming approach provides an efficient way to get local optima numerically which occasionally turns out to be global optimal [65, 66]. To find the efficient sub-optimal solution, this method involves successive convex approximation. That is, the sub-problem in each iteration j is obtained by linearization of $H(z)$ at point z^j, i.e. $H(z) = H(z^j) + H'(z^j)(z - z^j)$ where $H'(\cdot)$ represents the derivative of $H(\cdot)$. Note that z^j is update in z after j-th iteration. The algorithm to solve **P2** is presented in **Algorithm 1**. The complexity and convergence of **Algorithm 1** is well-established in [67].

Data: Initial point: z^0, Max Iterations $J_{\max}$, Error tolerance ϵ, Objective function

$Q(z)$ and reduction of candidate points based on $0 \leq O_k(z) \leq \tau$

Result: sub optimal desired solution z_{sub}

set $j = 0$; **while** $|Q(z^{j+1}) - Q(z^j)| \leq \epsilon$ *or* $j > J_{\max}$ **do**

- Convex approximation of $Q(x)$ at the point z^j,

  $$Q^j(z) = G(z) - H(z^j) - H'(z^j)(z - z^j)$$

- Solve $z^j = \operatorname{argmin} Q^{(j)}(z)$

- $j = j + 1$.

end

Algorithm 1: DC Algorithm

Next, I provide the discussion based on numerical results of the analysis and optimization presented earlier.

2.7 Numerical Results and Discussion

I verify the accuracy of our derived expressions by comparing it to the monte Carlo simulations and obtain insights related to the optimal ferrying distance, and performance of a UAV-assisted data ferrying distance system in a variety of scenarios. To perform monte Carlo simulations, we take average over 10,000 instants where in each instant the fading channel for uplink and downlink were random. Unless stated otherwise, the simulation parameters are $D = 5000m$, $H = 500$ m, $p_U = p_D = 50$ W, $\eta_1 = 0.009$, $\eta_D = 0.01$, $R = 200$ m, $\Gamma_0 = 10dB$, $q_U = q_D = -1.5$, $v_U = v_D = 3.5$, $w_U = w_D = 15$ dB, $z_U = z_D = 5$. The typical $N_0 = 10^{-17}$W/Hz [68], that justifies the values I used for γ_u and γ_k herein. Figure 2.4(a)
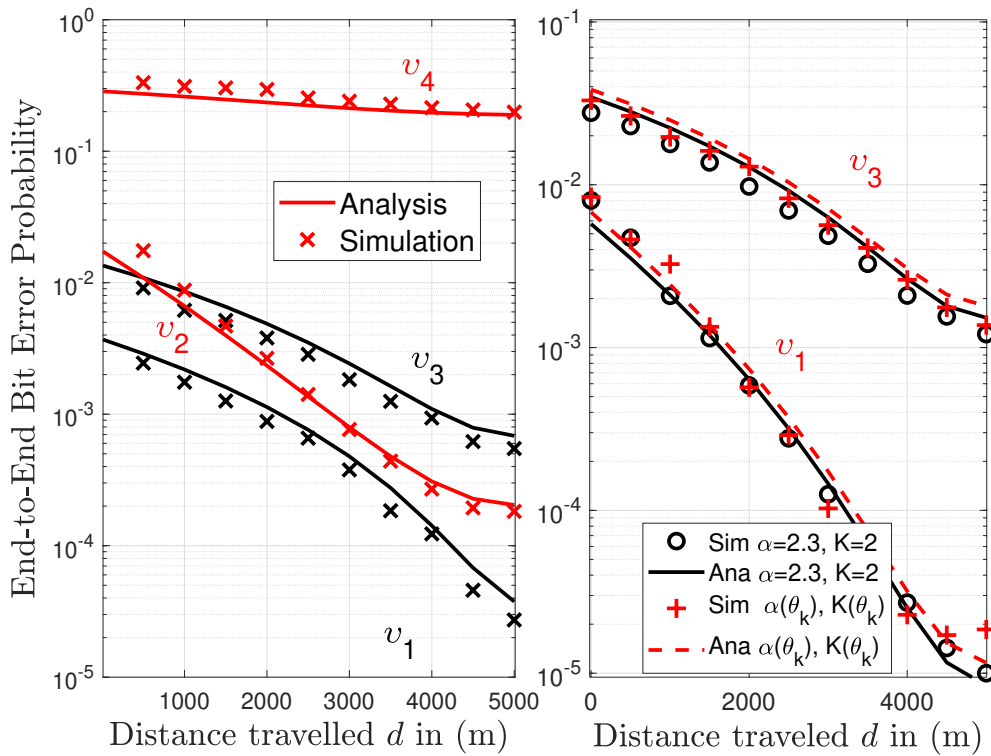
Figure 2.4 (a) BEP conditioned on d_k, $\gamma_u = 211dB$, $\gamma_k = 181dB$, $\Gamma_0 = 10dB$, $K(\theta_k)$ and $\alpha(\theta_k)$, (b) BEP with $K(\theta_k)$ ranging from [2.18 1.92] and $\alpha(\theta_k)$ ranging from [2.313 2.311] vs fixed K, α.

presents the end-to-end BEP of a typical RX as a function of the ferrying distance d considering the events v_1, v_2, v_3, and v_4 separately that appear in the order from bottom to

top. The BEP decreases monotonically as a function of d. Further, the theoretical results match well with the simulation results. Also, I observe that v_1 (Rician (LoS)-only) and v_4 (Rayleigh (NLoS)-only) have the minimum and maximum BEPs, respectively. The BEP in other events is similar to v_1 which shows that the significance of LoS transmissions in any one hop has a positive impact on the BEP.

Figure 2.4(b) depicts the comparison of the end-to-end BEP of two events v_1 and v_3 for Rician K-factor and path-loss exponent α as a function of elevation angle θ_k as in (2.9) and (2.10) to the fixed K and α. I note that the change in ferrying distance does not impact θ_k and in turn $K(\theta_k), \alpha(\theta_k)$ significantly. Thus the end-to-end BEP remains the same. This result also justifies our assumption to consider fixed value of K and α in the optimization problems presented in Section V. Note that the fixed K and α can not be chosen randomly but their value needs to be chosen close to $K(\theta_k), \alpha(\theta_k)$.
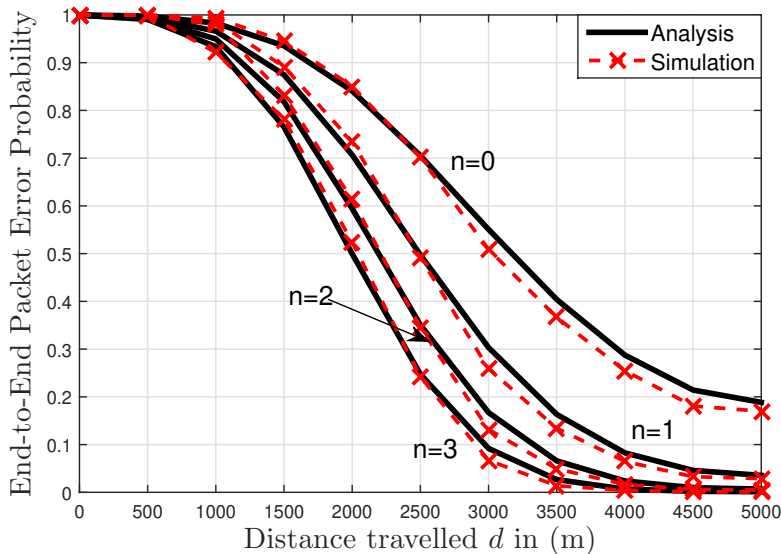
Figure 2.5 PEP conditioned on d_k: comparison of simulation and exact analysis for unconditioned on events and conditioned on d_k as a function d with and without ARQ.

Figure 2.5 depicts the end-to-end PEP as a function of d without and with ARQ retransmissions. Analytical and simulation results match well for $n = 0$, i.e. for single trans-

mission and $n = 1, 2, 3$ with two and three retransmissions, respectively. As expected, PEP decreases with d which means reliability is increasing. Figure 2.5 depicts that increasing retransmissions help in achieving the desired reliability with a lower traveled distance which will minimize the energy consumption. In addition, I also note that the reduction in PEP is significant $n = 0$ to $n = 1$ and the degree of reduction gradually reduces for $n = 2$ to $n = 3$ and onwards.
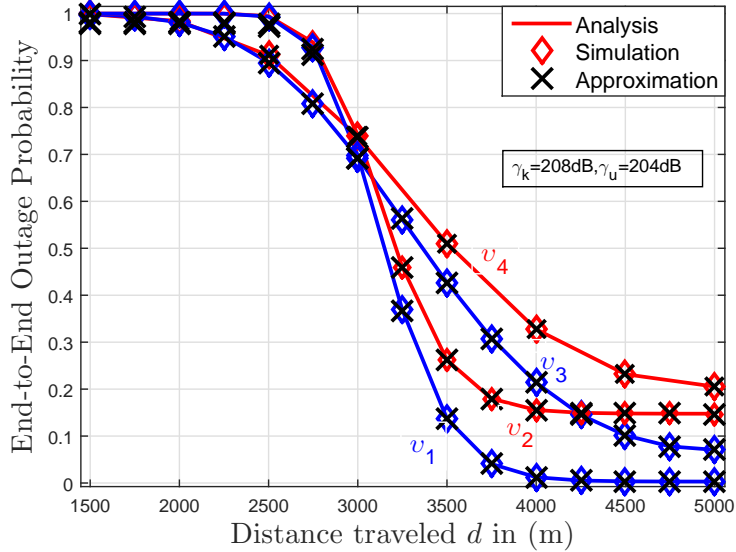
Figure 2.6 Outage probability conditioned on d_k comparison of simulation, exact, and approximate analysis for different d.

Figure 2.6 depicts the end-to-end outage probability of a typical RX as a function of the distance traveled by the UAV. Each curve corresponds to the events v_1, v_2, v_3, and v_4 separately. Theoretical results match well with the simulations. Figure. 2.6 demonstrates the efficacy of the Bessel approximation. The outage probability decreases monotonically as a function of the ferrying distance d due to reduction in path-loss. As such, d can be optimized to meet a specific outage probability constraint.

Note that v_1 (Rician-only) and v_4 (Rayleigh-only) shows the minimum and maximum outages, respectively, beyond a certain travel distance $d \approx 3500$m. For distances smaller than $d = 3500$m, Rician-only event v_1 (both uplink and downlink are LoS) performs similar to

64
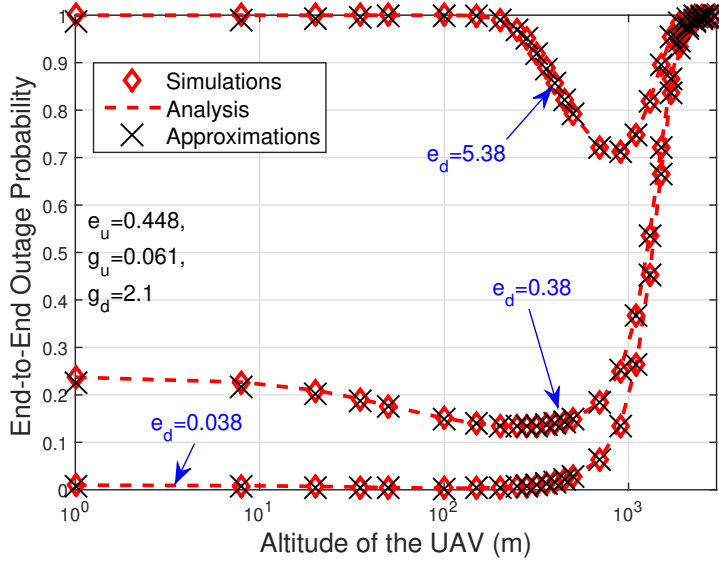
Figure 2.7 Outage probability as a function of the altitude of UAV considering $\gamma_u = 172\text{dB}$, $\gamma_k = 184\text{dB}$, and $d = 2000\text{m}$.

Rician-Rayleigh event υ_2 (uplink is LoS and downlink is NLoS). The reason is the dominance of uplink over downlink due to reduced path-loss in the uplink (when the UAV is close to **I**). Similarly, Rayleigh-only event υ_4 (both uplink and downlink channels are NLoS) performs similar to Rayleigh-Rician event υ_3 (uplink is NLoS and downlink is LoS). For distances more than $d = 4250\text{m}$, Rician-only event υ_1 performs similar to Rayleigh-Rician event υ_3 and Rayleigh-only event υ_4 performs similar to Rician-Rayleigh event υ_2. The reason is the dominance of downlink over uplink transmission when the UAV is close to **F**.

Figure 2.7 depicts the end-to-end outage probability of a typical RX as a function of the altitude taken by the UAV considering different values of e_k as given in (2.6). The derived theoretical results match well with the Monte-Carlo simulation results. As e_k decreases, the LoS probability increases (see (2.6)) and therefore the end-to-end outage decreases. Another interesting trend is that the SNR outage initially decreases with the increase in height (due to higher LoS probability); however, after a certain point the SNR outage tends to increase due to the increasing distance from the ground. It is also interesting to observe that the reduction in outage due to higher altitude is noticeable only for higher values of e_k. The
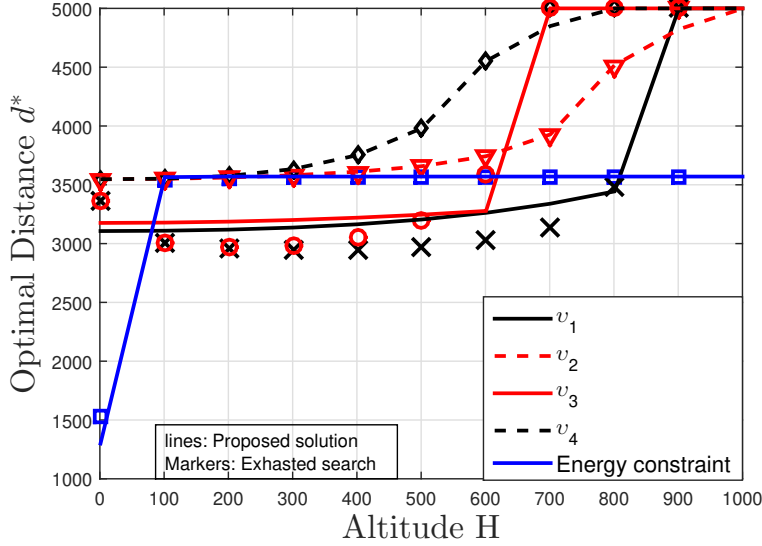
Figure 2.8 Optimal distance d^* plotted for (a) outage constrained energy minimization and (b) energy constrained outage minimization, $\gamma_u = 188dB$, $\gamma_k = 172$dB, & $K = 5.25$ with outage threshold $\tau = 0.2$, and energy budget $E_\tau = 1 \times 10^5$.

energy efficiency curve shows the inverse trend of outage probability.

Figure 2.8 shows the optimal distance d^* obtained by solving the optimization problems (i) outage constrained energy minimization and (ii) energy constrained outage minimization, for all four events v_1, v_2, v_3, and v_4 as a function of the UAV altitude H (please see Section 2.4). It is noted that the optimal ferrying distance d^* in the former problem gradually increases with the height of UAV for all events. The reason is that, with the increase of height, the channel becomes weaker due to path-loss dominance which causes UAV to travel more to meet the constraint on outage probability. For the latter problem, d^* increases first and then becomes a constant almost at $d^* = 3500$. The derived optimal solutions match well with the optimal results obtained through exhaustive search. I also note that the optimal distance for the event v_1 (Rician-only) is minimum because of improved channel condition. However, v_4 (Rayleigh-only) suffers with worst channel attenuation which causes the d^* to be the longest. The optimal distances of the v_2, v_3 lies between the v_1 and v_4.

Figure 2.9(a) shows the impact of λ on the utility function in (2.70). For smaller
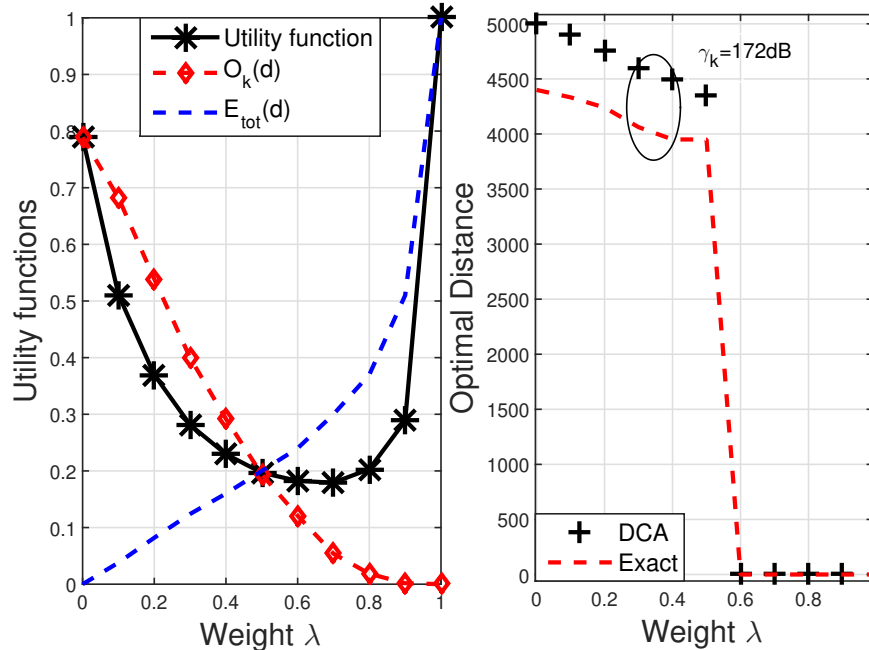
Figure 2.9 Multiobjective optimization with minimization of outage and energy consumption for a typical user comparison exhaustive vs difference of convex algorithm (DCA) based solution for Rician K-factor $K = 2$ for event υ_1, $\gamma_u = 176$dB and $\gamma_k = 180$dB as a function of weights λ.

values of λ, outage probability is dominant in the utility function. As λ increases, the bias towards energy consumption increases and at $\lambda = 0.5$ both outage probability and energy consumption are equally important. Figure 2.9(b) depicts the comparison of the optimal ferrying distance using exhaustive search to the optimal solution obtained from **Algorithm 1** with $0 \leq O_k(d_k) \leq 0.5$. In the region for $\lambda \geq 0.6$, the objective is biased towards minimizing the energy consumption which in turn minimizes the UAV distance traveled while meeting the outage constraints. With no outage constraints, the energy is minimum when UAV does not travel from **I**. In the region for $\lambda \leq 0.6$, the objective is biased towards minimizing the outage which in turn maximizes the UAV distance traveled while meeting the minimum energy consumption constraints. With no energy constraints, the outage is minimum when UAV is at **F**.

2.8 Conclusion

A summary of the major observations is as follows: The optimal data ferrying distance d^* gradually increases with the height of UAV since with the increase of height the channel becomes weaker and, in turn, the UAV needs to travel more to meet the constraint on outage probability. Increasing retransmissions help in achieving the desired reliability with a lower data ferrying distance. This minimizes the energy consumption. In addition, a reduction in packet error probability is higher with one retransmission and it gradually decreases for a higher number of retransmissions. Regarding the impact of weight λ on the utility function in our multi-objective optimization problem, for $\lambda = 0$, the outage probability is dominant; therefore, the UAV tends to travel a larger distance in order to minimize outage. When $\lambda = 1$, the bias towards energy consumption increases due to which the UAV tends to minimize its travel distance to minimize energy consumption. For any other value of λ, the UAV finds optimal distance somewhere between 0 to D to fulfill the outage-energy trade-off.

Chapter Three

Optimization of Wireless Relaying With Flexible UAV-Borne Reflecting Surfaces

This chapter characterize and design the system model for the proposed Integrated UAV-IRS scheme. The framework provide end-to-end performance analysis in terms of outage probability, Spectral efficiency, and energy efficiency for the three modes of operations, UAV-only mode, IRS-only mode, and integrated UAV-IRS mode. This chapter also presents variety of optimization problems under different constraints and objectives and their corresponding solution approach. In this chapter, I first provide introduction and then describe the system model in Section 3.2. In Section 3.3, I characterize the end-to-end energy efficiency, the SNR outage probability and data rate for the considered network modes. In Section 3.4, I propose approximations for ergodic capacity and energy efficiency. In Section 3.5, optimization is performed to maximize energy efficiency for IRS elements and UAV height for transmission modes. Mode selection probability and criteria are presented in the same section. Then, I present the numerical results in Section 3.6 before I conclude in Section 3.7.

3.1 Introduction

Intelligent reflecting surfaces (IRS) are emerging as a key enabling technique to smartly reconfigure wireless propagation environment in beyond 5G wireless networks [22]. The IRS consists of multiple small meta-surfaces that are also referred to as *IRS elements* that enables smart reconfiguration via software-controlled reflections of IRS. The comprehensive intelligent functionality of each element includes reflection, refraction, transmittance and absorption [22, 25]. The functionalities can be used all together or in separate based on the application requirement. In contrast to conventional relaying, IRS assisted communication offers multitude of benefits: **(i) Reduced energy consumption:** Since IRS simply reflects the incident transmission signals and does not require power consuming complex signal processing operations, the energy consumption can be reduced significantly. In addition, IRS can potentially minimize the on-board UAV energy consumption [28, 29] by putting the wireless transmitter at the UAV in sleep mode, in specific scenarios where desired quality-of-service (QoS) can be met with IRS-only transmissions. **(ii) Efficient spectrum utilization:** Since IRS simply reflects the incident transmission signals and does not require an additional frequency channel for transmission, network-wide spectrum consumption can be minimized. **(iii) Flexible deployment of metasurfaces in three dimensions:** The considered integrated UAV-IRS mode provides flexible placement of IRS in three dimensions and the number of IRS elements provides an additional degree of freedom to improve the channel quality. **(iv) Low hardware cost:** This IRS surface consists of large arrays of low-cost integrated electronics (e.g., polymer diode/switch or conductive square patches [23] [24]) which reflects the incoming signal to the desired direction with minimal hardware costs. The above benefits motivate us to characterize and optimize the performance of an integrated UAV-IRS system.

3.1.1   Background Work

As mentioned in the Introduction of Chapter 2, that series of research works [30–32, 34, 69] derive SNR outage characterization of UAV-assisted relaying assuming either LoS Rician or NLoS Nakagami-m faded aerial channels which are generally in the form of complicated mathematical functions which cannot be directly used for network planning and optimization purposes. In [69] and [34], the SNR outage probability was analyzed for Rician and Rayleigh fading channels considering LoS and NLoS channels with and without shadowing, respectively. [70] provided outage probability considering that channel is perfectly known. The aforementioned research works [30–32, 34, 69, 70] overlooked the impact of limited on-board energy of the UAV as well as the circuit and hovering power consumption of the UAV.

Another series of research works that focused on the energy efficiency maximization of UAV-enabled relaying networks include [13, 36, 71–76] and [Chapter 2 of the thesis]. These research works are solely based on numerical optimization techniques. Recently, I developed a mathematical framework to characterize the reliability, energy efficiency, and coverage probability in a UAV-assisted data-ferrying network considering Rician-faded aerial channels [Chapter 2 of the thesis]. Using the derived expressions, I optimized the data-ferrying distance for a UAV with the following three different objectives: (i) minimize the energy consumption under the constraint of outage probability, (ii) minimize the outage probability under the constraint of energy consumption, and (iii) minimize both the outage probability and energy consumption by considering multi-objective optimization [Chapter 2 of the thesis]. The aforementioned research works did not consider the IRS-assisted UAV systems.

To date, a number of research works considered the statistical performance characterization or optimization of IRS-assisted wireless networks either without UAV [23, 26, 77, 78] or with UAV [79, 80]. A pioneering effort to characterize an upper bound on the average symbol error probability was undertaken in [77]. The research work considered Rayleigh fading channels and simplified the instantaneous SNR given the optimal phase shifts for IRS.

71

The energy efficiency of the system was not considered. A number of research works [23, 26] focused on maximizing the energy efficiency by optimizing the IRS phase shifts with infinite and low phase resolution capability. An interesting research work is [78] where the authors compared the performance of decode and forward (DF) relaying with IRS-assisted transmission. The IRS and DF relay were placed in the same fixed location. They also considered maximal ratio combining between the direct and IRS assisted link. Nevertheless, the channel gain coefficients were assumed to be perfectly known. The authors in [79] considered an IRS to facilitate the transmission between a mobile UAV and a ground user. The UAV-to-IRS transmission link was modeled as LoS Rician fading channel whereas IRS-to-ground user link was modeled as NLoS Rayleigh fading channel. The authors maximized the rate by optimizing IRS phase shifts and the trajectory through numerical optimization considering known channel state information (CSI). In [80], the authors used reinforcement learning to optimize the location of UAV-IRS system in order to maximize the downlink transmission capacity.

3.1.2 Contribution

Except [77], most of the aforementioned research works focused on the optimization of the phase-shifts in IRS-assisted networks using numerical optimization techniques. This chapter develops a comprehensive mathematical framework to characterize the performance of an integrated UAV-IRS system and optimize critical network parameters such as the number of IRS elements and UAV altitude to maximize the spectral and energy efficiency. Note that an IRS micro-controller can perform the optimal switching of IRS elements (e.g. by turning the corresponding diodes between 'ON' and 'OFF' [81]. At this point, it is noteworthy that maximization of energy efficiency and optimization of the number of IRS elements (N) in an integrated UAV-IRS system is crucial due to two reasons: **(i)** given the limited UAV size,

the number of IRS elements that can be deployed on a UAV is limited[1], and **(ii)** due to the power consumption associated with each IRS element. Although the power consumption of each IRS element is low, the overall power consumption may become significant for a large number of active IRS elements depending on the *phase resolution power consumption* $\tilde{P}_r(b)$ as described in Section 1.3,3. The specific contributions of the chapter are as follows:

- I characterize the outage probability, ergodic capacity, and energy efficiency in an integrated UAV-IRS system (where IRS surface is mounted on the UAV) considering three different modes, (i) *UAV-only mode*, where the UAV performs relaying in full-duplex mode, (ii) *IRS-only mode*, where the IRS performs (reflective) relaying which is implicitly a full-duplex transmission without self-interference (SI) [22, 82, 83], and (iii) *Integrated UAV-IRS mode*, where both the UAV and IRS perform relaying and the receiver uses selection combining (SC). The considered model captures the LoS air-to-ground (AtG) Rician fading channels and power consumption of UAV and IRS.

- I provide approximate expressions to increase the mathematical tractability of the proposed framework for system optimization purposes. That is, I incorporate the derived expressions (after some transformations to tractable mathematical forms) into the optimization problems. The derived expressions are validated by comparing numerical results with those obtained from Monte-Carlo simulations.

- I formulate a variety of the optimization problems where objective functions have a fractional form for IRS-only mode and UAV-only mode, i.e. (i) maximize EE to optimize the number of IRS elements, (ii) maximize EE to optimize the height of the IRS, (iii) minimize IRS power consumption to optimize the the number of IRS element and transmission power subject to rate constraints, and (iv) maximize EE to optimize the height of the UAV. I solve the aforementioned problems and derive optimal solutions

---

[1]The size of one IRS element is typically in the range $\lambda/10 - \lambda/5$ [24], where λ denotes the wavelength of the transmitted wave. As such, this limitation becomes more evident in low frequencies.

using quadratic transformation as a tool from fractional programming. Closed-form optimal solutions are provided, wherever applicable.

- I derive an analytic criterion to optimally select the UAV-only and IRS-only transmission modes to maximize the capacity and EE for a given number of IRS elements.

- Numerical results compare the proposed optimal solutions with the solutions obtained through exhaustive search. It is noted that, compared to the UAV-only mode, the IRS-only mode is energy efficient at lower altitudes with low to moderate number of active IRS elements, and for larger distances between the UAV and the source or destination.

3.2 System Model and Assumptions

3.2.1 Spatial Deployment of UAV-IRS System

I consider an integrated UAV-IRS network in which a UAV carries a large array of IRS elements to assist communication between source $\mathbf{S}$ and destination $\mathbf{D}$ located on the ground. I assume that there exists no direct link between the $\mathbf{S}$ and $\mathbf{D}$. In particular, the IRS reflects the incident signal in the desired direction of destination with minimal power consumption. In addition, the UAV operates as an independent relay between $\mathbf{S}$ and $\mathbf{D}$ since I assume that the UAV has separate transmit and receive antennas. In Cartesian coordinates, the locations of $\mathbf{S}$ and $\mathbf{D}$ are denoted as $\mathbf{w}_s = (x_s, y_s, 0)$, and $\mathbf{w}_d = (x_d, y_d, 0)$, respectively (Fig. 3.1). I also assume that UAV can be placed at any height h such that $h \in [h_{\min}, h_{\max}]$ where $h_{\min}$ and $h_{\max}$ are decided by aviation authorities. I denote the UAV coordinate as $\mathbf{w_u} = (x_u, y_u, h)$. In two-dimensional Cartesian coordinates, the location of source, destination, and the UAV can be given by $\mathbf{z_s} = (x_s, y_s)$, $\mathbf{z_d} = (x_d, y_d)$, and $\mathbf{z_u} = (x_u, y_u)$, respectively.
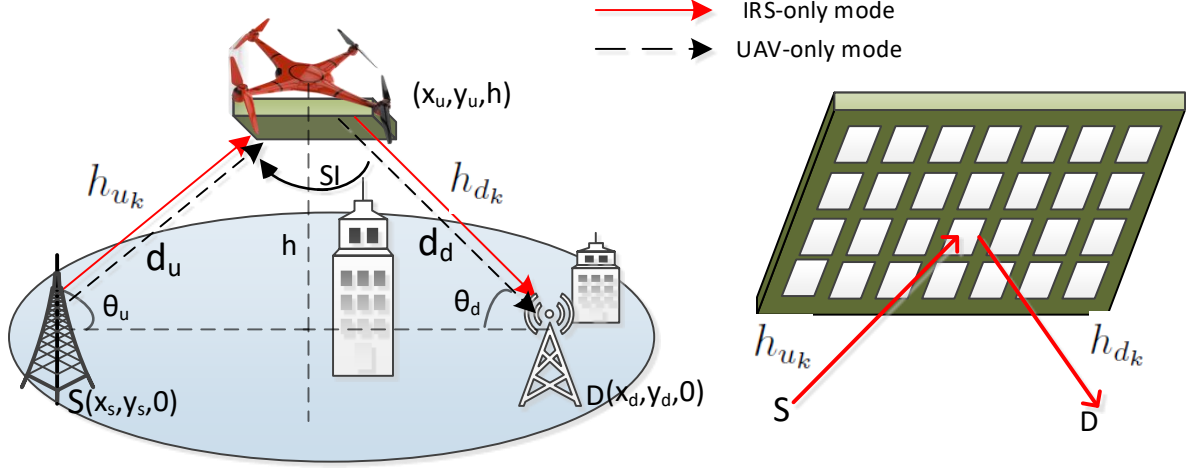
Figure 3.1 Integrated UAV-IRS communication system with self-interference (SI) at UAV.

3.2.2 Aerial Channel Model

The communication between the UAV and ground receiver **S** and **D** depends on the elevation angle between the nodes (and/or altitude of the UAV) and the environment (e.g. the intensity and height of buildings). The transmission to the ground users may have LoS or non-LOS based on the elevation angle (in rad) between the UAV and BS_i. The elevation angle can be given as follows:

$$\theta_u = \arctan\left(\frac{h}{|\mathbf{z_u} - \mathbf{z_s}|}\right), \qquad \theta_d = \arctan\left(\frac{h}{|\mathbf{z_u} - \mathbf{z_d}|}\right), \qquad (3.1)$$

where h, $\mathbf{z_s}$, and $\mathbf{z_d}$ are defined in 3.2.1. The probability of LoS in each link is a function of θ_i, i.e.

$$p_L(\theta_i) = (1 + e_i \exp(-g_i(\theta_i - e_i)))^{-1}, \qquad \forall i \in \{u, d\}, \qquad (3.2)$$

where e_u, e_d, g_u, and g_d, are the environment parameters obtained from the curve fitting using Damped Least-Squares (DLS) method [48]. The path-loss exponent α is a function of

the elevation angle [50], i.e.

$$\alpha(\theta_i) = p_L(\theta_i)q_i + v_i. \tag{3.3}$$

Here q_u, v_u, q_d, and v_d are constants depending on the uplink and downlink environment [48].

3.2.3   Spectrum Allocation

I consider that the destination BS $\mathbf{D}$ has a data rate requirement R_0 which is defined as $R_0 = B \log_2(1 + \Gamma_0)$, where Γ_0 is the minimum end-to-end SNR threshold required by the destination to achieve R_0, i.e. $\Gamma_0 = 2^{\frac{R_0}{B}} - 1$. Here, B represents the total transmission bandwidth available for IRS-only mode, UAV-only mode, and integrated UAV-IRS mode. The IRS does not need additional frequency to reflect the signals. For the sake of fairness, I consider in-band full-duplex (IBFD) operation at the UAV. This enables the UAV to transmit and receive simultaneously over the same frequency band B. The performance of IBFD communication is, however, limited by self interference (SI) which is introduced by the IBFD transmitter to its own receiver [17]. That is, the uplink receiver (which is the UAV) will see the interference from its own downlink transmission. The IBFD antenna is assumed to be equipped with a three-port circulator to prevent the leakage of transmit chains to receive chains; however, in practice, perfect SI cancellation is not possible [84].

3.2.4   Transmission Modes

I consider three different modes of data transmission, i.e. **(i)** *UAV-only mode*, when UAV provides coverage to the destination $\mathbf{D}$ with all IRS elements switched off (absorbing state of IRS) and UAV is operating in IBFD transmission mode, **(ii)** *IRS-only mode*, when only IRS is responsible to provide service to the destination $\mathbf{D}$ by acting as relay and the UAV does not communicate, and **(iii)** *Integrated UAV-IRS mode*, when both IRS and UAV transmit

the data and the receiver at the destination combines the data using *selection combining*[2], i.e. by opportunistically selecting the stronger signal between those received from the UAV and the IRS. I consider that the destination receiver is equipped with a buffer to store the observations from IRS transmission that arrives one time slot prior to the UAV transmission.

The IRS is equipped with linear arrays of elements and there is a controller associated with the IRS which is responsible for smart selection of the functionality of IRS elements such as absorption and beamforming.

Now I describe the transmission and channel models for each of the modes of operation.

UAV-only Mode

The transmission from **S** to UAV and the transmission from UAV to **D** can be given, respectively, as follows:

$$y_u = \sqrt{\hat{A} p_u \eta_u^{-1} d_u^{-\alpha(\theta_u)}} \, h_u \, s + R_{\text{SI}} + n_u, \qquad y_d = \sqrt{\hat{A} p_d \eta_d^{-1} d_d^{-\alpha(\theta_d)}} \, h_d \, y_u + n_d,$$

where s is the transmitted signal in binary phase shift keying (BPSK) from the source **S** to the UAV and y_u is the signal received by the IBFD UAV and relayed to **D**, η_i denotes the excess aerial path-loss, p_u is the transmission power of **S**, and p_d is the transmission power of UAV. Also, d_u is the distance between the **S** and the UAV, i.e. $d_u = \sqrt{|\mathbf{z}_u - \mathbf{z}_s|^2 + h^2}$ and d_d is the distance between UAV and **D**, i.e. $d_d = \sqrt{|\mathbf{z}_u - \mathbf{z}_d|^2 + h^2}$. Note that $\hat{A}$ reflects system parameters (e.g. operating frequency and antenna gain), n_i is additive white

---

[2]In selection combining, the combiner outputs the signal on the branch with the highest SNR, which requires one receiver switching to active branch, and co-phasing of multiple branches is not required as is the case the other combining techniques. Therefore, selection combining exhibits low overhead and is mathematically tractable. Also, this has a simplest receiver implementation since the IRS-only and UAV-only transmission links are independent and the selection combining is performed at the destination receiver. For the IRS communication mode, digital-to-analog converter (DAC) and RF chains are not required because IRS acts as a reflective array and has an advantage that the power is not consumed on the RF chains in IRS-assisted communication.

Gaussian noise (AWGN) with zero-mean and power spectral density N_0, R_{SI} denotes the residual SI experienced by the UAV [17], and h_i represents the i-th channel fading where $i \in (u, d)$. The SNR for the i-th link is given as follows:

$$\gamma_i = p_i \kappa_i \, d_i^{-\alpha(\theta_i)} \, X_i, \qquad \forall i \in \{u, d\}, \tag{3.4}$$

where $\kappa_u = \frac{\hat{A}\eta_u^{-1}}{R_{\mathrm{SI}}+N_0}$, $\kappa_d = \frac{\hat{A}\eta_d^{-1}}{N_0}$, and $X_i = |h_i|^2$ follows non-central chi square distribution with mean Ω_i, which is local mean power of i-th Rician fading channel whose probability density function (PDF) is:

$$f_{X_i}(x) = \frac{K_i + 1}{\Omega_i} e^{-K_i - \frac{(K_i+1)x}{\Omega_i}} I_0 \left(2\sqrt{\frac{K_i(K_i+1)x}{\Omega_i}} \right) = \sum_{\ell=0}^{\infty} \frac{b_i(b_i K_i)^{\ell}}{(\ell!)^2} x^{\ell} e^{-b_i x - K_i}, \tag{3.5}$$

in which K_i is the Rician factor in the i-th link and I_0 is a modified Bessel function of the first kind and $b_i = \frac{K_i+1}{\Omega_i}$ [49]. Note that in the UAV-only mode, the IRS absorbs the incoming signals to each element i.e. all the corresponding diodes are switched OFF, and therefore, no information is relayed from IRS to the destination. I call this state as the non-active state of the IRS.

Assuming that the UAV can perform decoding of y_u and then relay the decoded data, using (3.4), the end-to-end SNR Γ_{UAV} from **S** to **D** can be modeled as [58]:

$$\Gamma_{\mathrm{UAV}} = \min\{\gamma_u, \gamma_d\}. \tag{3.6}$$

IRS-only Mode

In this mode, I assume that the UAV does not transmit and the IRS controller adjusts the phase shift of each element intelligently to the optimal value [77, 85]. That is, the IRS maximizes the signal power by optimizing the phase shifts of the impinging signals and each element's functionality as a switch is controlled by switching the diode state between ON and OFF. In this setup, for the sake of symmetry, I consider an odd number of elements, i.e.
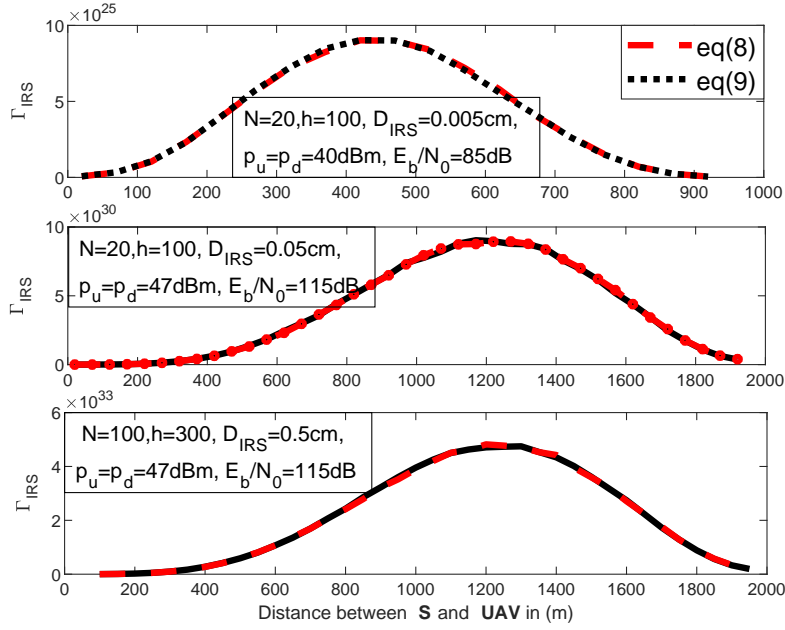
Figure 3.2 Comparison of Eq. (3.8) and its approximation in Eq. (3.9) for different parameters.

$N = 2n + 1$, where n is any arbitrary positive integer. The received signal at destination **D** via k-th IRS element is given by

$$y_{\text{IRS}_k} = \sqrt{\hat{A} p_u \eta_u^{-1} \; d_{u_k}^{-\alpha(\theta_{u_k})}} \; h_{u_k} e^{j(\phi_k)} \sqrt{\hat{A} \eta_d^{-1} \; d_{d_k}^{-\alpha(\theta_{d_k})}} h_{d_k} \; s + w_u,$$

where $k \in \{-n, -n+1, \cdots, 0, 1, \cdots, n\}$. The distance between j-th element to **S** and to **D** can be given as $d_{u_k} = \sqrt{|\mathbf{z}_s - \mathbf{z}_{u_k}|^2 + h^2}$ and $d_{d_k} = \sqrt{|\mathbf{z}_d - \mathbf{z}_{u_k}|^2 + h^2}$, respectively, where $\mathbf{z}_{u_k} = (x_{u_k}, y_{u_k})$ and $x_{u_k} = x_u - kD_{\text{IRS}}$, $y_{u_k} = y_u$, and D_{IRS} denotes the uniform spacing between two consecutive elements on IRS. Note that the $k = 0$-th element is at UAV location $\mathbf{z}_u$. The channel from **S** to k-th IRS element and k-th IRS element to **D** can be given as $h_{u_k} = |h_{u_k}| e^{-j\theta_{u_k}}$ and $h_{d_k} = |h_{d_k}| e^{-j\theta_{d_k}}$, respectively. The end-to-end SNR for IRS-only mode Γ_{IRS} [77] for an IRS with N elements can be given as follows:

$$\Gamma_{\text{IRS}} = V \left(\sum_{k=1}^{N} d_{u_k}^{-\alpha(\theta_{u_k})/2} d_{d_k}^{-\alpha(\theta_{d_k})/2} |h_{u_k}| |h_{d_k}| e^{-j(\theta_{u_k} + \theta_{d_k} - \phi_k)} \right)^2, \tag{3.7}$$

where $V = \hat{A}^2 p_u \eta_u^{-1} \eta_d^{-1} / N_0$. Given the limited size of UAV and the IRS, I assume that

the distance between **S** and k-th IRS element is approximately the same as the distance between **S** and UAV. Similarly, I assume that the distance between **D** and k-th IRS element is approximately the same as the distance between **D** and UAV. That is, $d_{u_k} \approx d_u$, $d_{d_k} \approx d_d$, $\theta_{u_k} \approx \theta_u$, and $\theta_{d_k} \approx \theta_d$. From this point onward, I will use α_u and α_d as $\alpha(\theta_{u_k})$, and $\alpha(\theta_{d_k})$, respectively, for brevity. Now the modified maximum SNR is given as follows:

$$\Gamma_{\text{IRS}} = V d_u^{-\alpha_u} d_d^{-\alpha_d} \left(\sum_{k=1}^{N} |h_{u_k}||h_{d_k}| e^{-j(\theta_{u_k} + \theta_{d_k} - \phi_k)} \right)^2. \tag{3.8}$$

It is evident from (3.8) that the maximum SNR is obtained by taking the channel phases as $\phi_k = \theta_{u_k} + \theta_{d_k}$, $\forall k \in (-n, -n+1, \cdots, n-1, n)$ which maximizes the exponential term to unity because $e^{-j(\theta_{u_k} + \theta_{d_k} - \phi_k)} = 1$ [77]. Subsequently, (3.8) can be simplified as follows:

$$\Gamma_{\text{IRS}} \approx V d_u^{-\alpha_u} d_d^{-\alpha_d} \left(\sum_{k=1}^{N} |h_{u_k}||h_{d_k}| \right)^2. \tag{3.9}$$

Also, [85] showed that a 3-bit phase resolution is practically sufficient to achieve maximum SNR/capacity performance that is achievable when infinite phase resolution is considered. Eq. (3.8) and its approximation in Eq. (3.9) are validated in Fig. 3.2 for different simulation parameters. Note that, the IRS implicitly operates in full-duplex mode (with zero self-interference) [22,82,83] and the incident signals on IRS reflect with minimal delay (typically less than the decoding delay experienced in DF relaying).

Integrated UAV-IRS Mode

Here, both the UAV and the IRS relay the signal transmitted from **S**, and the receiver uses SC to obtain the desired signal. The SNR at the receiver can be formulated as follows:

$$\Gamma_{\text{INT}} = \max\left(\Gamma_{\text{UAV}}, \Gamma_{\text{IRS}} \right) = \max \left\{ \min \left(p_u \kappa_u d_u^{-\alpha_u} X_u, p_d \kappa_d\, d_d^{-\alpha_d}\, X_d \right), V \frac{\left(\sum_{k=1}^{N} |h_{u_k}||h_{d_k}| \right)^2}{d_u^{\alpha_u} d_d^{\alpha_d}} \right\}. \tag{3.10}$$

Note that in both modes, the air to ground distances are very similar; thereby, the channels are highly correlated. Nevertheless, since the distances are not random variables

here, statistical correlation is not considered. The small-scale fading channels in both modes may not necessarily be correlated. In this work, I consider independent fading channels.

3.2.5 Energy Consumption Model

I consider that the UAV hovering time is equal to the time UAV can communicate and can be computed as $T_{hov} = \frac{E_B}{p_{\text{uav}}}$, where E_B is maximum UAV battery capacity and p_{uav} is the power consumption of the UAV. The total power consumption of the considered system includes (i) the power consumed by the UAV for hovering and supporting IRS transmissions (p_{uav}) and data transmission (p_d) in downlink and (ii) the hardware power consumption (p_{bs}) of the ground BS transmitter and receiver as well as (p_u).

UAV Power Consumption (p_{uav})

The total UAV power consumption is the sum of powers consumed by UAV in hovering p_h, circuit power consumption p_c [86], and the power consumed by UAV in the IRS hardware p_{IRS}. That is, the UAV power consumption can be given as $p_{\text{uav}} = p_c + p_{\text{IRS}} + p_h$. where p_h is hovering power consumption of UAV (please see Section 2.3.4 for detail).

Since I consider that the IRS is mounted on a UAV, IRS power consumption is a part of the total UAV power consumption. Note that, IRS is acting as a passive device and does not need any transmission power. The IRS power consumption is written as $p_{\text{IRS}} = N(P_F + \tilde{P}_r(b)) = NP_r(b)$ and N is number of IRS elements, P_F and $\tilde{P}_r(b)$ are power consumption of diode in forward biased mode to operate in ON state [81] and phase resolution power consumption [23], respectively. For instance, the power consumption of finite phase resolution for 6 bits is $\tilde{P}_r(6) = 78\text{mW}$ and for infinite phase resolution is $\tilde{P}_r(\infty) = 45\text{dBm}$ (Fig. 4 of [26]). Therefore, an increase in the resolution and the number of IRS elements increases its hardware power consumption as formulated in [23,26]. Moreover, for an element

to operate in absorbing state the corresponding diode is turned 'OFF' and the IRS element experiences reversed biased power consumption P_R. However, P_R is in the order of micro or nano Watts [87] and therefore it is negligible.

Terrestrial Circuit Power Consumption (p_{bs})

It is the hardware power consumption, i.e. the circuit power consumed by the source and destination ground BSs [88] given as p_{bs}.

Transmission Power Consumption

The transmission power consumption includes transmission power of the source BS in the uplink (p_u) and that of the UAV in the downlink (p_d).

Subsequently, I can define the total ene-to-end power consumption of each transmission mode as $P_{\text{UAV}} = p_u + p_d + C$, $P_{\text{IRS}} = p_u + p_{\text{IRS}} + C$, and $P_{\text{INT}} = p_u + p_d + p_{\text{IRS}} + C$, where $C = p_c + p_h + 2p_{\text{bs}}$. Note that the definition of power consumption here includes terrestrial power consumption unlike Chapter 1. This is because in Chapter one, the major power consumption was coming from the traveling distance of UAV so the hardware power cost was not important. However, the effect of terrestrial power consumption can be ignored by using $p_{\text{bs}} = 0$ in C.

3.3 Performance Characterization of Integrated UAV-IRS Relaying

In this section, I characterize the outage probability O_m, ergodic capacity R_m and energy-efficiency EE_m for each of the modes (i.e. UAV-only, IRS-only, and integrated UAV-IRS modes) for the considered integrated UAV-IRS relaying system. The subscript m denotes

the mode of operation.

3.3.1 UAV-only Mode of Relaying

Conditioned on the distances d_u and d_d, the end-to-end SNR Γ_{UAV} can be given using (3.6). Subsequently, the SNR outage probability can be defined as follows:

$$O_{\text{UAV}} = \mathbb{P}(\Gamma_{\text{UAV}} < \Gamma_0) = \mathbb{P}[\min(\gamma_u, \gamma_d) < \Gamma_0] = 1 - (1 - F_{\gamma_u}(\Gamma_0))(1 - F_{\gamma_d}(\Gamma_0)), \quad (3.11)$$

where $F_{\gamma_u}(\Gamma_0)$ and $F_{\gamma_d}(\Gamma_0)$ represent the CDFs of the SNR received on the channel from **S** to UAV and UAV to **D**, respectively, evaluated at the desired SNR threshold Γ_0. Using (3.4), the i-th link SNR outage can be given as follows:

$$F_{\gamma_i}(\Gamma_0) = \mathbb{P}(\gamma_i \leq \Gamma_0) = \mathbb{P}\left(X_i \leq \Gamma_i' d_i^{-\alpha_i}\right) = F_{X_i}(\Gamma_i' d_i^{-\alpha_i}), \qquad i \in \{u, d\}, \quad (3.12)$$

where $X_i = |h_i|^2$ represents non-central chi square distribution and $\Gamma_i' = \frac{\Gamma_0}{\kappa_i p_i}$. Using the alternate exact expression for PDF in (3.5), the CDF of X_i can be given as follows [49,59,60]:

$$F_{X_i}(x_i) = 1 - \sum_{\ell=0}^{\infty} \sum_{m=0}^{\ell} f_i(m, l) x_i^m e^{-bx_i}, \quad (3.13)$$

where $f_i(m, \ell) = e^{-K_i} \frac{K_i^\ell b_i^m}{\ell! m!}$, $b_i = \frac{K_i + 1}{\Omega_i}$, Ω_i is the mean local power of the Rician channel in the i-th link, and K_i is the Rician factor. Substituting $x_i = \Gamma_i' d_i^{\alpha_i}$ in (3.13), I obtain

$$F_{\gamma_i}(\Gamma_0) = F_{X_i}(\Gamma_i' d_i^{\alpha_i}) = 1 - \sum_{\ell=0}^{\infty} \sum_{m=0}^{\ell} f_i(m, l)(\Gamma_i' d_i^{\alpha_i})^m \exp\left(-b_i \Gamma_i' d_i^{\alpha_i}\right), \qquad i \in (u, d). \quad (3.14)$$

By using (3.14) for $i = u$ and $i = d$ in (3.11), the end-to-end SNR outage O_{UAV} is given as

$$O_{\text{UAV}} = 1 - \sum_{\ell=0}^{\infty} \sum_{m=0}^{\ell} f_u(m, l)(\Gamma_u' d_u^{\alpha_u})^m \exp\left(-b_u \Gamma_u' d_u^{\alpha_u}\right) \sum_{\ell=0}^{\infty} \sum_{m=0}^{\ell} f_d(m, l)(\Gamma_d' d_d^{\alpha_d})^m \exp\left(-b_d \Gamma_d' d_d^{\alpha_d}\right).$$

$$(3.15)$$

Corollary 3. *In scenarios where NLoS components are dominant (i.e. for $K_u = 0$ and $K_d = 0$) than LoS components, the Rician distribution follows Rayleigh distribution. As*

such, the CDF in (3.14) can be expressed as $F_{X_u}(\Gamma'_u d_u^{-\alpha_u}) = 1 - e^{-\Gamma'_u d_u^{-\alpha_u}/\Omega_u}$, $F_{X_d}(\Gamma'_d d_d^{-\alpha_d}) = 1 - e^{-\frac{\Gamma'_d}{\Omega_d} d_d^{\alpha_d}}$. *The end-to-end SNR outage for UAV-only mode of relaying can be simplified as follows:*

$$O_{\text{UAV}}(d_d) = 1 - e^{-\frac{\Gamma'_u}{\Omega_u} d_u^{-\alpha_u} - \frac{\Gamma'_d}{\Omega_d} d_d^{-\alpha_d}}. \tag{3.16}$$

3.3.2 Outage Probability for IRS-only Mode of Relaying

Using (3.9), the end-to-end SNR outage in the IRS-only mode of relaying can be given as:

$$O_{\text{IRS}} = \mathbb{P}\left(\Gamma_{\text{IRS}} \leq \Gamma_0\right) = \mathbb{P}\left(V d_u^{-\alpha_u} d_d^{-\alpha_d} Z^2 \leq \Gamma_0\right) = \mathbb{P}\left(Z^2 \leq t\Gamma_0\right), \tag{3.17}$$

where $Z = \sum_{k=1}^{N} |h_{u_k}||h_{d_k}|$ and $t = \frac{d_u^{\alpha_u} d_d^{\alpha_d}}{V}$. The SNR outage probability can then be derived as follows.

Proposition 6. *The outage probability of IRS-only mode can be given as follows:*

$$O_{\text{IRS}} = \frac{1}{2}\left(\text{erf}\left(\frac{\sqrt{t\Gamma_0} - \sqrt{\lambda}}{\sqrt{2}}\right) + \text{erf}\left(\frac{\sqrt{t\Gamma_0} + \sqrt{\lambda}}{\sqrt{2}}\right)\right), \tag{3.18}$$

where $t = \frac{d_u^{\alpha_u} d_d^{\alpha_d}}{V}$, $\lambda = \frac{1}{2}\frac{\mu_Z^2}{\sigma_Z^2}$, $\mu_z = (N+1)\mathbb{E}[|h_{u_k}||h_{d_k}|]$, *and* $\sigma_Z^2 = (N+1)var(|h_{u_k}||h_{d_k}|)$.

Proof. In general, a meta-surface is made up of a large number of reflecting elements, i.e. $N \gg 1$ and optimal phase is realizable using because $\phi_k = \theta_{u_k} + \theta_{d_k}$ [77]. Therefore, I apply central limit theorem (CLT) on $Z = \sum_{k=1}^{N} |h_{u_k}||h_{d_k}|$, where $|h_{u_k}||h_{d_k}| \; \forall k = 1, 2, \cdots, N$ are identically and independently distributed (i.i.d) random variables with the mean and variance $\mathbb{E}[|h_{u_k}||h_{d_k}|]$ and $var(|h_{u_k}||h_{d_k}|)$, respectively, for $i \in (u, d)$. Subsequently, the distribution of Z will converge to the Gaussian distribution with mean and variance, respectively, given by

$$\mu_z = (N+1)\mathbb{E}[|h_{u_k}||h_{d_k}|] \qquad \text{and} \qquad \sigma_Z^2 = (N+1)var(|h_{u_k}||h_{d_k}|).$$

Note that $|h_{u_k}|$ and $|h_{d_k}|$ are independent, but may not be identically distributed Rician variables. The aforementioned product follows the double-Rician distribution [89] with the

mean and variance given as:

$$\mathbb{E}[|h_{u_k}||h_{d_k}|] = \sigma \frac{\pi}{2} {}_1F_1\left(\frac{-1}{2}; 1; \frac{-\mu_u^2}{2\Omega_u}\right) {}_1F_1\left(\frac{-1}{2}; 1; \frac{-\mu_d^2}{2\Omega_d}\right),$$

and

$$var(|h_{u_k}||h_{d_k}|) = 2^2\sigma^2\left(1 + \frac{\mu_u^2}{2\Omega_u}\right)\left(1 + \frac{\mu_d^2}{2\Omega_d}\right) - \left(\sigma\frac{\pi}{2}\right)^2\left[{}_1F_1\left(\frac{-1}{2}; 1; \frac{-\mu_u^2}{2\Omega_u}\right) {}_1F_1\left(\frac{-1}{2}; 1; \frac{-\mu_d^2}{2\Omega_d}\right)\right]^2,$$

where $\sigma^2 = \Omega_u\Omega_d$ and ${}_1F_1(.)$ is the Confluent Hypergeometric function. Now taking $X = Z^2$, the distribution of X follows the non-central chi square distribution with unity degree of freedom and non-centrality parameter $\lambda = \frac{1}{2}\frac{\mu_Z^2}{\sigma_Z^2}$. Subsequently, the probability density function (PDF) of X is given as:

$$f_X(x) = \frac{1}{2}\left(\frac{x}{\lambda}\right)^{-1/4} e^{-\frac{\lambda+x}{2}} I_{-1/2}\left(\sqrt{\lambda x}\right), \tag{3.19}$$

where I_β is the modified Bessel function of first kind of order β. Fig. 3.3 shows that the PDF of X obtained from simulations converges to non-central chi square variable for $N \geq 20$, as is implied by CLT.

$$O_{\text{IRS}} = \mathbb{P}\left(Z^2 \leq t\Gamma_0\right) = \mathbb{P}\left(-\sqrt{t\Gamma_0} \leq X \leq \sqrt{t\Gamma_0}\right)$$
$$= \int_{x=0}^{t\Gamma_0} \frac{1}{2}\left(\frac{X}{\lambda}\right)^{-1/4} e^{-\frac{\lambda+X}{2}} I_{-1/2}\left(\sqrt{\lambda X}\right) dX. \tag{3.20}$$

$\blacksquare$

For $\mu_u = \mu_d = 0$, the mean and variance of the double Rician variable can be simplified as follows.

Corollary 4. *For $\mu_u = \mu_d = 0$, the double Rician variable converts to double Rayleigh variable. Thus, the mean and variance of the product $|h_{u_k}||h_{d_k}|$ can be simplified as $\mathbb{E}[|h_{u_k}||h_{d_k}|] = \sigma\frac{\pi}{2}$ and $var(|h_{u_k}||h_{d_k}|) = 2^2\sigma^2(1 - \pi^2/16)$ with $\sigma^2 = \Omega_u\Omega_d$ [90], respectively. After applying central limit theorem for Rayleigh fading, I obtain $\mu_z = (N+1)\sigma\frac{\pi}{2}$, $\sigma_Z^2 = (N+1)2^2\sigma^2(1 - \pi^2/16)$.*

85
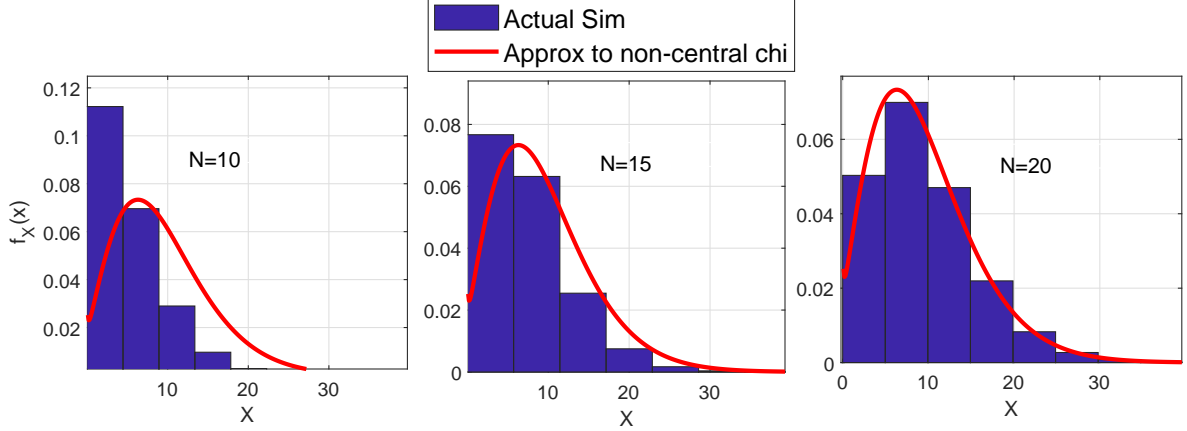
Figure 3.3 Comparison of the exact PDF of X through simulations and the PDF of X when $N \to \infty$ that follows non-central chi-square distribution.

3.3.3 Outage Probability of Integrated UAV-IRS Mode of Relaying

In integrated UAV-IRS mode of relaying, I assume that the receiver applies SC and selects the mode of operation associated to the maximum SNR. This implies additional degree of freedom, however, at the expense of increased resource consumption, since both the UAV and the IRS are actively transmitting to **D**. The outage probability of this mode can thus be derived using (3.10) as follows:

$$O_{\mathrm{INT}} = \Pr\left(\Gamma_{\mathrm{UAV}} \leq \Gamma_0\right) \Pr\left(\Gamma_{\mathrm{IRS}} \leq \Gamma_0\right) = O_{\mathrm{UAV}} O_{\mathrm{IRS}}, \tag{3.21}$$

where O_{UAV} and O_{IRS} are given in Section III.A and III.B, respectively.

3.3.4 Ergodic Capacity R_m and Energy Efficiency EE_m for Mode m

Given mode m, the exact end-to-end ergodic capacity at the receiver can be derived as follows [46]:

$$C_m = \mathbb{E}[B\log_2(1 + \Gamma_m)] = \frac{1}{\ln(2)} \int_{t=0}^{\infty} \frac{\Pr(\Gamma_m > t)}{1 + t} dt = \frac{B}{\ln(2)} \int_{\Gamma_0=0}^{\infty} \frac{1 - O_m}{1 + \Gamma_0} d\Gamma_0, \tag{3.22}$$

where $\Pr\left(\Gamma_m > \Gamma_0\right) = 1 - O_m$ and O_m is derived in (3.15), (3.18), and (3.21) for UAV-only, IRS-only and integrated UAV-IRS modes, respectively. Along the similar lines, using the

definition of energy efficiency EE_m of each mode m (which is defined as the ratio of ergodic capacity to the corresponding power consumption P_m), I can derive the exact end-to-end energy-efficiency as follows:

$$EE_m = \frac{B}{\ln(2)P_m} \int_{\Gamma_0=0}^{\infty} \frac{1-O_m}{1+\Gamma_0} \, d\Gamma_0. \tag{3.23}$$

3.4 Approximate Performance Characterizations for UAV-IRS Relaying

In this section, I first derive a bound on the ergodic capacity R_m and energy efficiency EE_m for each mode of relaying (i.e. UAV-only, IRS-only, and UAV-IRS modes).

UAV-only Mode of Relaying: Applying Jensen's inequality to the ergodic capacity expression, an upper bound on the ergodic capacity (in bps) can be derived as follows:

$$\mathbb{E}\left[\log_2\left(1+\mathrm{SNR_m}\right)\right] \leq \log_2\left(1+\mathbb{E}\left[\mathrm{SNR_m}\right]\right). \tag{3.24}$$

Subsequently, I derive tractable expressions of the ergodic capacity and energy-efficiency in UAV-only mode as shown in the following Proposition.

Proposition 7. *The ergodic capacity R_{UAV} and energy-efficiency EE_{UAV} expressions in UAV-only mode can be given, respectively, as follows:*

$$R_{\mathrm{UAV}} \leq B\log_2\left(1 + \min\left(p_u\kappa_u \, d_u^{-\alpha_u} \ \Omega_u, p_d\kappa_d \, d_d^{-\alpha_d} \ \Omega_d\right)\right), \tag{3.25}$$

$$EE_{\mathrm{UAV}} \approx \frac{B\log_2\left(1 + \min\left(p_u\kappa_u \, d_u^{-\alpha_u} \ \Omega_u, p_d\kappa_d \, d_d^{-\alpha_d} \ \Omega_d\right)\right)}{p_u + p_d + C}. \tag{3.26}$$

Proof. The ergodic capacity R_{UAV} in (3.22) can be bounded as follows:

$$\begin{aligned}
R_{\mathrm{UAV}} &\overset{(a)}{\leq} B\log_2\left(1 + \mathbb{E}\left[\min\left(p_u\kappa_u \, d_u^{-\alpha_u} \ X_u, p_d\kappa_d \, d_d^{-\alpha_d} \ X_d\right)\right]\right) \\
&\overset{(b)}{\approx} B\log_2\left(1 + \min\left(\mathbb{E}\left[p_u\kappa_u \, d_u^{-\alpha_u} \ X_u, p_d\kappa_d \, d_d^{-\alpha_d} \ X_d\right]\right)\right) \\
&\overset{(c)}{=} B\log_2\left(1 + \min\left(p_u\kappa_u \, d_u^{-\alpha_u} \ \mathbb{E}\left[X_u\right], p_d\kappa_d \, d_d^{-\alpha_d} \ \mathbb{E}\left[X_d\right]\right)\right),
\end{aligned} \tag{3.27}$$
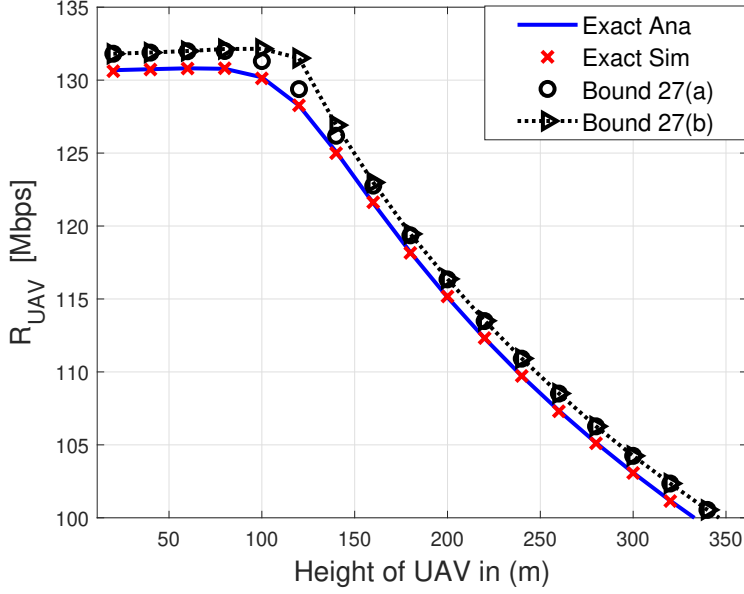
Figure 3.4 The comparison of exact ergodic capacity (via analysis and simulations) to the UAV-only bounds provided in Eq. 3.27(step a) and Eq. (3.27) (step b). Approximation in Eq. (3.27) (step b) is validated by analytically solving Eq. (3.27) (step a).

where X_u and X_d follow non-central chi square distribution. Note that (a) is obtained by using Jensen's inequality [91], (b) is obtained by interchanging $\min(.)$ and $\mathbb{E}(.)$ (validated in Fig. 3.4), (c) follows from non-central chi-square distribution with mean Ω_u and Ω_d, respectively, and results in (3.25). Finally, using ergodic capacity in (3.25), I obtain $\mathrm{EE}_{\mathrm{UAV}}$ in (3.26). ∎

Fig. 3.4 validates the accuracy of our proposed bounds in (3.27) (step a) using Jensen's inequality and (3.27) (step b) using interchange of $\min(\cdot)$ and the expectation operator $\mathbb{E}[\cdot]$ with exact Monte-Carlo simulations. To further justify the approximation in (b), I calculate the expectation of the minimum of two random variables, i.e. $\mathbb{E}[\Gamma_{\mathrm{UAV}}] = \mathbb{E}[\min\left(p_u\kappa_u\,d_u^{-\alpha_u}\,X_u, p_d\kappa_d\,d_d^{-\alpha_d}\,X_d\right)]$ in an exact form. That is, I first determine the PDF of Γ_{UAV}, by taking the derivative of the CDF of Γ_{UAV}. The CDF of Γ_{UAV} can be derived using (3.15), by substituting Γ_u' and Γ_d' and replacing Γ_0 with z. Finally, I calculate $\mathbb{E}[\Gamma_{\mathrm{UAV}}] = \int_{z=0}^{\infty} z f_{\Gamma_{\mathrm{UAV}}}(z)dz$, under the condition that $m_u + m_d$ and $m_u + m_d > 0$ and

$$\left(\frac{b_u d_u^{\alpha_u}}{\kappa_u p_u} + \frac{b_d d_d^{\alpha_d}}{\kappa_d p_d} \right) \geq 0.$$

Corollary 5. *When NLoS components are dominant, the Rician distribution follows Rayleigh distribution, i.e. $\Omega_u = 1$ and $\Omega_d = 1$. The end-to-end $\mathrm{EE}_{\mathrm{UAV}}$ for UAV-only mode in (3.26) can be simplified as follows:*

$$\mathrm{EE}_{\mathrm{UAV}} \approx \frac{B\log_2\left(1 + \min\left(p_u \kappa_u \, d_u^{-\alpha_u}, p_d \kappa_d \, d_d^{-\alpha_d}\right)\right)}{p_u + p_d + C}. \tag{3.28}$$

IRS-only Mode of Relaying: For IRS-only mode, the ergodic capacity and EE expressions are derived in the following.

Proposition 8. *The ergodic capacity expression can be obtained for IRS-only mode as follows:*

$$R_{\mathrm{IRS}} \overset{(a)}{\leq} B\log_2\left(1 + \mathbb{E}\left[V d_u^{-\alpha_u} d_d^{-\alpha_d} X\right]\right) \overset{(b)}{=} B\log_2\left(1 + V d_u^{-\alpha_u} d_d^{-\alpha_d} \left(v + \lambda\right)\right), \tag{3.29}$$

where (a) is obtained using Jensen's inequality and (b) is obtained using $\mathbb{E}[X] = \nu + \lambda$ [92]. Using (3.29) (step b), I bound $\mathrm{EE}_{\mathrm{IRS}}$ as follows:

$$\mathrm{EE}_{\mathrm{IRS}} \approx \frac{B\log_2\left(1 + V d_u^{-\alpha_u} d_d^{-\alpha_d} \left(\nu + \lambda\right)\right)}{P_{\mathrm{IRS}}}. \tag{3.30}$$

Here, I want to highlight that R_{IRS} in (3.30) has the order of $\log_2(N^2)$ for large values of N that is achieved by ignoring the normalization factor from $\mathbb{E}[X]$ as provided in [22, 78].

Integrated UAV-IRS Mode of Relaying: For integrated UAV-IRS mode ($m = \mathrm{INT}$), the ergodic capacity in (3.22) can be formulated as:

$$R_{\mathrm{INT}} = B\mathbb{E}\left[\log_2\left(1 + \max\left(V d_u^{-\alpha_u} d_d^{-\alpha_d} X, \min\left(p_u \kappa_u \, d_u^{-\alpha_u} X_u, p_d \kappa_d \, d_d^{-\alpha_d} X_d\right)\right)\right)\right], \tag{3.31}$$

where X, X_u, and X_d follow non-central chi square distribution representing end-to-end channel fading power in IRS transmission, channel fading power from **S** to UAV and UAV

to $\mathbf{D}$, respectively. After applying SC, the ergodic capacity (3.31) can be approximated as follows:

$$
\begin{aligned}
R_{\text{INT}} &\overset{(a)}{\leq} B\log_2\left(1 + \mathbb{E}\left[\max\left(Vd_u^{-\alpha_u}d_d^{-\alpha_d}X, \min\left(p_u\kappa_u\, d_u^{-\alpha_u}\, X_u, p_d\kappa_d\, d_d^{-\alpha_d}\, X_d\right)\right)\right]\right) \\
&\overset{(b)}{\approx} B\log_2\left(1 + \max\left(Vd_u^{-\alpha_u}d_d^{-\alpha_d}\,\mathbb{E}[X], \mathbb{E}\left[\min\left(\hat{A}p_u\eta_u^{-1}\, d_u^{-\alpha_u}\, X_u, \hat{A}p_d\eta_d^{-1}\, d_d^{-\alpha_d}\, X_d\right)\right]\right)\right) \\
&\overset{(c)}{\approx} B\log_2\left(1 + \max\left(Vd_u^{-\alpha_u}d_d^{-\alpha_d}\,\mathbb{E}[X], \min\left(p_u\kappa_u\, d_u^{-\alpha_u}\,\mathbb{E}[X_u], p_d\kappa_d\, d_d^{-\alpha_d}\,\mathbb{E}[X_d]\right)\right)\right) \\
&\overset{(d)}{=} B\log_2\left(1 + \max\left(Vd_u^{-\alpha_u}d_d^{-\alpha_d}\,(\nu+\lambda), \min\left(p_u\kappa_u\, d_u^{-\alpha_u}\,\Omega_u, p_d\kappa_d\, d_d^{-\alpha_d}\,\Omega_d\right)\right)\right),
\end{aligned}
$$

$$(3.32)$$

where (a) is obtained using Jensen's inequality, (b) and (c) are obtained by interchanging max(.) and min(.) operators with the $\mathbb{E}(.)$ operator, respectively, and (d) is obtained by substituting the mean of X, X_u and X_d with $\nu+\lambda$, Ω_u and Ω_d, respectively. Finally, using (d) I approximate EE_{INT} as follows:

$$
\text{EE}_{\text{INT}} \approx \frac{B\log_2\left(1 + \max\left(Vd_u^{-\alpha_u}d_d^{-\alpha_d}\,(\nu+\lambda), \min\left(p_u\kappa_u\, d_u^{-\alpha_u}\,\Omega_u, p_d\kappa_d\, d_d^{-\alpha_d}\,\Omega_d\right)\right)\right)}{P_{\text{INT}}}. \quad (3.33)
$$

3.5   Optimization of UAV-IRS Relaying

In this section, I consider two optimization problems for maximizing the network energy efficiency and minimizing the network power consumption subject to rate constraints, considering the UAV-only mode and the IRS-only mode of relaying. For the IRS-only mode, I optimize the number of active IRS elements N and height of the IRS surface (i.e. UAV height). For the UAV-only mode, I optimize the UAV height.

3.5.1 IRS-only Mode: Optimizing the Number of IRS Elements

EE Maximization

Using (3.30) where λ is a function of N, i.e. $\lambda = (N+1)\lambda'$, where $\lambda' = \frac{1}{2}\frac{\left(\mathbb{E}[|h_{u_k}||h_{d_k}|]\right)^2}{var(|h_{u_k}||h_{d_k}|)}$ can be taken from (3.18), the EE maximization problem can be formulated as follows:

$$\mathbf{P1}: \max_N \ \mathrm{EE_{IRS}} = \frac{B\log_2\left(1 + Vd_u^{-\alpha_u}d_d^{-\alpha_d}(v+\lambda)\right)}{p_u + NP_r(b) + C}$$

$$\text{s.t. } \mathbf{C1}: N_{\min} \leq N \leq N_{\max},$$

(3.34)

where $N_{\max}$ is the maximum number of IRS elements that can be calculated as a ratio of the size of UAV to the size of one IRS element, $N_{\min}$ is the minimum number of IRS elements that can be deployed at a surface in practical settings and for which the objective function is accurate [refer to Fig. 3.3]. Since λ is directly proportional to N, I reformulate the problem **P1** as follows:

$$\mathbf{P2}: \max_\lambda \ \frac{B\log_2\left(1 + Vd_u^{-\alpha_u}d_d^{-\alpha_d}(v+\lambda)\right)}{p_u + \left(\frac{\lambda-\lambda'}{\lambda'}\right)P_r(b) + C}$$

$$\text{s.t. } \mathbf{C1}: (N_{\min}+1)\lambda' \leq \lambda \leq (N_{\max}+1)\lambda'.$$

(3.35)

The problem P2 is non-convex in general; however, it is in the form of ratio of concave and convex function w.r.t variable λ. Fortunately, due to the structure of the problem, the globally optimal solution can be obtained by applying quadratic transform proposed in [93]. The quadratic transform converts the ratio of concave and convex function to the convex form by introducing an auxiliary variable y. Thus, I optimize the primal variable λ and the auxiliary variable y_j at each iteration j.

The iterative algorithm is guaranteed to converge to the globally optimal solution for the single ratio objective function in **P1** [93]. As such, using Quadratic Transform, the problem

P2 can be reformulated as:

$$\textbf{P3}: \max_{\lambda, y} \; Q(\lambda) = 2y\sqrt{B\log_2\left(1 + Vd_u^{-\alpha_u}d_d^{-\alpha_d}(\,v + \lambda)\right)} - y^2\left(p_u + (\frac{\lambda - \lambda'}{\lambda'})P_r(b) + C\right)$$

s.t. **C1**.

$$(3.36)$$

For a given λ, in each iteration j, y_j^* can be found in closed-form as $y_j^\star = \dfrac{\sqrt{B\log_2\left(1 + Vd_u^{-\alpha_u}d_d^{-\alpha_d}(\,v + \lambda)\right)}}{p_u + (\frac{\lambda-\lambda'}{\lambda'})P_r(b) + C}$.
Now I solve **P3** using **Algorithm 1** for which the convergence to the global optimal solution is proved in [94].

Data: Initialize λ with any arbitrary value, $j = 1$, Maximum Iterations $J_{\max}$, Error
   tolerance ϵ, $Q(\lambda^j)$

Find $y_j^\star$ by solving $Q(\lambda^j)$ and set $j = 2$;

while $|y_{j-1}^\star - y_j^\star| \geq \epsilon$ *and* $j < J_{\max}$ **do**

- Update λ by solving $Q(\lambda^j)$ for fixed $y_{j-1}^\star$ using any convex optimization tool, e.g.
  CVX.

- update $y_j^\star$

- $j = j + 1$.

end

Result: optimal desired solution $N^\star$ is then obtained from $\lambda^\star$ using $N^\star = \lceil\frac{\lambda^\star - \lambda'}{\lambda'}\rceil$
   Algorithm 2: Optimization of Number of IRS Elements in IRS-only Mode

---

Minimization of Power Consumption Under Rate Constraint

The problem can be formulated as:

$$\textbf{P1}: \min_{N} \ p_u + NP_r(b) + C$$

$$\text{s.t. } \textbf{C1}: B\log_2\left(1 + Vd_u^{-\alpha_u}d_d^{-\alpha_d}\left(\,v + (N+1)\lambda'\right)\right) \geq R_0 \tag{3.37}$$

$$\textbf{C2}: N_{\min} \leq N \leq N_{\max}.$$

The objective function in **P1** is convex and monotonically decreasing w.r.t N and the IRS ergodic capacity is monotonically increasing function of N. Therefore, the solution to the optimization problem lies at the boundary of the constraint **C1**, which is given as follows:

$$N^\star = \lceil \frac{1}{\lambda'}\left(\sqrt{\frac{\left(2^{\frac{R_0}{B}} - 1\right)}{V}d_u^{\alpha_u}d_d^{\alpha_d}} - \nu - \lambda'\right)\rceil. \tag{3.38}$$

The generalized optimal solution $N^\star$ is provided by incorporating the bound **C2** as follows:

$$N^\star = \begin{cases} N_{\min} & N^\star \leq N_{\min} \\ N_{\max} & N^\star \geq N_{\max} \\ \lceil \frac{1}{\lambda'}\left(\sqrt{\frac{\left(2^{\frac{R_0}{B}}-1\right)}{V}d_u^{\alpha_u}d_d^{\alpha_d}} - \nu - \lambda'\right)\rceil & \text{otherwise} \end{cases} \tag{3.39}$$

In addition, the optimization problem (3.37) can be solved to optimize the variable p_u given a fixed N. The objective function in **P1** is convex and monotonically increasing w.r.t p_u, whereas the ergodic capacity is monotonically increasing function on p_u. Therefore, the solution to the optimization problem lies at the boundary of the constraint **C1** and the optimal solution for $p_u^\star$ can be given as follows:

$$p_u^\star = \frac{2^{\frac{R_0}{B}} - 1}{\hat{A}^2\eta_u^{-1}\eta_d^{-1}}\frac{d_u^{\alpha_u}d_d^{\alpha_d}N_0}{v + (N+1)\lambda'}. \tag{3.40}$$

3.5.2   IRS-only Mode: Height Optimization

Here, I maximize EE_{IRS} which is equivalent to maximizing the ergodic capacity R_{IRS} in (3.29) w.r.t height, since the IRS-only power consumption does not depend on height. The problem can then be formulated as follows:

$$\mathbf{P1} : \max_{h} \ R_{IRS} = B \log_2 \left(1 + V d_u^{-\alpha_u} d_d^{-\alpha_d} (\nu + \lambda) \right)$$

$$\text{s.t. } \mathbf{C1} : h_{\min} \leq h \leq h_{\max}.$$

$$(3.41)$$

In (3.41), I note that only numerator $d_u^{-\alpha_u} d_d^{-\alpha_d}$ is a function of h. Therefore, to reformulate **P1** I ignore the logarithm and constants in the objective function of **P2** as shown below:

$$\mathbf{P2} : \max_{h} \ d_u^{-\alpha_u} d_d^{-\alpha_d}$$

$$\text{s.t. } \mathbf{C1}.$$

$$(3.42)$$

The optimal h obtained from **P2** can be substituted back in (3.41) to obtain maximum EE_{IRS}. By combining (3.1), (3.2), and (3.3), I note that $\alpha_u = \frac{q_u}{1 + \varsigma_u \exp\left(-g_u \arctan\left(\frac{h}{\hat{z}_u}\right)\right)} + v_u$ is a function of h, where $\varsigma_u = e_u e^{g_u e_u}$ and $\hat{z}_u = |\mathbf{z_u} - \mathbf{z_s}|$. Similarly, $\alpha_d = \frac{q_d}{1 + \varsigma_d \exp\left(-g_d \arctan\left(\frac{h}{\hat{z}_d}\right)\right)} + v_d$ is a function of h, where $\varsigma_d = e_d e^{g_d e_d}$ and $\hat{z}_d = |\mathbf{z_u} - \mathbf{z_d}|$. Clearly, the reformulated objective function in **P2** depends on α_i, $i \in \{u, d\}$ which is non-linear due to tangent inverse function of variable h in the denominator of α_u and α_d.

Subsequently, I apply the following transformations to simplify the problem:

- Taking the log of objective function of **P2**, the transformed objective function becomes

$$-\alpha_u \log (d_u) - \alpha_d \log (d_d) = -\frac{\alpha_u}{2} \log \left(\hat{z}_u^2 + h^2 \right) - \frac{\alpha_d}{2} \log \left(\hat{z}_d^2 + h^2 \right).$$

- Using $\arctan(x) \approx \frac{3x}{1 + 2\sqrt{1 + x^2}}$, I get

$$\alpha_i \approx q_i \left(1 + \varsigma_i \exp \left(\frac{-3 g_i h}{\hat{z}_i + 2\sqrt{\hat{z}_i^2 + h^2}} \right) \right)^{-1} + v_i, \quad i \in \{u, d\}$$

.

94

- Applying the second-order Taylor series approximation $\exp(-x) \approx 1 - x + \frac{x^2}{2}$ and some algebraic manipulations, I obtain

$$\alpha_i(h) \approx \frac{A_i \left(\hat{z}_i + 2\sqrt{\hat{z}_i^2 + h^2}\right)^2 - B_i h \left(\hat{z}_i + 2\sqrt{\hat{z}_i^2 + h^2}\right) + C_i h^2}{(1 + \varsigma_i)\left(\hat{z}_i + 2\sqrt{\hat{z}_i^2 + h^2}\right)^2 - B_i' h \left(\hat{z}_i + 2\sqrt{\hat{z}_i^2 + h^2}\right) + C_i' h^2}, \quad i \in \{u, d\}, \quad (3.43)$$

where $A_i = q_i + v_i(1 + \varsigma_i)$, $B_i = 3\varsigma_i v_i g_i$, $C_i = 9/2 v_i \varsigma_i g_i^2$, $B_i' = 3\varsigma_i g_i$, $C_i' = 9/2\varsigma_i g_i^2$. Following the above approximations, the original (3.42) is given as follows:

$$\textbf{P3} : \max_h \; -\frac{1}{2}\alpha_u(h) \log\left(\hat{z}_u^2 + h^2\right) - \frac{1}{2}\alpha_d(h) \log\left(\hat{z}_d^2 + h^2\right)$$

$$\text{s.t. } \textbf{C1}. \tag{3.44}$$

The mismatch in the optimal solutions is found to be negligibly small and is mainly due to the considered `arctan` and Taylor approximations, as validated in Fig. 3.5. Clearly, the problem in **P3** is in the form of sum of ratio of concave-convex function as is shown in the following Proposition. This guarantees that an optimal solution for **P3** can be obtained.

Proposition 9. *The $-\frac{1}{2}\alpha_i(h) \log\left(\hat{z}_i^2 + h^2\right)$ is ratio of concave-convex when*

$$\hat{z}_i > 10 \quad \& \quad \begin{cases} \hat{z}_i \geq h^{5/4} \left(\frac{78A_i + 14C_i}{11B_i}\right)^{1/4} & \hat{z}_i \geq h \\ h \geq \hat{z}_i \left(\frac{(78A_i\hat{z}_i + B_i + 14C_i\hat{z}_i)}{12B_i}\right)^{1/4} & h > \hat{z}_i \end{cases}. \tag{3.45}$$

Proof. See **Appendix**. ∎

Now, **P3** can be reformulated as follows:

$$\textbf{P3}' : \min_h \; \frac{1}{2}\alpha_u(h) \log\left(\hat{z}_u^2 + h^2\right) + \frac{1}{2}\alpha_d(h) \log\left(\hat{z}_d^2 + h^2\right)$$

$$\text{s.t. } \textbf{C1}. \tag{3.46}$$

Note that **P3** is a multiple-ratio fractional programming problem and can be solved by applying the quadratic transform method, as applied earlier. For the sake of simplicity, I

rewrite **P3′** by using a general notation i, where $i = (u, d)$, as follows [93]:

$$\textbf{P4}: \min_h \sum_{i=(u,d)} \frac{O_i(h)}{T_i(h)}$$

(3.47)

$$\text{s.t. } \textbf{C1},$$

where $O_i(h) = 0.5 \log(h^2 + \hat{z}_i^2) \times \left(A_i \left(\hat{z}_i + 2\sqrt{\hat{z}_i^2 + h^2} \right)^2 - B_i h(\hat{z}_i + 2\sqrt{\hat{z}_i^2 + h^2}) + C_i h^2 \right)$ and $T_i(h) = (1 + \varsigma_i)(\hat{z}_i + 2\sqrt{\hat{z}_i^2 + h^2})^2 - B_i' h \left(\hat{z}_i + 2\sqrt{\hat{z}_i^2 + h^2} \right) + C_i' h^2$. Note that, the complexity arises due to the negative sign in $O_i(h)$ that makes $\sqrt{O_i(h)}$ a complex number. To avoid the negative sign, I rewrite the problem **P3′** in the minimization form of sum of ratio of convex functions[3]. Thus, after introducing auxiliary variable y_i and applying quadratic transform, **P5** becomes a convex problem in h [93]:

$$\textbf{P5}: \min_{h, y_i} \sum_{i=(u,d)} 2y_i \sqrt{O_i(h)} - y_i^2 \left(T_i(h) \right)$$

(3.48)

$$\text{s.t. } \textbf{C1} \ \& \ y_i \in \mathbb{R}.$$

For a given h, the optimal y_i can thus be obtained in closed form as $y_i^\star = \frac{\sqrt{O_i(h)}}{T_i(h)}$. The solution to the problem **P5** with $Q_i(h) = 2y_i \sqrt{O_i(h)} - y_i^2 T_i(h)$ in the objective function can be obtained using **Algorithm 2** that iteratively solves the minimization problem for h.

Fig. 3.5 shows the comparison between the optimal solution obtained from solving Eq. (3.42), Eq. (3.44) and Eq. (3.48), which are represented by blue, black, and red curves, respectively. Evidently, due to the considered approximations of (3.42), the optimal solution obtained by solving (3.42) has a slight mismatch with the exact solution obtained by solving (3.44) using exhaustive search method. However, it is noteworthy that the transformation of (3.44) into (3.48) does not impact the optimality of the solution.

---

[3]Note that this alternation is particularly applicable to the case where quadratic transform **P5** is convex, not otherwise.
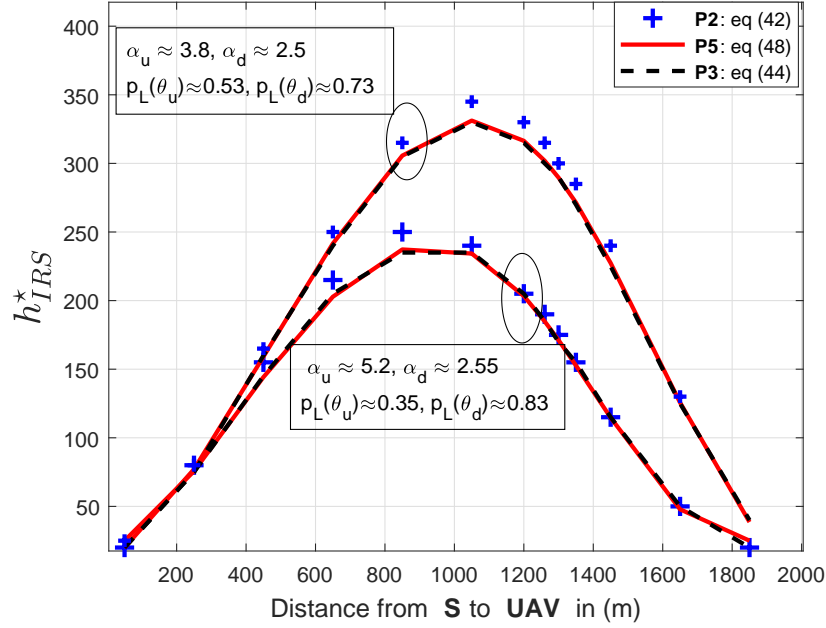
Figure 3.5 The validation of solution obtained from Eq. (3.42), Eq. (3.44) and Eq. (3.48) for IRS-only mode for $E_b/N_0 = 130$dB, $N = 30$, $p_u = p_d = 50$dBm for different environment parameters, where (E_b represents per symbol energy).

Data: Initialize h, $j = 1$, Maximum Iterations $J_{\max}$, Error tolerance ϵ, $Q_i(h^j)$

Find $y^\star_{i,j}$ by solving $Q_i(h^j)$ and set $j = 2$;

while $|y^\star_{i,j+1} - y^\star_{i,j}| \geq \epsilon$, *and* $j < J_{\max}$ **do**

- Update h by solving $Q_i(h^j)$ for fixed $y^\star_{i,j-1}$ using any convex optimization tool e.g, CVX.

- update $y^\star_{i,j}$ $\forall i \in (u, d)$

- $j = j + 1$.

end

Result: optimal desired solution $h^\star$

Algorithm 3: Height Optimization in IRS-only Mode

3.5.3 UAV-only Mode: Height Optimization

I formulate the height optimization problem using (3.26), which is an approximation of (3.23), for the UAV-only mode as follows:

$$\textbf{P1} : \max_{h} \ R_{\text{UAV}} = B\log_2 \left(1 + \min \left(p_u \kappa_u \ d_u^{-\alpha_u} \ \Omega_u, p_d \kappa_d \ d_d^{-\alpha_d} \ \Omega_d \right) \right)$$

$$\textbf{C1} : h_{\min} \leq h \leq h_{\max}.$$

(3.49)

Using an approach similar to that followed for (3.42), i.e. by ignoring logarithm and constant scaling function and considering only the terms that are function of h, I recast the optimization problem **P1** as follows:

$$\textbf{P2} : \max_{h} \ \min \left(I_u d_u^{-\alpha_u}, I_d d_d^{-\alpha_d} \right) = \max_{h} \ \min_{i} \ I_i d_i^{-\alpha_i}$$

$$\text{s.t. } \textbf{C1},$$

(3.50)

where $I_u = p_u \kappa_u \ \Omega_u$, $I_d = p_d \kappa_d \ \Omega_d$, $d_u = \sqrt{\hat{z}_u^2 + h^2}$, $d_d = \sqrt{\hat{z}_d^2 + h^2}$, and α_i for $i \in (u, d)$ is given in (3.43). where d_u and d_d are convex functions of h, whereas α_u and α_d are ratio of concave and convex functions of h. Clearly, this problem is non-convex and cannot be solved directly. Therefore, I take log of **P2** which is an increasing function and does not effect the solution of the original objective. **P2** can then be reformulated as follows:

$$\textbf{P3} : \max_{h} \ \min_{i} \ \left(\log(I_i) - \alpha_i(h) \log \left(h^2 + \hat{z}_i^2 \right) \right)$$

$$\text{s.t. } \textbf{C1},$$

(3.51)

where α_i is a ratio of concave and convex functions of h, thus the objective function is a ratio of two functions of h for $i \in (u, d)$. However, the ratio in the objective may not necessarily be concave-convex form. However, under a certain condition, I am able to prove that the objective in **P3** is indeed a concave-convex form in terms of h). This guarantees that an optimal solution for P3 can be obtained under specific condition. By substituting $\alpha_i(h)$ and simplifying the objective of **P3**, I get

$$O_i(h) = G_1 \left(\hat{z}_i + 2\sqrt{\hat{z}_i^2 + h^2} \right)^2 - G_2 h \left(\hat{z}_i + 2\sqrt{\hat{z}_i^2 + h^2} \right) + G_3 h^2,$$

(3.52)

where $G_1 = 2\log(I_i)(1+\varsigma_i) - A_i \log(h^2 + \hat{z}_i^2)$, $G_2 = 2\log(I_i)B_i' - B_i \log(h^2 + \hat{z}_i^2)$, and $G_3 = 2\log(I_i)C_i' - C_i \log(h^2 + \hat{z}_i^2)$ and denominator function is $T_i(h) = (1+\varsigma_i)\left(\hat{z}_i + 2\sqrt{\hat{z}_i^2 + h^2}\right)^2 - B_i' h\left(\hat{z}_i + 2\sqrt{\hat{z}_i^2 + h^2}\right) + C_i' h^2$. It is straight-forward to see that $T_i(h)$ is convex. In the following Proposition, I show that $O_i(h)$ in (3.52) is a concave function of h under a certain condition.

Proposition 10. *The $O_i(h)$ in (3.52) is concave when*

$$2G_1 \hat{z}_i^3 + (4G_1 + G_3)(\hat{z}_i^2 + h^2)^{3/2} - G_2 h(3\hat{z}_i^2 + 2h^2) \tag{3.53}$$

is negative. Using the identity that norm is less than the sum of the sides, i.e. $\sqrt{h^2 + \hat{z}_i^2} \leq h + \hat{z}_i$, I obtain an upper bound on (3.53) after simplification as

$$(6G_1 + G_3)\hat{z}_i^3 + (4G_1 + G_3 - 2G_2)h^3 + (4G_1 + G_3)\hat{z}_i h^2 + (4G_1 + G_3 - 3G_2)\hat{z}_i^2 h. \tag{3.54}$$

Now, for the cases $\hat{z}_i \geq h$ and $\hat{z}_i < h$ and replacing $\min(h, \hat{z}_i)$ with $\max(h, \hat{z}_i)$ (which gives an upper bound), I obtain the simplified condition for concavity after substituting G_1, G_2 and G_3 as

$$\log(I_i) \leq \frac{(18A_i - 5B_i + 4C_i)}{36(1 + \varsigma_i) - 10B_i' + 8C_i'} \log\left(h^2 + \hat{z}_i^2\right).$$

Now to solve **P3**, I apply quadratic transformation available for max-min problem [93]. The steps include recasting the problem as maximization of z under the constraint on h such that $z \leq \frac{O_i(h)}{R_i(h)}$. The constraint $z \leq \frac{O_i(h)}{R_i(h)}$ can be written using quadratic transform as $2y_i\sqrt{O_i(h)} - y_i^2 T_i(h) \geq z$, $\forall i \in (u, d)$ with y_i as an auxiliary optimization variable. The equivalent problem of (3.51) can then be given as:

$$\mathbf{P3'} : \max_{h, y_i, z} z \tag{3.55}$$
$$\mathbf{C1} \quad \& \quad \mathbf{C2} : 2y_i\sqrt{O_i(h)} - y_i^2 T_i(h) \geq z, \quad \forall i.$$

The above problem cannot be solved since $O_i(h)$ is a negative valued function. Therefore, I

change z to $-z \geq -\frac{O_i(h)}{T_i(h)}$ to make $O_i(h)$ positive inside the square root in **C2** as follows:

$$\mathbf{P4} : \max_{h,y_i,z} \; -z$$
$$\mathbf{C1} \quad \& \quad \mathbf{C2} : 2y_i\sqrt{-O_i(h)} - y_i^2 T_i(h) \geq -z, \;\; \forall i \tag{3.56}$$

Now changing maximization over h to minimization over h, the above problem can be reformulated as:

$$\mathbf{P5} : \min_{h,y_i,z} \; z$$
$$\mathbf{C1} \quad \& \quad \mathbf{C2}, \tag{3.57}$$

which is solved using **Algorithm 3** for UAV only mode.

Data: Initialize h, z, $j = 1$, Maximum Iterations $J_{\max}$, Error tolerance ϵ, $O_i(h^j)$ &

  $R_i(h^j)$

Find $y_{i,j}^\star$ by solving $y_{i,j}^\star = \frac{\sqrt{O_i(h_j)}}{R_i(h_j)}$ and set $j = 2$;

while $|y_{i,j+1}^\star - y_{i,j}^\star| \geq \epsilon$, *and* $j \leq J_{\max}$ **do**

  - Update h and z by solving (3.57) for fixed $y_{i,j-1}^\star$ using any convex optimization tool, e.g. CVX.

  - update $y_{i,j}^\star \;\; \forall i \in (u, d)$

  - $j = j + 1$.

end

Result: optimal desired solution $h^\star$
Algorithm 4: Height Optimization in UAV-only Mode

Fig. 3.6 shows the comparison between the optimal solution obtained from solving (3.49), (3.51), and (3.57), which are represented by blue, black, and red curves, respectively. Clearly, due to the considered approximations the optimal solution obtained by solving (3.51) has a slight mismatch with the exact solution obtained by solving (3.49) using an exhaustive
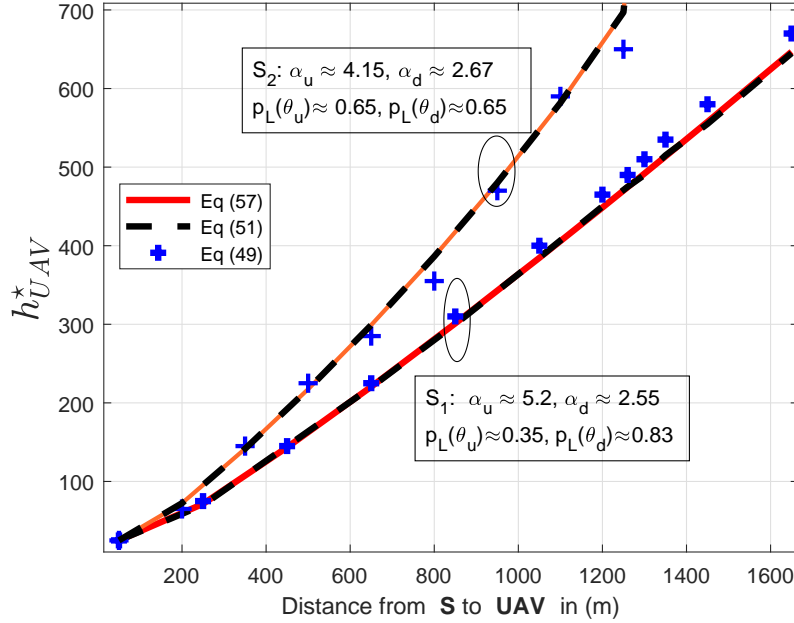
Figure 3.6 The validation of solution obtained from Eq. (3.49), Eq. (3.51) and Eq. (3.57) for UAV-only mode for $E_b/N_0 = 122$dB, $R_{SI} = 5$dB, $p_u = 56$dBm, $p_d = 45$dBm. For given parameters $I_i < 10^{10} \ \forall i \in (u,d)$ assures the concavity of $O_i(h)$.

search. However, it is noteworthy that the transformation of (3.51) into (3.57) does not impact the optimality of the solution.

3.5.4 Mode Selection

In this section, I derive the probabilities of selecting modes (UAV-only, IRS-only, integrated UAV-IRS) to maximize the energy efficiency. However, first I would like to clarify that the denominator (i.e. power consumption) of energy efficiency in integrated UAV-IRS mode will always be higher than the power consumption in UAV-only and IRS-only modes. The reason is that the power consumption of the integrated UAV-IRS mode (the sum of the power consumption of UAV-only and IRS-only modes) is always higher than the power consumption of the UAV-only and IRS-only modes. Furthermore, the numerator which is ergodic capacity in (3.31) chooses between the maximum SNR of either IRS-only mode or UAV-only mode.

As such, the integrated UAV-IRS mode (which is optimal when the objective is to maximize the rate) is not selected when the objective is to maximize energy efficiency. Therefore, the mode selection is essentially performed between UAV-only and IRS-only modes. In what follows, I derive the mode selection probabilities given the instantaneous fading channels and devise a criterion to select how many active IRS elements are needed to maximize energy efficiency in IRS-only mode. I use the proposed criterion for mode selection and obtain optimal heights to maximize the overall energy efficiency of the integrated UAV-IRS system.

The probability of selecting IRS-only mode can be formulated as follows:

$$\mathbb{P}_{\text{IRS}} = \Pr\left(\Gamma_{\text{IRS}} \geq \frac{\Gamma_{\text{UAV}} \text{P}_{\text{IRS}}}{\text{P}_{\text{UAV}}}\right) = 1 - \Pr\left(\Gamma_{\text{IRS}} < \frac{\Gamma_{\text{UAV}} \text{P}_{\text{IRS}}}{\text{P}_{\text{UAV}}}\right). \tag{3.58}$$

Conditioned on Γ_{UAV}, the probability in (3.58) can be derived as follows:

$$\mathbb{P}_{\text{IRS}} = \mathbb{E}_{\Gamma_{\text{UAV}}}\left[1 - F_{\Gamma_{\text{IRS}}}\left(\frac{\Gamma_{\text{UAV}} P_{IRS}}{P_{\text{UAV}}}\right)\right] \stackrel{(a)}{=} 1 - \int_0^\infty F_{\Gamma_{\text{IRS}}}\left(\frac{\Gamma_{\text{UAV}} P_{IRS}}{P_{\text{UAV}}}\right) f_{\Gamma_{\text{UAV}}}(z) dz, \tag{3.59}$$

where $F_{\Gamma_{\text{IRS}}}\left(\frac{\Gamma_{\text{UAV}} P_{\text{IRS}}}{P_{\text{UAV}}}\right)$ is obtained by replacing Γ_0 with $\frac{\Gamma_{\text{UAV}} P_{\text{IRS}}}{P_{\text{UAV}}}$ in (3.17). The density function of Γ_{UAV} in (3.6) is obtained by using order statistics and differentiating (3.11) as $f_{\Gamma_{\text{UAV}}}(z) = (1 - F_{X_u}(z))f_{X_d}(z) + (1 - F_{X_d}(z))f_{X_u}(z)$, where $f_{X_i}(z)$ and $F_{X_i}(z)$ are given in (3.5) and (3.14), respectively. Subsequently, the probability of UAV-only mode selection can be given as $\mathbb{P}_{\text{UAV}} = 1 - \mathbb{P}_{\text{IRS}}$.

Now, to maximize the energy efficiency at an arbitrary height, I design the following mode selection criterion based on the average SNR[4] to select the IRS-only mode, i.e.

$$\mathbb{E}[\Gamma_{\text{IRS}}] \geq \frac{\mathbb{E}[\Gamma_{\text{UAV}}] P_{\text{IRS}}}{P_{\text{UAV}}}.$$

$$N > \frac{(p_u - P_r(b) + C)\min\left(p_u\kappa_u d_u^{-\alpha_u}\Omega_u, p_d\kappa_d d_d^{-\alpha_d}\Omega_d\right) - \nu(p_u + p_d + C)V d_u^{-\alpha_u} d_d^{-\alpha_d}}{\lambda'(p_u + p_d + C)\left(V d_u^{-\alpha_u} d_d^{-\alpha_d}\right) - P_r(b)\min\left(p_u\kappa_u d_u^{-\alpha_u}\Omega_u, p_d\kappa_d d_d^{-\alpha_d}\Omega_d\right)} - 1 = N_{\text{th}}.$$

$$\tag{3.60}$$

That is, the number of IRS elements should be greater than N_{th} to enable the IRS-only mode. Another way to maximize the energy efficiency is to calculate $\frac{\mathbb{E}[\Gamma_{IRS}]}{P_{\text{IRS}}}$ and $\frac{\mathbb{E}[\Gamma_{UAV}]}{P_{\text{UAV}}}$ with their

---

[4]Generally, the instantaneous CSI may not be available at the receiver.

optimal heights calculated in Section V.B (**Algorithm 2**) and Section V.C (**Algorithm 3**), respectively. Then choose the mode and optimal height corresponding to whichever term becomes the maximum.

Remark: For mode selection based on the power consumption, the integrated UAV-IRS mode will never be selected due to its higher power consumption compared to the UAV-only and IRS-only modes. Furthermore, the IRS-only mode will be selected when $N \leq \frac{p_d}{P_r(b)}$ and vice versa for the UAV-only mode. Similarly, for the SNR-based mode selection, then integrated UAV-IRS mode will always be selected as it chooses the maximum SNR of the IRS-only and UAV-only modes.

3.6 Numerical Results and Discussion

In this section, I verify the accuracy of our derived expressions and obtain insights related to the number of IRS elements and the optimal height of UAV for different communication modes. Unless stated otherwise, the simulation parameters are: $D = 2000$m, $B = 5$MHz, $H = 550$m, $p_u = p_d = 49$dBm, $\eta_u = \eta_d = 0.002$, $\Gamma_0 = 20$dB, $q_u = q_d = -1.7$, $v_u = v_d = 3.05$, $w_u = w_d = 15$dB, $z_u = z_d = 5$, Ω_i, $R_{\text{SI}} = 6$dB, $D_{\text{IRS}} = 0.5$cm, $P_F = 1$mW, and $E_b/N_0 = 50$dB.

Fig. 3.7 compares the outage probability and ergodic capacity w.r.t the number of IRS elements for the UAV-only, IRS-only and integrated UAV-IRS modes. Clearly, the UAV-only mode is independent of N. However, as N increases, the IRS-only mode and the integrated UAV-IRS mode minimize the outage probability and maximize the capacity due to enhanced IRS transmission link. For larger values of N, the IRS-only transmissions become strong and the opportunistic selection between the UAV-only and IRS-only modes improves the performance of integrated UAV-IRS mode. As expected, the integrated UAV-IRS mode outperforms the IRS-only and UAV-only mode for all N in terms of outage and
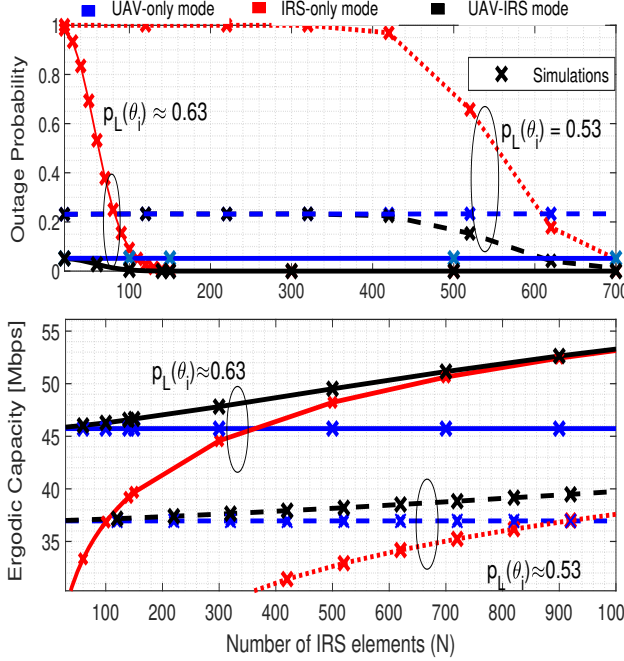
Figure 3.7 Performance comparison of outage probability, and ergodic capacity for IRS-only, UAV-only and integrated UAV-IRS mode for $P_r(b) = 15 \times 10^{-2}$W and $d = 1250$m.
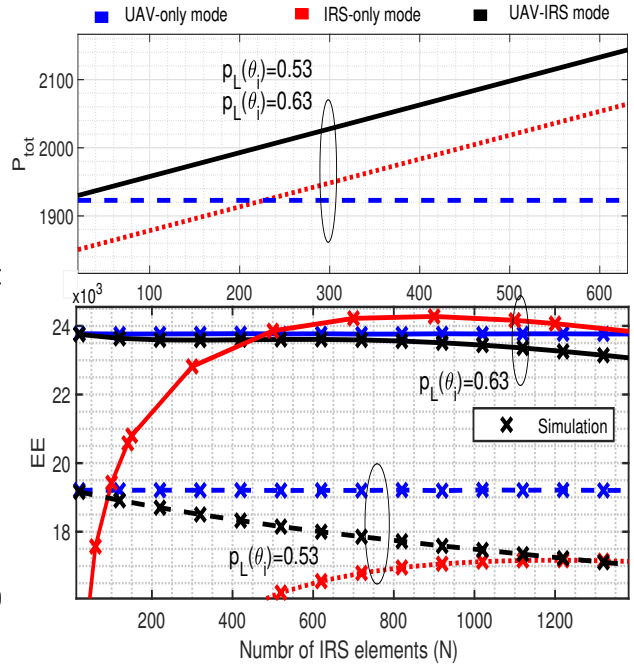
Figure 3.8 Performance comparison of power consumption, and energy-efficiency for IRS-only, UAV-only and integrated UAV-IRS mode for $P_r(b) = 15 \times 10^{-2}$W and $d = 1250$m.

ergodic capacity. An interesting observation is that the lower LoS probability worsens the performance of all schemes. That is, a higher value of N is needed to minimize the outage and maximize the transmission capacity for scenarios with lower LoS.

Fig. 3.8 compares power consumption and energy-efficiency w.r.t the number of IRS elements for the UAV-only, IRS-only, and integrated UAV-IRS modes. Clearly, the power consumption and energy efficiency of UAV-only mode do not depend on N. However, for the IRS-only mode, the power consumption increases with N with the slope given by the power consumption per IRS element $P_r(b)$. Note that the power consumption does not change with the LoS probability; therefore, the reduction in energy efficiency with the decrease in LoS probability is only due to the reduction in transmission capacity. Furthermore, the energy efficiency first increases up to a certain value of N, because the capacity is dominant than
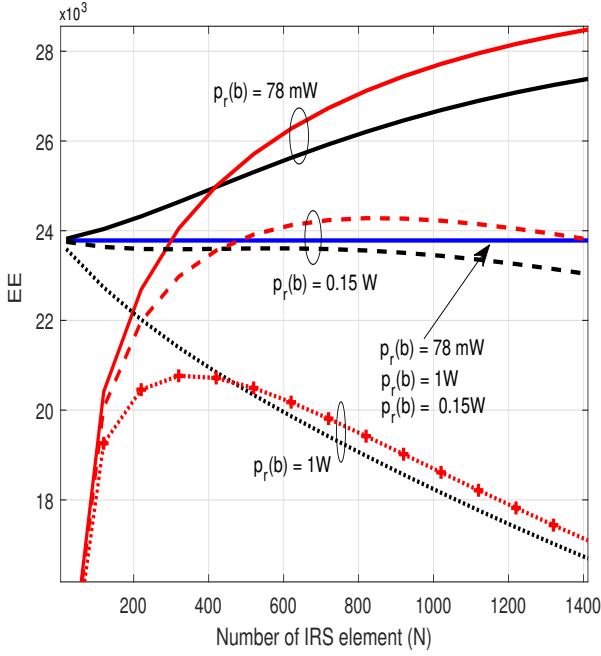
Figure 3.9 Energy-efficiency EE w.r.t numbr of IRS elements N for different different bit resolution power consumption $P_r(b)$ for $d = 1250$m.
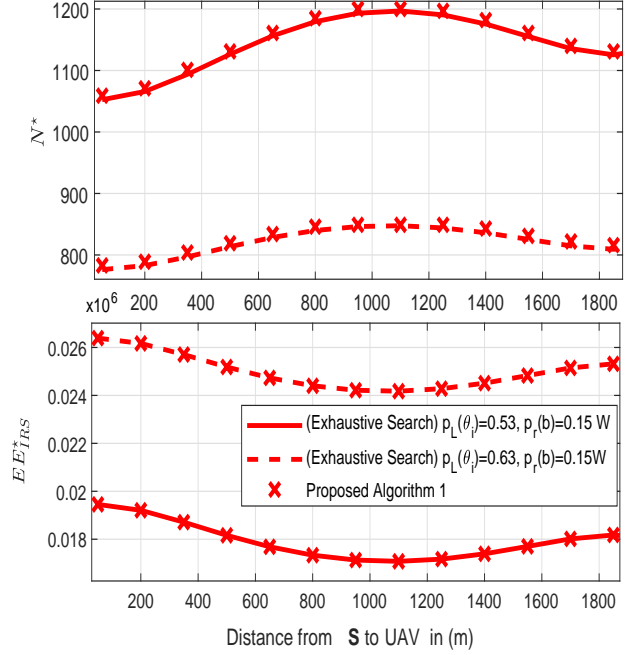
Figure 3.10 Optimal number of IRS elements and the optimal $EE^\star_{\text{IRS}}$ comparison for different source to UAV distance provided in Fig. 3.7 and Fig. 3.8 for $p_r(b) = 15 \times 10^{-2} W$.

power consumption in this regime. Later, for larger values of N, the power consumption becomes dominant and thus the reduction in energy efficiency is evident. Finally, it is intuitive to see that the power consumption of the integrated UAV-IRS mode is higher than the other modes; therefore, an efficient mode selection mechanism is important.

Fig. 3.9 shows the effect of power consumption of bit resolution $P_r(b)$ on the energy efficiency of the three communication modes. It is clear that the UAV-only mode is independent of $P_r(b)$. However, the IRS-only and integrated UAV-IRS modes show that an optimal number of IRS elements exists which increases with the reduction in $P_r(b)$. In particular, for smaller values of $P_r(b)$, the EE continues to increase for a wider range of N, because the increase in N does not significantly increase the power consumption, whereas the capacity keeps increasing. For higher values of $P_r(b)$, the power consumption of IRS elements becomes

105

more dominant than the impact of IRS elements on the ergodic capacity. As such, after a specific value of N, a decreasing energy-efficiency trend can be observed. Clearly, for very high values of $P_r(b)$, minimizing IRS elements is necessary to maximize energy efficiency. Similar trends are observed for EE in integrated UAV-IRS mode with lower gain than the IRS-only mode, because this mode consumes more power then the IRS-only and UAV-only modes.
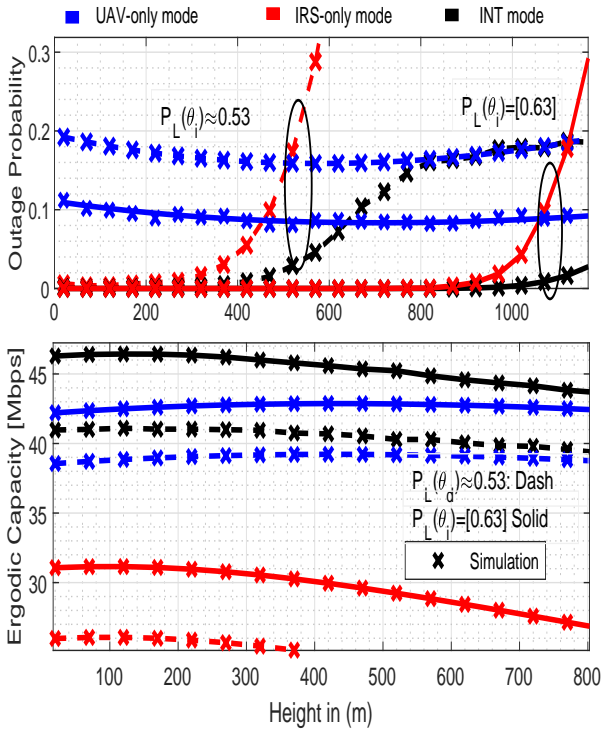
Figure 3.11 Performance comparison of outage probability and ergodic capacity for IRS-only, UAV-only and integrated UAV-IRS mode for $d = 1250$ m, $N = 260$, $P_r(b) = 35 \times 10^{-3}$ W, w.r.t height of UAV.
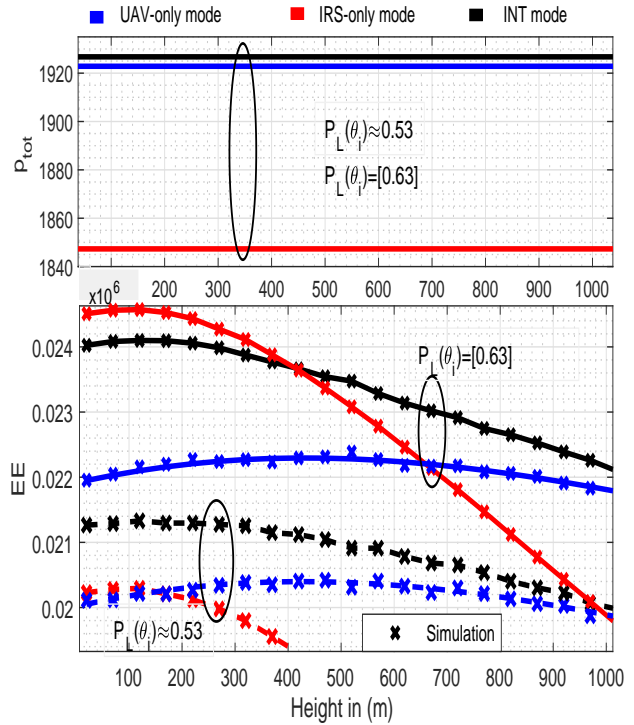
Figure 3.12 Performance comparison of power consumption and energy efficiency for IRS-only, UAV-only and integrated UAV-IRS mode for $d = 1250$ m, $N = 260$, $P_r(b) = 35 \times 10^{-3}$W w.r.t height of UAV.

Fig. 3.10 shows the optimal number of IRS elements $N^\star$ (obtained using **Algorithm 1**) continues to increase as a function of the distance between the source and UAV. However, the corresponding values of optimum energy efficiencies continue to decrease with the increasing distance between the source and UAV. On the other hand, when the distance from
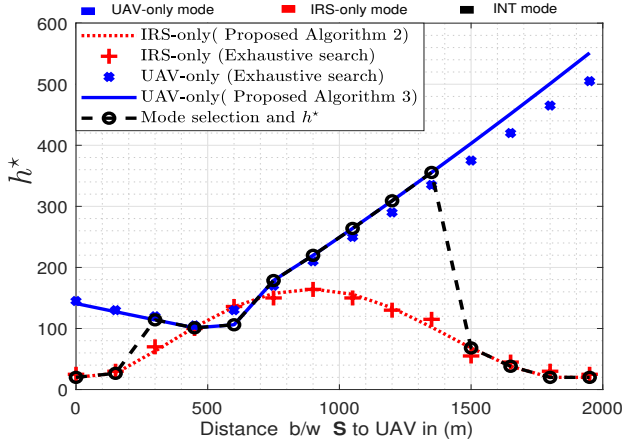
Figure 3.13 Optimal UAV height for different source to UAV distance for $N = 260$, $P_r(b) = 15 \times 10^{-3}$ W.
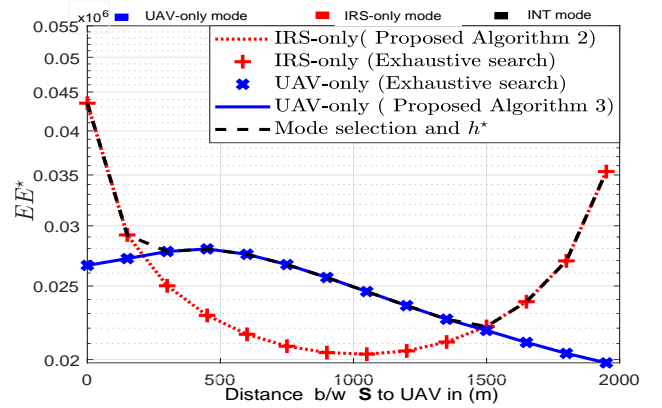
Figure 3.14 Optimal EE for different source to UAV distance for $N = 260$, $P_r(b) = 15 \times 10^{-3}$ W.

the source to UAV decreases, higher values of optimum energy-efficiency can be achieved with less number of IRS elements. This trend is also true when the distance from UAV to destination decreases. The proposed optimal solution (shown by marker) matches well with the optimal solutions obtained by an exhaustive search. Furthermore, it is noted that a low LoS probability $p_L(\theta_i) = 0.53$ requires more IRS elements for optimal function while the maximum energy-efficiency values obtained are still low. On the other hand, when $p_L(\theta_i) = 0.63$, a smaller number of IRS elements provide higher optimum energy efficiency values. In summary, I can conclude that if bit resolution power is very small, then using maximum number of IRS elements is optimal, whereas when the bit resolution power is significantly large, then using small number of IRS elements is optimal.

Fig. 3.11 shows variations in outage probability and ergodic capacity with the height of the UAV considering the UAV-only, IRS-only, and integrated UAV-IRS modes. I note that the optimal height varies depending on the selected communication mode. For weak LoS, I have a higher outage probability in general. However, I note that for weak LoS $P_L(\theta_i) \approx 0.53$, the UAV-only mode outperforms the IRS-only mode for $h \geq 500$m, and as expected, the integrated mode performs better than both modes. However, for strong LoS,

107

the IRS-only mode performs better than the UAV-only mode for a wide range of heights for the outage probability. Also, significant energy efficiency gains can be seen with IRS-only mode compared to UAV-only mode in Fig. 3.12.

Fig. 3.12 depicts power consumption and energy efficiency performance with respect to height. The power consumption is independent of the LoS probability and height of UAV. The energy-efficiency in strong LoS $P_L(\theta_i) = [0.65\ 0.75]$ outperforms the EE in weak LoS $P_L(\theta_i) = 0.5$. For weak LoS, EE_{IRS} is the least energy-efficient. However, for strong LoS, the IRS-only mode becomes the most energy-efficient mode for a wide range of UAV altitudes, since the IRS only mode power consumption is much lower than the other communication modes (i.e. small $P_r(b)$ and N).

Fig. 3.13 compares the optimal heights for different distances between source and UAV. This figure shows that the height calculated from the proposed **Algorithms 2** and **3** matches well with the exact optimal height obtained from exhaustive search. The performance of analytical mode selection criterion and its corresponding optimal height can also be seen. This shows that for the distance between source and UAV in [300 1300] m, the UAV-only mode is optimal, whereas when the UAV is close to the destination or the source the IRS-only mode is optimal. Hence, the optimal height switches to IRS-only height. The same trend is also observed from Figure 3.14 which represents the optimal energy efficiency vs distance between **S** and UAV and follows the same trend as in Fig. 3.13.

3.7 Conclusion

I have analyzed the end-to-end performance in terms of SNR outage probability, ergodic capacity, and energy efficiency for an integrated UAV-IRS relaying system that can operate in three different modes, namely, IRS-only mode, UAV-only mode and integrated UAV-IRS mode. For the IRS-only mode, I have optimized the number of IRS elements and UAV

height, whereas I have optimized the UAV height for the UAV-only mode. I have observed that the optimal height varies based on the selected transmission mode. I have also provided an analytical criterion for optimal height and mode selection in terms of energy efficiency. The extension of analysis and optimization of integrated UAV-IRS system with correlated fading channels is a potential future research work.

Chapter Four

Stochastic Geometry Analysis of IRS-Assisted Downlink Cellular Networks

This chapter proposed IRS-assisted downlink cellular network scheme. Then the system model of the proposed scheme is presented followed by the major performance analysis of coverage probability, spectral efficiency and EE of both IRS-assisted user and direct user. Validation of the analysis is provided with the monte-Carlo simulations followed by numerical insights. Lastly, summary of observations is provided.

4.1   Introduction

Intelligent reflecting surfaces (IRSs) are considered as a key enabling technology for the sixth generation (6G) wireless communications systems. IRSs enable a smart manipulation of the wireless propagation environment [22, 95]. Each IRS consists of many antenna elements (a.k.a IRS elements) [23] and each IRS element is controlled via a controller that assists each IRS element to steer the incident signal into the desired direction [24].

Also, with the advances in the wireless technology and extravagant demand of higher data rate to millions of indoor/outdoor devices, it has become inevitable to utilize the resources wisely to enable massive connectivity. In this context, IRSs operate as a low cost solution to extend the communication range and to provide service to more users. In order to achieve this goal, the transmissions can happen in three modes, i.e., (i) *Joint Transmission:* in which a user receives the IRS signals combined with the direct signal from the base-stations (BSs), (ii) *IRS-only Transmission:* in which a user receives only IRS transmissions and the direct transmissions get blocked, and (iii) *Direct Transmission:* in which a user is served only through direct transmissions.

It is noteworthy that combining the signals coming from the direct and indirect IRS-assisted path may suffer from incoherent multi-path delays and it may necessitate sophisticated synchronization, detection, and co-phasing techniques resulting in complex hardware/software design. Furthermore, the impact of IRS transmissions is generally more understandable in the absence of direct link; therefore, it is crucial to investigate the significance of IRS-only transmissions without direct links. Similarly, the fact that the direct transmissions from BSs may be impacted by the presence of IRSs, it is important to study the performance of direct transmissions in a large-scale IRS-assisted network comprehensively. Also, the analysis of users with joint transmissions has already been done in [96, 97] and is thus currently beyond the scope of this chapter. In this chapter, I develop a novel framework to analyze the performance of various types of transmissions in a multi-BS, multi-IRS network.

4.1.1 Background Work

To date, there have been a number of research works that considered the performance analysis of IRS-assisted communication systems assuming a single IRS, single source and destination [77, 97–103]. For instance, the authors in [77] applied the central limit theorem

(CLT) to derive the approximate symbol error probability expressions under independent Rayleigh fading channels. In [98], the authors derived the approximate outage probability, symbol error rate, and upper and lower bounds on ergodic capacity by applying CLT and assuming uncorrelated Rayleigh fading channels. Later, [99] derived the average bit error rate, capacity, and outage probability with Rayleigh fading. In [100], the exact outage probability, symbol error rate, and ergodic capacity expressions under Rayleigh fading were derived. In [101] and [102], using moment generating function (MGF)-based approach, the exact outage probability was derived considering *Nakagami-m* and generalized fading channels, respectively. The direct link transmission was ignored in [77, 98, 99, 101]; however [102] considered both the direct and IRS-assisted transmissions. In [97], the authors derived the outage probability and ergodic capacity expressions considering IRS link modeled with Rician fading and direct channel modeled as Rayleigh fading. The joint direct and IRS-assisted transmission was considered.

All of the aforementioned research works were limited to single IRS, single source, and single destination under varying fading channels. That is, the impact of interference is ignored and the IRS is deployed at a fixed location. Furthermore, the analyses assume optimal phase-shifts and apply CLT, which simplifies the cascaded signal model substantially. Recently, in [103], using moment matching method, the authors derived the outage probability and capacity expressions under correlated Rayleigh fading channel while considering arbitrary phase shifts. This work considered both the direct and IRS-assisted links; however, again the framework was limited to a single IRS, single source, and single destination. Another work is [104] where multi-pair D2D network is considered with a single IRS and the authors derive average achievable rate expressions assuming arbitrary phase-shifts. However, the authors considered approximating the signal and interference power with their respective statistical averages.

Another series of research works considered multiple IRSs, single source, and single

destination [105–107]. In [105], the authors derived the outage probability considering Rayleigh fading with the direct transmission blocked. The transmission is conducted by only one IRS that provides the maximum SNR. Instead of applying CLT, the authors proposed Generalized-K approximation. In [106], the authors applied CLT to derive the outage probability and rate considering Nakagami-m fading. Both the direct and indirect transmissions were considered. Similarly, in [107], the authors derived the outage probability by approximating the end-to-end IRS-assisted channel with the log-normal and gamma distribution.

The aforementioned research works ignored interference from IRSs, assumed a single BS, and ideal phase shifts were assumed. Recently, a couple of research works considered a realistic multi-IRS set-up with multiple BSs [96, 108]. In [108], the authors derived the average achievable rate of the IRS-assisted multi-BS network and derived the Laplace Transform (LT) of the aggregate interference from all BSs and IRSs. However, the interference from all BSs to a specific IRS is replaced by its average value. The resulting rate expressions require four-fold integral evaluations. Another relevant research work is [96] where the authors derived the coverage probability expressions considering joint direct and IRS transmission. The signal power is approximated with the Gamma distribution and approximated the interference from all IRS with the mean IRS interference and considering only users with joint direct and IRS-assisted transmissions. Both of the aforementioned works [96, 108] assumed optimal phase-shifts in the desired signal and interference which makes the application of CLT possible.

4.1.2   Contribution and Organization

in this chapter, I develop a comprehensive framework to analyze the coverage probability and rate of various types of users (e.g., users performing direct transmissions and indirect IRS-assisted transmissions) in a realistic large-scale multi-BS, multi-IRS network. The pro-

posed framework can capture the impact of arbitrary phase-shifts on the received signal power as well as the aggregate interference from all IRSs on users that are served by direct transmissions from BS or IRS-assisted transmissions. More specifically, I have the following main contributions:

- For IRS-assisted downlink transmissions, I approximate the desired signal power from the nearest IRS as a sum of scaled generalized gamma (GG) random variables whose parameters are a function of the IRS phase shifts. Then, I derive the novel LT expression and validate its accuracy considering both the optimized and randomized phase-shifts of the IRS.

- I approximate the aggregate interference from multiple IRSs in a multiple BS scenario as the sum of normal random variables. Then, I derive the LT of the aggregate interference from all IRSs. The derived expressions can be customized for both types of users, i.e., those served by direct BS transmissions and those served by IRS-assisted transmissions.

- Based on the LT expressions, I characterize the coverage probability, ergodic capacity, and energy-efficiency of both the IRS-assisted users and direct users.

- Finally, I derive the overall coverage probability, ergodic capacity, and energy efficiency based on the fraction of direct and indirect IRS-assisted users in the network. This fraction is derived as a function of the **(i)** deployment intensity of IRSs as well as **(ii)** blockage probability of direct transmission links.

- The analytical results are validated by Monte-Carlo simulations. Numerical results extract useful insights related to the impact of IRS interference on IRS-assisted as well as direct transmissions in a large-scale network as a function of the number of IRS elements, intensity of IRSs and BSs, and the transmit power of BSs.

114

Note that stochastic geometry analyses of wireless systems follow more or less similar methodologies; however, the novelty of a stochastic geometry framework comes from the novelty in system set-up, modeling of channel, interference, and the corresponding random variables and their statistics such as PDF or LT expressions. Nonetheless, our provided expressions expressions are tractable, novel, and can be implemented in any standard software such as Matlab and Mathematica to gain insights and optimize network parameters in a large-scale network model without running lengthy Monte-Carlo simulations.

The remainder of the chapter is organized as follows. Section 4.2 describes the system model and assumptions and the methodology of analysis. I characterize the statistics of the received signal power, aggregate interference and the corresponding LT of users supported by IRS in Section 4.3 and Section 4.4, respectively. The coverage probability, ergodic capacity and energy efficiency of users supported by IRS transmissions and users supported by direct transmission, also the overall coverage of the network and achievable data rate is provided in Section 4.5. Then, in Section 4.6, I present selected numerical results followed by conclusions in Section 4.7. A list of the major notations is presented in **Table 4.1**.

4.2   System Model and Assumptions

In this section, I present the network, transmission, signal and interference models for users who are served by direct BS transmissions and those served by IRS-assisted transmissions, and also our methodology for large-scale analysis of the system.

4.2.1   Network Deployment and Transmission Model

I consider a two-tier downlink cellular network consisting of IRS surfaces, BSs, and users. The locations of the BSs follow a two-dimensional(2D) homogeneous Poisson Point Process (PPP) denoted as Φ_B with intensity λ_B, whereas the locations of the IRSs follow Binomial

Point Process (BPP) in which M IRSs are distributed in a finite region $\mathcal{A} \subset \mathbb{R}^2$. I consider $\mathcal{A} = \mathbf{b}(\mathbf{o}, R)$ is a disc of radius R centered at origin $\mathbf{o} = (0,0)$ [109]. For simplicity, I refer to $\lambda_R = \frac{M}{\pi R^2}$ as the IRS intensity throughout the chapter. I assume that the IRSs are deployed at a fixed height H_R and are equipped with N elements each, whereas all the BSs have a fixed height H_B. I assume that there are two different types of users in the considered multi-BS and multi-IRS network, i.e.,

- *Direct users:* who are served by direct BS transmissions, and

- *IRS-assisted users:* who are served by indirect IRS-assisted transmissions.

The typical user who is deployed at origin would reflect the performance of any user within the coverage region without loss of generality. The Slivnyak's theorem [110, 111] states that adding a user to the PPP at any location, such as the origin or at a fixed distance from the origin, do not change the statistical behaviour. The user anywhere has an identical statistical behavior to the origin [112] therefore, the boundary effect will not exist. I also consider $\mathcal{A}$ IRS-assisted users and $1 - \mathcal{A}$ direct users in the system. For direct transmission from the BS, the typical user is associated to the nearest BS. In the indirect IRS-assisted transmission mode, the user associates to the nearest IRS, and then, that nearest IRS associates to the nearest BS.

I assume that an IRS can relay information from only one BS to only one user at a predefined time/frequency resource to maintain orthogonality. I consider that the *direct* communication (i.e., BS to the typical user) and *indirect* IRS-assisted communication (i.e., BS to IRS and IRS to the typical user) share different frequency spectrum such that a BS can serve both the direct and indirect IRS-assisted users. Now let us assume that F_1 and F_2 is the frequency of direct user and IRS-assisted user, respectively. Overall, there exist four types of transmissions. (i) IRS-assisted transmission on F_2, (ii) direct transmission on F_1, (iii) Interference due to direct transmissions at F_1 and the interference due to reflection
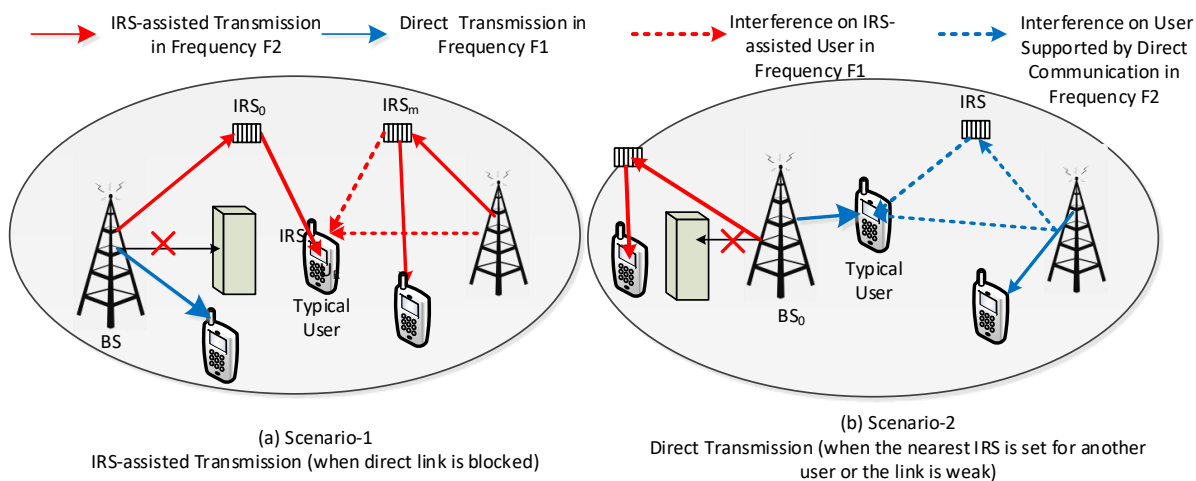
Figure 4.1 System model for direct and IRS-assisted communication in multi-IRS and multi-BS setup: (a) Scenario 1: when the user is connected with a BS through nearest IRS and the direct link to the nearest BS is blocked, and (b) Scenario 2: when the user is connected with a nearest BS in the presence a weak IRS link.

transmissions from IRSs at F_1, and (iv) Interference due to IRS-assisted transmissions at F_2 and the interference due to direct transmissions from BSs at F_2 as shown in Fig. 1.

I assume that an IRS can relay information from only one BS to only one user at a predefined time/frequency resource to maintain orthogonality. I consider that the *direct* communication (i.e., BS to the typical user) and *indirect* IRS-assisted communication (i.e., BS to IRS and IRS to the typical user) share different frequency spectrum such that a BS can serve both the direct and indirect IRS-assisted users.

Table 4.1 Chapter 4: Summary of the main symbols and their definitions

Notation	Description
R	Coverage radius
N	Number of IRS elements
M	Total number of IRSs

Table 4.1 – *Continued from previous page*

Notation	Description
λ_B	BS intensity
Φ_B	PPP for BSs
H_B, H_R	BS height, IRS height
α	Path-loss exponent
BS_j	j-th interfering BS to the typical user in direct mode
BS_0	Nearest BS to the typical user in direct mode
ℓ_j	Direct distance of BS_j in 2D
d_j	Direct distance of BS_j in 3D
ℓ_0	Direct distance of nearest BS_0 in 2D
d_0	Direct distance of BS_j in 3D
h_j	Fading channel between typical user and BS_j
h_0	Fading channel between typical user and BS_0
$\hat{p}_t, p_t$	Transmission power of BSs in direct and IRS-assisted mode
IRS_{m_n}	The n-th element of interfering IRS m
IRS_{0_n}	The n-th element of nearest IRS_0 to user
$\lvert g_{0,m_n} \rvert, \phi_{0,m_n}$	Fading magnitude and phase from the user to the IRS_{m_n}
r_{0,m_n}	Distance of the user to the IRS_{m_n}
$\lvert f_{m_n,j} \rvert, \psi_{m_n,j}$	Fading magnitude and phase from IRS_{m_n} to BS_j
$t_{m_n,j}$	Distance from IRS_{m_n} to BS_j
Θ_{m_n}	Phase shift of IRS_{m_n}
Θ_{0_n}	Phase shift of IRS_{0_n}
$\lvert g_{0,0_n} \rvert, \phi_{0,0_n}$	Fading magnitude and phase from the user to the IRS_{0_n}
$r_{0,0_n}$	Distance of the user to the IRS_{0_n}

118

Table 4.1 – *Continued from previous page*

Notation	Description
$\|f_{0_n,j}\|, \psi_{0_n,j}$	Fading magnitude and phase from IRS_{0_n} to BS_j
$t_{0_n,j}$	Distance from IRS_{0_n} to BS_j
I_B	Aggregate interference from all BSs in IRS-assisted mode
I_R	Aggregate interference from all IRS in IRS-assisted mode
$\hat{I}_B$	Aggregate interference from all BSs in direct mode
$\hat{I}_R$	Aggregate interference from all IRS in direct mode
S_{D_0}	Received signal power from BS_0
S_{R_0}	Received signal power from IRS_0
C_D	Coverage probability in the direct transmission mode
C_{ID}	Coverage probability in the IRS-assisted mode
γ_D	Direct mode SINR
γ_{ID}	Direct mode SINR
τ	SINR threshold
$\mathcal{A}$	Fraction of users assisted by IRS
$X_G(\kappa, \zeta)$	Gamma RV and parameters
$X_{GG}(a, d, p)$	Generalized gamma RV and parameters
R_D	Rate achieved in direct mode
R_{ID}	Rate achieved in indirect mode
t_j	Approximation of $t_{m,j}$
N_0	Noise power spectral density
$p_{\text{BS}}, p_{\text{U}}$	Static power consumption of BS and user
p_{IRS}	IRS power consumption
$p_{\text{ID}}, p_{\text{D}}$	Total system power consumption per user in indirect and direct mode

Table 4.1 – *Continued from previous page*

Notation	Description
$\mathcal{A}$	Fraction of user associated with IRS-assisted ID communication
β	Reference channel power gain on free space path loss at 1-meter distance

4.2.2 Signal and Interference Models (IRS-Assisted Users)

Desired Signal Power

4.2.3 Signal and Interference Models (IRS-Assisted Users)

Desired Signal Power

The signal power received at the typical user from the nearest IRS (IRS$_0$) is given as [104,113]:

$$S_{R_0} = p_t \; |\hat{\mathbf{g}}_{0,0}^H \Theta_0 \; \hat{\mathbf{f}}_{0,j}|^2 = p_t |\sum_{n=1}^{N} r_{0,0_n}^{-\alpha/2} t_{0_n,j}^{-\alpha/2} f_{0_n,j} g_{0,0_n} e^{j\theta_{0_n}}|^2, \tag{4.1}$$

where p_t is the transmission power of the BSs in IRS-assisted mode, $g_{0,0_n} = |g_{0,0_n}|e^{-j\phi_{0,0_n}}$ is the Rayleigh fading channel gain from the typical user to the n-th element of IRS$_0$, thus $\hat{g}_{0,0_n} = \beta \left(r_{0,0_n}\right)^{-\alpha/2} g_{0,0_n}$, where $\alpha \geq 2$ represents the path-loss exponent, $\beta = \left(\frac{4\pi f_c}{c}\right)^{-2}$ is the channel power gain on free-space path-loss model at a reference distance of one meter, f_c is carrier frequency, c represents the speed of light, and $\hat{\mathbf{g}}_{0,0} \in \mathbb{C}^{1 \times N}$, where $r_{0,0_n} = \sqrt{\ell_{0_n}^2 + H_R^2}$ represents the distance from the n-th element of the IRS$_0$ to the typical user. Note that $|g_{0,0_n}|$ and $\phi_{0,0_n}$ represent the magnitude and phase component of the fading channel from the n-th element of IRS$_0$ to the typical receiver. Similarly, $f_{0_n,j} = |f_{0_n,j}|e^{-j\psi_{0_n,j}}$ is the fading channel gain from the n-th element of IRS$_0$ to j-th BS, thus $\hat{f}_{0_n,j} = \beta \left(t_{0_n,j}\right)^{-\alpha/2} f_{0_n,j}$ and

$\hat{\mathbf{f}}_{0,j} \in \mathbb{C}^{N \times 1}$, where

$$t_{0_n,j} = \sqrt{r_{0,0_n}^2 + d_j^2 - 2r_{0,0_n}d_j \cos(\angle t_{0_n,j})}$$

represents the distance from the n-th element of IRS_0 to the typical user, where $\angle t_{0_n,j}$ denotes the angle opposite to $t_{0_n,j}$. Note that $|f_{0_n,j}|$ and $\psi_{0_n,j}$ represent the magnitude and phase component of the fading channel from j-th BS to n-th element of IRS_0. Finally, Θ_0 denotes the phase shift of the IRS_0 and $\Theta_0 = \text{diag}\{e^{j\theta_{0_1}}, e^{j\theta_{0_2}}, \cdots, e^{j\theta_{0_N}}\}$.

Interference Power

The interference at a typical user in the IRS-assisted mode is composed of two parts (i) interference from the BSs, and (ii) interference from the IRSs. The aggregate interference from all the BSs (excluding the nearest BS) is given as follows:

$$I_B = \sum_{j \in \Phi_B \backslash 0} p_t \beta^2 |h_j|^2 d_j^{-\alpha} = \sum_{j \in \Phi_B \backslash 0} p_t \beta^2 |h_j|^2 (\ell_j^2 + H_B^2)^{-\alpha/2}, \tag{4.2}$$

On the other hand, the aggregate interference from the IRSs can be modeled as follows:

$$I_R = \sum_{j \in \Phi_B} \sum_{m=1}^{M \backslash 0} p_t \ |\hat{\mathbf{g}}_{0,m}^H \Theta_m \ \hat{\mathbf{f}}_{m,j}|^2 = \sum_{j \in \Phi_B} \sum_{m=1}^{M \backslash 0} p_t |\sum_{n=1}^{N} r_{0,m_n}^{-\alpha/2} t_{m_n,j}^{-\alpha/2} f_{m_n,j} g_{0,m_n} e^{j\theta_{m_n}}|^2, \tag{4.3}$$

where $g_{0,m_n} = |g_{0,m_n}|e^{-j\phi_{0,m_n}}$ is the fading channel gain from the typical user to the n-th element of IRS m, thus $\hat{g}_{0,m_n} = \beta (r_{0,m_n})^{-\alpha/2} g_{0,m_n}$ and $\hat{\mathbf{g}}_{0,m} \in \mathbb{C}^{1 \times N}$, where $r_{0,m_n} = \sqrt{\ell_{m_n}^2 + H_R^2}$ represents the distance from n-th element of m-th IRS to the typical user. Note that $|g_{0,m_n}|$ and ϕ_{0,m_n} represent the magnitude and phase component of the fading channel from n-th element of m-th IRS to the typical receiver. Similarly, $f_{m_n,j} = |f_{m_n,j}|e^{-j\psi_{m_n,j}}$ is the fading channel gain from the n-th element of IRS m to j-th BS, thus $\hat{f}_{m_n,j} = \beta (t_{m_n,j})^{-\alpha/2} f_{m_n,j}$ and $\hat{\mathbf{f}}_{m,j} \in \mathbb{C}^{N \times 1}$, where $t_{m_n,j} = \sqrt{r_{0,m_n}^2 + d_j^2 - 2r_{0,m_n}d_j \cos(\angle t_{m_n,j})}$ represents the distance from n-th element of m-th IRS to the typical user where $\angle t_{m_n,j}$ denotes the angle opposite to $t_{m_n,j}$. Note that $|f_{m_n,j}|$ and $\psi_{m_n,j}$ represent the magnitude and phase component of the fading channel from j-th BS to n-th element of m-th IRS. Finally, Θ_m denotes the phase shift of the IRS and $\Theta_m = \text{diag}\{e^{j\theta_{m_1}}, e^{j\theta_{m_2}}, \cdots, e^{j\theta_{m_N}}\}$.

4.2.4 Signal and Interference Models (Direct Mode)

Desired Signal Power

The signal power from the desired BS to the typical user is:

$$S_{D_0} = \hat{p}_t \beta^2 |h_0|^2 d_0^{-\alpha} = \hat{p}_t \beta^2 |h_0|^2 (\ell_0^2 + H_B^2)^{-\alpha/2}, \qquad (4.4)$$

where $\hat{p}_t$ is the transmission power of the BSs in direct mode, h_0 and d_0 are the small scale fading channel and the distance between the typical user to the nearest BS, respectively.

Interference Power

The interference at a typical user in the direct mode is composed of two parts (i) interference from the BSs, and (ii) interference from the IRSs. The aggregate interference from the BSs (excluding the desired BS) is given as follows:

$$\hat{I}_B = \sum_{j \in \Phi_B \backslash 0} \hat{p}_t \beta^2 |h_j|^2 d_j^{-\alpha} = \sum_{j \in \Phi_B \backslash 0} \hat{p}_t \beta^2 |h_j|^2 (\ell_j^2 + H_B^2)^{-\alpha/2}, \qquad (4.5)$$

where h_j and d_j are the small scale fading channel and the distance between the typical user to the nearest BS, respectively. On the other hand, the aggregate interference from all IRSs can be modeled as follows:

$$\hat{I}_R = \sum_{j \in \Phi_B} \sum_{m=1}^{M} \hat{p}_t \, |\hat{\mathbf{g}}_{0,m}^H \Theta_m \, \hat{\mathbf{f}}_{m,j}|^2 = \sum_{j \in \Phi_B} \sum_{m=1}^{M} \hat{p}_t |\sum_{n=1}^{N} r_{0,m_n}^{-\alpha/2} t_{m_n,j}^{-\alpha/2} f_{m_n,j} g_{0,m_n} e^{j\theta_{m_n}}|^2. \qquad (4.6)$$

4.2.5 Power Consumption Model

I consider the transmission power of IRS-assisted mode and direct mode is p_t and $\hat{p}_t$. respectively. The IRS is acting as a passive device and does not have any additional transmission power consumption. However, the IRS power consumption is required for the IRS operation and is associated with the number of IRS elements and the phase resolution [23] as

mentioned in chapter 2. Therefore, hardware power consumption increases with an increase in resolution and the number of IRS elements as provided in [23, 26]. The system power consumption per user in the IRS-assisted indirect mode p_{ID} is given as $p_{\text{ID}} = U + p_t + p_{\text{IRS}}$, whereas the power consumption of direct mode $\hat{p}_{\text{D}}$ is given as $\hat{p}_{\text{D}} = U + \hat{p}_t$. Here U denotes the sum of static power consumption of a BS and a user.

4.2.6 Methodology of Analysis

To derive the coverage probability of different types of users in a large-scale IRS-assisted network, our methodology is as follows:

- (**IRS-assisted User**) Model the received signal power S_{R_0} as a sum of scaled generalized gamma random variables and then derive the LT of S_{R_0} (**Section III**).

- (**IRS-assisted User**) Derive the LT of the aggregate interference observed at a typical IRS-assisted user from all BSs, i.e., LT of I_{B}. Then, I model the aggregate interference observed at a typical IRS-assisted user from all IRSs as sum of normal random variables and derive its corresponding LT, i.e., LT of I_{R} (**Section IV**).

- Then, apply Gil-Pelaez inversion to obtain C_{ID} conditioned on the distance $r_{0,0}$[1].

- (**Direct User**) Derive the LT of $\hat{I}_{\text{B}}$ and $\hat{I}_{\text{R}}$, i.e., $\mathcal{L}_{\hat{I}_{\text{B}}}(s)$ and $\mathcal{L}_{\hat{I}_{\text{R}}}(s)$, respectively, and obtain C_{D} conditioned on distance d_0.

- Derive the ergodic capacity using Hamdi's lemma [47] and energy-efficiency of typical IRS-assisted user and direct user.

---

[1]I approximate $r_{0,0_n} \approx r_{0,0}$ since the distance between the typical user and different elements of the nearest IRS is almost the same, i.e., the distance between IRS elements is negligible compared to the distance between the nearest IRS and the typical user. Similarly $t_{0_n,j} \approx t_{0,j}$, $r_{0,m_n} \approx r_{0,m}$, and $t_{m_n,j} \approx t_{m,j}$.

4.3 Statistics of the Received Signal Power (IRS-assisted Transmission)

In what follows, I model the received power at a typical IRS-assisted user S_{R_0} as a a sum of scaled generalized gamma random variables and derive the LT of S_{R_0} conditioned on $r_{0,0}$.

Lemma 11. *The desired signal power through nearest IRS $S_{R_0}(r_{0,0})$ in (4.1) can be approximated as a sum of scaled generalized gamma random variable as follows:*

$$S_{R_0} \approx p_t r_{0,0}^{-\alpha} t_{0,j}^{-\alpha} \sum_{q=1}^{N^2} |a_q| X_{GG_q}(\zeta^2, 0.5m, 0.5), \tag{4.7}$$

where $a_q = \cos(\beta_{0_n} - \beta_{0_k}), \forall q = 1, \cdots, n+k, \cdots, N^2, n = \{1, \cdots, N\}, k = \{1, \cdots, N\}$.

Proof. The desired signal power through nearest IRS $S_{R_0}(r_{0,0})$ in (4.1) is simplified using the following steps:

$$
\begin{aligned}
S_{R_0}(r_{0,0}) &\overset{(a)}{\approx} p_t r_{0,0}^{-\alpha} t_{0,j}^{-\alpha} |\sum_{n=1}^{N} |f_{0_n,j}||g_{0,0_n}|e^{-j\beta_{0_n}}|^2 \\
&\overset{(b)}{=} p_t r_{0,0}^{-\alpha} t_{0,j}^{-\alpha} \sum_{n=1}^{N} \sum_{k=1}^{N} \cos(\beta_{0_n} - \beta_{0_k})|f_{0_n,j}||g_{0,0_n}||f_{0_k,j}||g_{0,0_k}| \\
&\overset{(c)}{\approx} p_t r_{0,0}^{-\alpha} t_{0,j}^{-\alpha} \sum_{n=1}^{N} \sum_{k=1}^{N} \cos(\beta_{0_n} - \beta_{0_k}) X_{NG} = p_t r_{0,0}^{-\alpha} t_{0,j}^{-\alpha} \sum_{n=1}^{N} \sum_{k=1}^{N} \cos(\beta_{0_n} - \beta_{0_k}) X_{GG}(\zeta^2, 0.5m, 0.5) \\
&\overset{(d)}{=} p_t r_{0,0}^{-\alpha} t_{0,j}^{-\alpha} \sum_{q=1}^{N^2} |a_q| X_{GG}(\zeta^2, 0.5m, 0.5),
\end{aligned}
$$

$$\tag{4.8}$$

where (a) is obtained by approximation as discussed in footnote-1, (b) follows from the simplification using $|x|^2 = \operatorname{Re}(x)^2 + \operatorname{Im}(x)^2$ and trigonometric identity $\cos(\alpha - \beta) = \cos(\alpha)\cos(\beta) - \sin(\alpha)\sin(\beta)$, (c) is followed by noting that $|g_{0,0_n}||f_{0_n,j}||g_{0,0_k}||f_{0_k,j}|$ is the product of four independent Rayleigh distributed random variables with mean and variance $\mu_x = \sigma\pi/2$ and $\sigma_x^2 = 2^2\sigma^2(1 - \pi^2/16)$, respectively. However, the exact distribution of the product of

four independent Rayleigh random variables in [90] is complicated. Therefore, to maintain tractability, I approximate it as a transformed Nakagami-m random variable [114] with the density function

$$f_{X_{NG}}(x) = 2\left(\frac{m}{\Omega}\right)^m \frac{1}{\hat{n}\Gamma(m)\sigma^{\frac{2m}{\hat{n}}}} x^{\frac{2m}{\hat{n}}-1} \exp(-\frac{m}{\Omega\sigma^{\frac{2}{\hat{n}}}} x^{\frac{2}{\hat{n}}}),$$

where $m = 0.6102\hat{n} + 0.4263 = 2.8671$, and $\Omega = 0.8808n^{-0.9661} + 1.12 = 1.3508$, and $\hat{n} = 4$. Here $\hat{n} = 4$ represents the product of four-independent Rayleigh random variables. Now by substituting $\hat{n} = 4$ and $\zeta = \frac{\Omega}{m}$, $f_{X_{NG}}(x)$ can be rewritten as $f_{X_{GG}}(x) = \frac{0.5}{\zeta^m\Gamma(m)}x^{0.5m-1}e^{-\sqrt{\frac{x}{\zeta^2}}}$, which is the PDF of a generalized Gamma random variable [115]. Finally, in (d), the double summation $n = 1, \cdots, N$, $k = 1, \cdots, N$ and $a_q = \cos(\beta_{0_n} - \beta_{0_k})$ is transformed to single summation $q = 1, \cdots, n + k, \cdots, N^2$, where $-\pi/2 \leq \beta_{0_n} - \beta_{0_k} \leq \pi/2$. ∎

In what follows, I derive the conditional LT of the received signal power in the IRS-assisted communication mode.

Lemma 12. *Conditioned on $r_{0,0}$, the LT of the S_{R_0} experienced by the typical user through nearest IRS $\mathcal{L}_{S_{R_0}}$ in the IRS-assisted indirect communication mode is given as follows:*

$$\mathcal{L}_{S_{R_0}|r_{0,0}}(s) = \mathbb{E}\left[\prod_{q=1}^{N^2} \frac{1}{(2\zeta^2 s\ \hat{a}_q)^d} \exp\left(\frac{1}{8\ \zeta^2 s\ \hat{a}_q}\right) D_{-2d}\left(\frac{1}{2\zeta^2 s\ \hat{a}_q}\right)\right], \qquad (4.9)$$

*where $\hat{a}_q = p_t r_{0,0}^{-\alpha} t_{0,j}^{-\alpha} a_q$, a_q is defined in **Lemma 11** and $D_{-v}(\cdot)$ is the parabolic cylinder function.*

Proof. The LT of S_{R_0} is given by using step (d) of (4.8) as follows:

$$\begin{aligned}
\mathcal{L}_{S_{R_0}|r_{0,0}}(s) &= \mathbb{E}[e^{-sS_{R_0}}] \\
&= \mathbb{E}[e^{-sp_t r_{0,0}^{-\alpha} t_{0,j}^{-\alpha} \sum_{q=1}^{N^2} a_q X_{GG_q}(\zeta^2, 0.5m, 0.5)}] \\
&= \prod_{q=1}^{N^2} \mathbb{E}[e^{-sp_t r_{0,0}^{-\alpha} t_{0,j}^{-\alpha} a_q X_{GG_q}(\zeta^2, 0.5m, 0.5)}],
\end{aligned} \qquad (4.10)$$
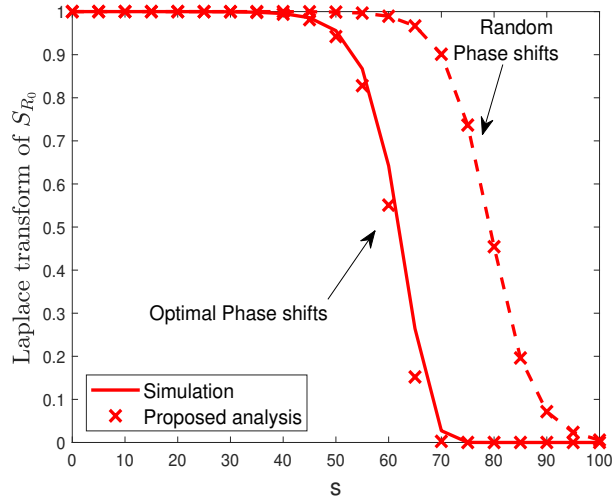
Figure 4.2 Validation of conditional LT in (4.7) of the desired received signal power $S_{R_0}(r_0)$ considering (i) random IRS phase shifts and (ii) optimal IRS phase shifts obtained from CVX, using Monte-Carlo simulations.

where (4.10) follows from the fact that MGF of the linear combination of independent variables can be rewritten as the product of MGFs of each of the independent variables, and

$$
\begin{aligned}
\mathbb{E}\big[e^{-sp_t r_{0,0}^{-\alpha} t_{0,j}^{-\alpha} a_q X_{GG_q}(\zeta^2, 0.5m, 0.5)}\big] &= \int_0^\infty e^{-s\hat{a}_q X_{GG_q}} f_{X_{GG}}(x)dx \\
&\overset{(a)}{=} \int_0^\infty \frac{0.5}{\zeta^m \Gamma(m)} x^{0.5m-1} e^{-s\hat{a}_q x - \sqrt{\frac{x}{\zeta^2}}} dx \\
&\overset{(b)}{=} \frac{2}{\zeta^m \Gamma(m)} \int_0^\infty g^{m-1} e^{-s\hat{a}_q g^2 - \frac{g}{\zeta}} dg \\
&\overset{(c)}{=} \frac{1}{(2\zeta^2 s\,\hat{a}_q)^{0.5m}} \exp\left(\frac{1}{8\,\zeta^2 s\,\hat{a}_q}\right) D_{-m}\left(\frac{1}{2\zeta^2 s\,\hat{a}_q}\right),
\end{aligned}
\tag{4.11}
$$

where (a) is obtained by substituting the probability density function of GG random variable $f_{XX_G}(x) = \frac{0.5}{\zeta^m \Gamma(m)} x^{0.5m-1} e^{-\sqrt{\frac{x}{\zeta^2}}}$ [114], (b) is obtained by changing variable $g = \sqrt{x}$, (c) is derived by using the identity $\int_0^\infty g^{\nu-1} e^{-\beta g^2 - \gamma g} dg = (2\beta)^{-\frac{\nu}{2}} \Gamma[\nu] \exp(\frac{\eta^2}{8\beta}) D_{-\nu}\left(\frac{\eta}{\sqrt{2\beta}}\right)$ from Eq. 3.462 of [116], where $D_{-\nu}(.)$ represents the parabolic cylinder function. Finally, by using $\hat{a}_q = p_t r_{0,0}^{-\alpha} t_{0,j}^{-\alpha} a_q$ in step (c) of (4.11) and (4.10) results in **Lemma** 12. ∎

Fig. 2 validates the accuracy of the LT of the received signal power (derived in **Lemma 2**) of the typical IRS-assisted user with the Monte-Carlo simulations. Our derived expressions

126

match well with the simulations confirming the accuracy of our S_{R_0} model and its corresponding LT. In both Lemma 2 and simulations, the phase-shifts are obtained optimally from CVX. Specifically, I solve the following problem (**P1**) to maximize the received signal power (given in (4.1)) and obtain the optimal phase-shifts:

$$\textbf{P1} : \max_{\theta_{0_n}, \forall n} \ S_{R_0} = P|\sum_{n=1}^{N} C_{0_n,j} f_{0_n,j} g_{0,0_n} e^{j\theta_{0_n}}|^2$$

$$\text{s.t. } 0 \leq \theta_{0_n} \leq \pi, \forall n = 1, \cdots, N.,$$

(4.12)

Substituting $f_{0_n,j} = |f_{0_n,j}|e^{-j\psi_{0_n,j}}$, $g_{0,0_n} = |g_{0,0_n}|e^{-j\phi_{0,0_n}}$, $\Theta_0 = \text{diag}\{e^{j\theta_{0_1}}, e^{j\theta_{0_2}}, \cdots, e^{j\theta_{0_N}}\}$ and $C_{0_n,j} \approx C_{0,j} = r_{0,0}^{-\alpha} t_{0,j}^{-\alpha}$ defined in Sec. IIB, the objective function can be rewritten as $Pr_{0,0}^{-\alpha} t_{0,j}^{-\alpha} |\sum_{n=1}^{N} |f_{0_n,j}||g_{0,0_n}|e^{-j\beta_{0_n}}|^2$. Since $Pr_{0,0}^{-\alpha} t_{0,j}^{-\alpha}$ is independent of the optimization variable, I can discard this term. Now, I transform the objective to equivalent matrix form as $|\tilde{\mathbf{g}}_{0,0}^{H} \mathbf{B_0} \ \tilde{\mathbf{f}}_{0,j}|^2$, where $\tilde{\mathbf{g}}_{0,0} \in \mathbb{R}^{1 \times N}$, $\tilde{\mathbf{f}}_{0,j} \in \mathbb{R}^{N \times 1}$, and $\mathbf{B_0} = \text{diag}\{e^{j\beta_{0_1}}, e^{j\beta_{0_2}}, \cdots, e^{j\beta_{0_N}}\}$. Since the objective function is a scalar, I can convert absolute square to norm square as $\|\tilde{\mathbf{g}}_{0,0}^{H} \mathbf{B_0} \ \tilde{\mathbf{f}}_{0,j}\|^2$. Finally, defining $\mathbf{v} = [v_1, \cdots, v_n]^H$, where $v_n = e^{j\beta_{0_n}}, \forall n$, and $\Phi = \text{diag}(\tilde{\mathbf{g}}_{0,0}^{H})\tilde{\mathbf{f}}_{0,j}$, I reformulate $\|\tilde{\mathbf{g}}_{0,0}^{H} B_0 \ \tilde{\mathbf{f}}_{0,j}\|^2 = \|\mathbf{v}^H \Phi\|^2$. The problem **P1** can thus be reformulated as follows:

$$\textbf{P2} : \max_{\mathbf{v}} \ \mathbf{v}^H \Phi \Phi^H \mathbf{v}$$

$$\text{s.t. } |v_n|^2 = 1, \forall n = 1, \cdots, N.$$

(4.13)

P2 is non-convex quadratically constrained quadratic program (QCQP) in the homogeneous form and the constraint is rank one [117]. Now, defining $\mathbf{V} = \mathbf{vv}^H$, I apply semi-definite relaxation (SDR) to relax the constraint as follows:

$$\textbf{P3} : \max_{\mathbf{V}} \ \text{Tr} \ (\Phi\Phi^H \mathbf{V})$$

$$\text{s.t. } \mathbf{V}_{n,n} = 1, \forall n = 1, \cdots, N, \quad \mathbf{V} \geq 0.$$

(4.14)

Since the problem is now transformed in to a convex semidefinite program (SDP), similar to [25], I solve it for the optimal value using CVX.

Furthermore, Fig. 2 also compares the LT of S_{R_0} with optimal IRS phase-shifts to LT of S_{R_0} with random IRS phase shifts. For a given value of s, the LT of S_{R_0} with optimal IRS phase-shifts is lower than the LT of S_{R_0} with random IRS phase-shifts. Thus, it is evident that the received signal power S_{R_0} with optimal phase-shifts significantly outperforms the received signal power S_{R_0} with random phase shifts.

Corollary 6. *The optimal received signal power can be obtained if I substitute $\beta_{0_n,j} = \theta_{0_n} - \psi_{0_n,j} - \phi_{0,0_n} = 0$ in (4.7), which maximizes a_q to unity $\forall n \in \{1, \cdots, N\}$ [77] and results in maximum S_{R_0} as $S_{R_0} = p_t r_{0,0}^{-\alpha} t_{0,j}^{-\alpha} W$. In this case, $W = \sum_{q=1}^{N^2} X_{GG_q}(\zeta^2, 0.5m, 0.5)$ can be modeled as a normal random variable Since the square of the number of IRS elements can be a large number, using CLT with mean $\mu_w = N^2 \mu_{GG}$ and variance $\sigma_w^2 = N^2 \sigma_{GG}^2$. where $\mu_{GG} = \zeta^2 \frac{\Gamma(m+2)}{\Gamma(m)}$ and $\sigma_{GG} = \zeta^4 \left(\frac{\Gamma(m+4)}{\Gamma(m)} - \mu_{GG}^2 \right)$ [115], I have the mean and the variance of S_{R_0} as $\mathbb{E}[S_{R_0}] = p_t r_{0,0}^{-\alpha} t_{0,j}^{-\alpha} \mu_{GG}$ and $\mathbb{V}[S_{R_0}] = p_t^2 r_{0,0}^{-2\alpha} t_{0,j}^{-2\alpha} \sigma_{GG}$, respectively.*

4.4 Statistics of the Aggregate Interference (IRS-Assisted Transmission)

In this section, I first derive the LT of the aggregate interference observed at a typical IRS-assisted user from all BSs. Then, I model the worst-case aggregate interference observed at a typical IRS-assisted user from all IRSs and derive its corresponding LT.

The LT of the aggregate interference observed at a typical IRS-assisted user from all BSs (excluding the blocked nearest direct BS) $\mathcal{L}_{I_B}(s)$ is derived as follows:

$$\mathcal{L}_{I_B|d_0}(s) = \mathbb{E}\big[e^{-s\sum_{j\in\Phi_B\backslash 0} p_t\beta^2|h_j|^2(\ell_j^2+H_B^2)^{-\alpha/2}}\big]$$

$$\overset{(a)}{=} \mathbb{E}_{\Phi_B}\left[\prod_{j\in\Phi_B\backslash 0} \frac{1}{1 + s\,p_t\beta^2(\ell_j^2 + H_B^2)^{-\alpha/2}}\right]$$

$$\overset{(b)}{=} \exp\left(-2\pi\lambda_B \int_{\ell_0}^{\infty}\left(1 - \frac{1}{1 + p_t\beta^2(\ell_j^2 + H_B^2)^{-\alpha/2}}\right)\ell_j d\ell_j\right) \quad (4.15)$$

$$\overset{(c)}{=} \exp\left(-2\pi\lambda_B \int_{d_0}^{\infty}\left(1 - \frac{1}{1 + p_t\beta^2 d_j^{-\alpha}}\right)d_j\,dd_j\right),$$

where (a) is obtained by applying the LT of $|h_j|^2$ and $|h_j|^2 \sim \exp(1)$, and (b) is derived using PGFL² for PPP w.r.t the two-dimensional distance ℓ_j of the interfering BSs [96], and (c) is obtained by substituting $d_j = \sqrt{\ell_j^2 + H_B^2}$. The closed-form expression can then be obtained as follows:

$$\mathcal{L}_{I_B|d_0}(s) = \exp\left(-2\pi\lambda_B \frac{d_0^{2-\alpha}sp_t\beta^2}{\alpha-2}\,{}_2F_1\left(1, \frac{-2+\alpha}{\alpha}; 2 - \frac{2}{\alpha}; -s\,p_t\beta^2 d_0^{-\alpha}\right)\right). \quad (4.16)$$

Corollary 7. *For $\alpha = 4$, the LT of the aggregate interference to the typical user through all the BSs (except the associated BS_0) $\mathcal{L}_{\hat{I}_B}$ in the the direct mode can simplified as:*

$$\mathcal{L}_{\hat{I}_B|d_0}(s) = \exp\left(-\pi\lambda_B \sqrt{s\hat{p}_t\beta^2}\arctan\left(\sqrt{s\,\hat{p}_t\beta^2 d_0^{-4}}\right)\right),$$

using ${}_2F_1\left(1, 0.5; 1.5; -X^2\right) = \frac{\arctan X}{X}$, for $|X| < 1$ [118][Eq. 15.4.3].

Note that **Corollary 2** is the special case of (4.16), which is mostly applicable for the outdoor communication setup.

Lemma 13 (Lower Bound on the Aggregate Interference from Multiple IRSs)**.** *I reformulate the aggregate interference observed at a typical user from all IRSs (excluding nearest IRS) in a multi-IRS, multi-BS scenario as $I_R \leq \sum_{j\in\Phi_B} PZ_j$, where $Z_j = \sum_{m=1}^{M-1} r_{0,m}^{-\alpha}\,t_{m,j}^{-\alpha}\,Y_m$.*

---

²PGFL of any function $f(r)$ for a PPP Φ is defined as $\mathbb{E}[\prod_{r\in\Phi} f(r)] = \exp\left(-\lambda\int_{\mathbb{R}^2}(1 - f(r))dr\right) = \exp\left(-2\pi\lambda\int_r^{\infty}(1 - f(r))\,rdr\right)$.

Proof. Taking $\beta_{m_n,j} = \theta_{m_n} - \psi_{m_n,j} - \phi_{0,m_n}$, the I_R expression in (4.3) can be rewritten as follows:

$$
\begin{aligned}
I_R &\overset{(a)}{=} \sum_{j\in\Phi_B} p_t \sum_{m=1}^{M-1} r_{0,m}^{-\alpha} t_{m,j}^{-\alpha} \quad |\sum_{n=1}^{N} |f_{m,j}| \, |g_{0,m_n}| e^{j\beta_{m_n,j}}|^2 \\
&\overset{(b)}{\leq} \sum_{j\in\Phi_B} p_t \sum_{m=1}^{M-1} r_{0,m}^{-\alpha} t_{m,j}^{-\alpha} |\sum_{n=1}^{N} |f_{m,j}| \, |g_{0,m_n}||^2 \\
&\overset{(c)}{=} \sum_{j\in\Phi_B} p_t \sum_{m=1}^{M-1} r_{0,m}^{-\alpha} t_{m,j}^{-\alpha} Y_m \overset{(d)}{=} \sum_{j\in\Phi_B} p_t Z_j,
\end{aligned}
\tag{4.17}
$$

where (a) is obtained by the approximation $r_{0,m} \approx r_{0,m_n}$, $t_{m,j} \approx t_{m_n,j}$ as discussed in footnote-1, (b) follows from $\beta_{m_n,j} = \theta_{m_n} - \psi_{m_n,j} - \phi_{0,m_n} = 0$ which results in the maximum interference (excluding nearest IRS) and hence referred to as *worst case interference*. Finally, step (c) and step (d) follow by defining $Y_m = |\sum_{n=1}^{N}|f_{m_n,j}| \, |g_{0,m_n}||^2$ and $Z_j = \sum_{m=1}^{M-1} r_{0,m}^{-\alpha} t_{m,j}^{-\alpha} Y_m$, respectively. ∎

In what follows, I derive the statistics of the aggregate interference observed at a typical user from multiple IRSs in a multi-BS scenario.

Lemma 14 (Distribution of the Aggregate Interference from Multiple IRSs (Excluding the Nearest IRS) in a Multi-BS Scenario). *Leveraging the results in* **Lemma 3**, *given* $I_R \leq \sum_{j\in\Phi_B} P Z_j$, *where* $Z_j = \sum_{m=1}^{M-1} r_{0,m}^{-\alpha} t_{m,j}^{-\alpha} Y_m$ *follows a Normal distribution with mean and variance given by*

$$
\mu_{Z_j} = \mathbb{E}[r_{0,m}^{-\alpha}]((M-1)t_j^2)^{-\alpha/2}(1+\lambda) \quad \text{and} \quad \sigma_{Z_j}^2 = 2\mathbb{V}[r_{0,m}^{-\alpha}]((M-1)t_j^2)^{-\alpha}(1+2\lambda),
$$

and Y_m *represents the non-central Chi-square random variable with mean and variance* $\mu_Y = (1+\lambda)$ *and* $\sigma_Y^2 = 2(1+2\lambda)$, *respectively.*

Proof. Let $X_n = |g_{0,m_n}||f_{m_n,j}|$ denote the product of two independent Rayleigh distributed random variables with mean and variance $\mu_x = \sigma\pi/2$ and $\sigma_x^2 = 2^2\sigma^2(1-\pi^2/16)$, respectively [119]. Since the IRS elements are typically large, I leverage on central limit theorem (CLT)
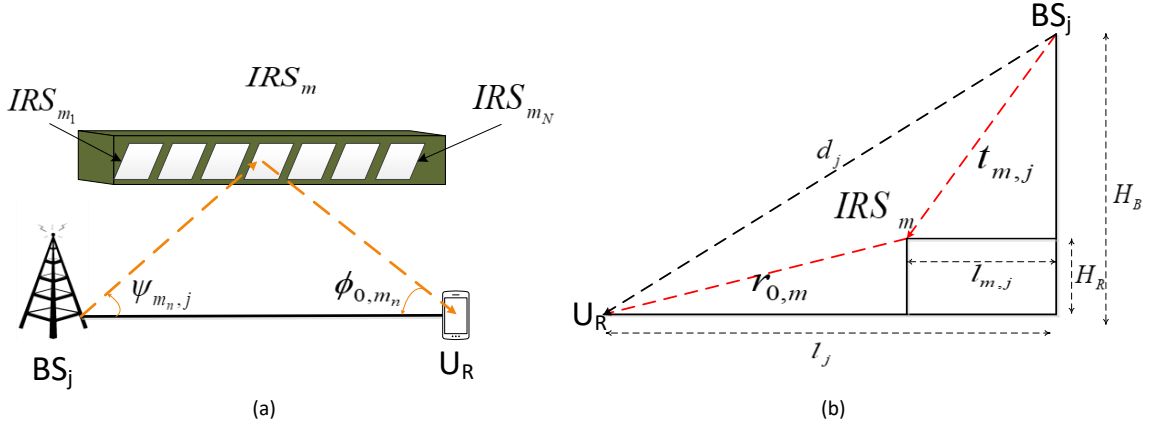
Figure 4.3 (a): Zoomed view of IRS functionality as a reflector, and (b) triangle explaining the IRS distance approximation.

to depict $X' = \sum_{n=1}^{N} X_n$ follows a normal distribution with the mean and variance given by $\mu_{X'} = N\mu_X$ and $\sigma_{X'}^2 = N\sigma_X^2$, respectively. I refer to this approximation as *Level-1 Gaussian approximation*. Consequently, $Y_m = |\sum_{n=1}^{N} X_n|^2$ will follow a non-central chi-square distribution with unity degree of freedom $\nu = 1$ and non-centrality parameter $\lambda = \frac{1}{2}\frac{\mu_{X'}}{\sigma_{X'}^2}$ [119]. Therefore, the mean and variance of Y_m can be obtained as in **Lemma 14**.

Let $Y'_m = r_{0,m}^{-\alpha} t_{m,j}^{-\alpha} Y_m$ denote the product of three random variables $t_{m,j}^{-\alpha}$, $r_{0,m}^{-\alpha}$, and Y_m, where $t_{m,j}^{-\alpha}$, and $r_{0,m}^{-\alpha}$ are correlated by cosine law as $t_{m,j}^{-\alpha} = \left(r_{0,m}^2 + d_j^2 - 2r_{0,m}d_j \cos\psi_m\right)^{-\alpha/2}$ [108, 120]. To simplify the analysis, I propose an alternate formulation of $t_{\mathrm{m,j}}$, i.e., instead of using cosine law I alternatively define $t_{m,j} = \sqrt{\ell_{m,j}^2 + (H_B - H_R)^2}$ (refer to the triangle in Fig. 4.3(b)). Next, to enhance tractability, I consider that the typical IRS is located in the middle of the BS_{j} and typical user (i.e., $\ell_{\mathrm{m,j}} \approx \frac{\ell_{\mathrm{j}}}{2}$) which upon substitution gives

$$t_{\mathrm{m,j}} \approx t_{\mathrm{j}} = \sqrt{\left(\frac{\ell_{\mathrm{j}}}{2}\right)^2 + (H_B - H_R)^2}. \tag{4.18}$$

Subsequently, I have $Y'_m \approx r_{0,m}^{-\alpha} t_j^{-\alpha} Y_m$, and $Z = \sum_{m=1}^{M-1} Y'_m$ will follow a normal distribution using CLT as shown in **Lemma 4**. I refer to this as *Level-2 Gaussian approximation*. ■

The factor $r_{0,m}^{-\alpha} t_{m,j}^{-\alpha}$ is important in modeling Y'_m as is evident in **Lemma 4**. Note that

131
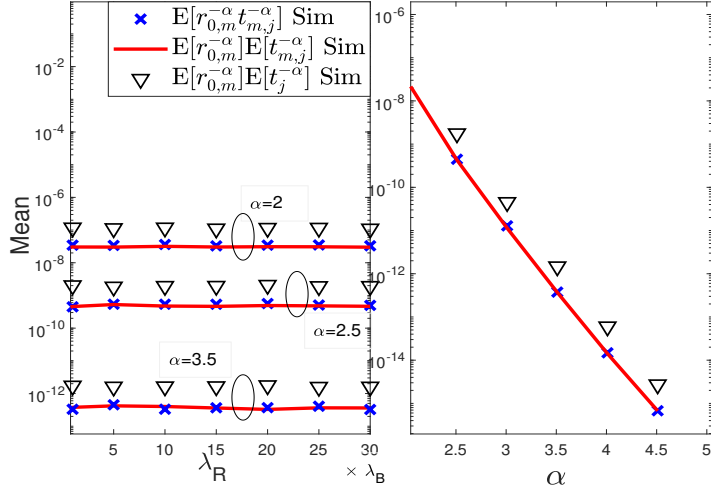
Figure 4.4 Comparison of $\mathbb{E}[r_{0,m}^{-\alpha}t_j^{-\alpha}]$, $\mathbb{E}[r_{0,m}^{-\alpha}]\mathbb{E}[t_{m,j}^{-\alpha}]$ and the proposed approximation of $\mathbb{E}[r_{0,m}^{-\alpha}]\mathbb{E}[t_j^{-\alpha}]$ in (4.18).

$r_{0,m}^{-\alpha}$ and $t_{m,j}^{-\alpha}$ are correlated using cosine law. However, Fig. 4 shows that the correlation is weak and thus the approximation in (4.18) is accurate. In the sequel, I first compare $\mathbb{E}[r_{0,m}^{-\alpha}]\mathbb{E}[t_{m,j}^{-\alpha}]$, and $\mathbb{E}[r_{0,m}^{-\alpha}t_j^{-\alpha}]$ to show the weak correlation. Then, I demonstrate the validity of the proposed approximation $\mathbb{E}[r_{0,m}^{-\alpha}]\mathbb{E}[t_j^{-\alpha}]$ to validate its accuracy in Fig. 4.4. It is also clear from the figure that λ_R does not have any impact on the distances $t_{m,j}$ and $r_{0,m}$ on average. It is clear from the right figure that increase in path-loss exponent α causes an increase in the path-loss distance term and hence decreases in $\mathbb{E}[r_{0,m}^{-\alpha}]\mathbb{E}[t_{m,j}^{-\alpha}]$, $\mathbb{E}[r_{0,m}^{-\alpha}t_j^{-\alpha}]$ and $\mathbb{E}[r_{0,m}^{-\alpha}]\mathbb{E}[t_j^{-\alpha}]$ are evident.

In what follows, I derive the first and second moment of $r_{0,m}^{-\alpha}$ as is required in **Lemma 4**.

Lemma 15. *The LT of interference experienced by the typical user through the all IRSs (except nearest IRS to the typical user) $\mathcal{L}_{I_R}$ in the IRS- assisted communication mode is given as follows:*

$$\mathcal{L}_{I_R|r_{0,0}}(s) \approx \exp\left(2\pi\lambda_B \frac{4}{\alpha}\sum_{i=1}^{\infty}\frac{b_i(s)}{i-\frac{2}{\alpha}}\left(X_R^{i-\frac{2}{\alpha}} - X_0^{i-\frac{2}{\alpha}}\right)\right), \tag{4.19}$$

where $b_i(s)$ denotes the Taylor's series expansion coefficients of $\exp(-k_1(s)x - k_2(s)x^2)$ and $k_1(s) = \mu_{Z_j}s\,p_t/t_j^{-\alpha}$, and $k_2(s) = \frac{1}{2t_j^{-2\alpha}}\sigma_{Z_j}^2 s^2 p_t^2$.

132

Proof. Using (4.17) in (4.3), I derive LT $\mathcal{L}_{I_R}(s)$ as:

$$\mathcal{L}_{I_R|r_{0,0}}(s) = \mathbb{E}[e^{-sI_R}] = \mathbb{E}[e^{-s\sum_{j\in\Phi_B} p_t Z_j}] = \mathbb{E}[\prod_{j\in\Phi_B} e^{-s\, p_t Z_j}]$$

$$\overset{(a)}{=} \mathbb{E}[\prod_{j\in\Phi_B} \mathbb{E}_Z[e^{-s\, p_t Z_j}]] = \mathbb{E}[\prod_{j\in\Phi_B} e^{-(\mu_{Z_j} s\, p_t + \frac{1}{2}\sigma_{Z_j}^2 s^2 p_t^2)}]$$

$$\overset{(b)}{=} \exp\left(-2\pi\lambda_B \int_0^R \left(1 - e^{-(k_1(s)t^{-\alpha}+k_2(s)t^{-2\alpha})}\right) \ell d\ell\right)$$

$$\overset{(c)}{=} \exp\left(-2\pi\lambda_B \frac{-4}{\alpha} \int_{X_0}^{X_R} \left(1 - e^{-(k_1(s)X+k_2(s)X^2)}\right) X^{-\frac{2}{\alpha}-1} dX\right) \tag{4.20}$$

$$\overset{(d)}{=} \exp\left(2\pi\lambda_B \frac{4}{\alpha} \int_{X_0}^{X_R} \sum_{i=1}^{\infty} b_i(s)\, X^{i-\frac{2}{\alpha}-1} dX\right)$$

$$\overset{(e)}{=} \exp\left(2\pi\lambda_B \frac{4}{\alpha} \sum_{i=1}^{\infty} \frac{b_i(s)}{i-\frac{2}{\alpha}} \left(X_R^{i-\frac{2}{\alpha}} - X_0^{i-\frac{2}{\alpha}}\right)\right),$$

where (a) follows from the LT of Z_j where Z_j is a Gaussian random variable with μ_{Z_j}, and $\sigma_{Z_j}^2$ is given by **Lemma 4**, (b) follows by substituting $k_1(s) = \mu_{Z_j}s\, p_t/t_j^{-\alpha}$ and $k_2(s) = \frac{1}{2t_j^{-2\alpha}}\sigma_{Z_j}^2 s^2 p_t^2$ and then I apply PGFL w.r.t ℓ_j where $t = \sqrt{(\frac{\ell}{2})^2 + (H_B - H_R)^2}$ and t_j is given in (4.18). For simplicity, (c) is obtained by changing of variable ℓ to X, i.e., $X = \left(\frac{\ell^2}{4} + (H_B - H_R)^2\right)^{-\alpha/2}$, where $X_0 = (H_B - H_R)^{-\alpha}$ and $X_R = \left(\frac{R^2}{4} + (H_B - H_R)^2\right)^{-\alpha/2}$. Note that (d) is obtained by using Taylor's series expansion of $\exp(-k_1 x - k_2 x^2)$ and $b_i(s)$ denotes the coefficients of the expanded Taylor series. Finally, (e) is obtained by solving the integral. ∎

Fig. 4.5 validates the accuracy of LT of aggregate interference from IRSs for different number of IRSs, i.e., $M = 300$ and $M = 1500$ and transmission power $p_t = 1$ W and $p_t = 20$ W. This figure shows that, for a given value of s, increasing transmission power and IRS intensity decreases IRS interference. Clearly, the interference in higher power and higher intensity trend dominates compared to all other combinations of power and IRS intensity. Similarly, Fig. 4.6 validates the accuracy of the LT of the aggregate interference from BSs (excluding the nearest BS) given in (4.16) as a function of s. Again, the LT of aggregate interference decreases with increasing transmission power of BSs (i.e., the interference in-
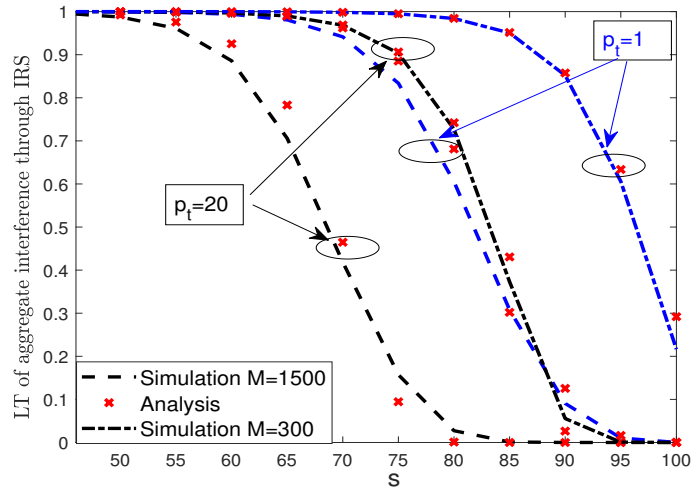
Figure 4.5 Conditional LT of aggregate interference from IRSs (excluding the nearest IRS), $\mathcal{L}_{I_R}(s)$ in (4.19), for $\lambda_R = 2\lambda_0, M = 300$ and $\lambda_R = 10\lambda_0, M = 1500$ with $P = 1$ and $P = 20$, using Monte-Carlo simulations.
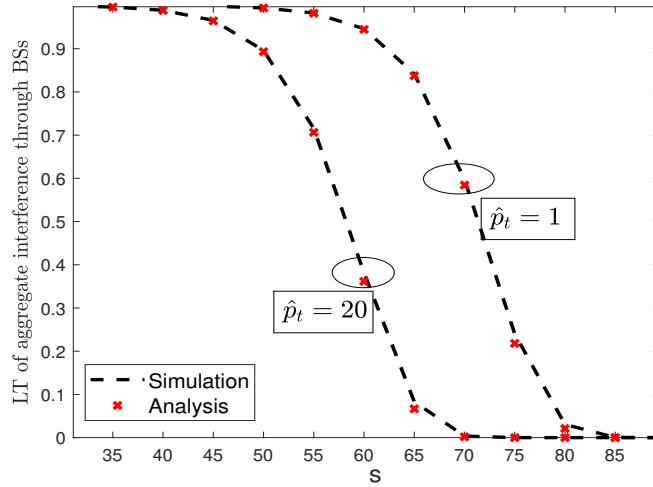
Figure 4.6 Conditional LT of aggregate interference from BSs (excluding the nearest BS in direct mode), $\mathcal{L}_{I_B}(s)$ (4.16), for $\hat{P} = P = 1$, $\hat{P} = P = 20$, and $\lambda_R = 2\lambda_0, M = 300$, using Monte-Carlo simulations.

creases). Unlike Fig. 4.5, neither the IRS intensity nor the total number of IRSs M have any effect on $\mathcal{L}_{I_B}$ as the direct transmissions are independent of λ_R or M.

4.5 Coverage Probability and Ergodic Capacity Characterization

In this section, I first derive the coverage probability of an IRS-assisted user and then the coverage probability of users who are supported by direct transmissions. Then, I derive the ergodic capacity and energy efficiency of an IRS-assisted user and the user supported by direct transmission from BS. Finally, I derive the overall network coverage, ergodic rate, and energy-efficiency considering the fraction of IRS-assisted and direct users in the network.

4.5.1 Coverage Probability (IRS-assisted Transmission)

The coverage probability of the typical user associated to nearest IRS in the IRS-assisted indirect mode of communication is defined as $C_{\mathrm{ID}} = \Pr(\gamma_{ID} \geq \tau)$, where the SINR for IRS-assisted indirect transmission is given as follows:

$$\gamma_{ID} = \frac{S_{R_0}}{I_{\mathrm{B}} + I_R + N_0}. \tag{4.21}$$

The coverage probability can be calculated numerically by using Gil-Paleaz inversion theorem [121] as shown in the following:

$$
\begin{aligned}
C_{\mathrm{ID}} &= \Pr\left(\gamma_{ID} \geq \tau\right) \\
&= \Pr\left(S_{R_0}(r_{0,0}) - \tau I_R \geq \tau\, I_B + \tau\, N_0\right) = \Pr\left(\Omega \geq \tau I_B + \tau N_0\right) \\
&= \mathbb{E}_{r_{0,0}}\left[\frac{1}{2} - \frac{1}{\pi}\int_0^\infty \frac{\mathrm{Im}[\phi_{\Omega|r_{0,0}}(\omega)\mathcal{L}_{I_B}(-j\omega\tau)e^{j\omega\tau N_0}]}{\omega}d\omega\right] \\
&= \frac{1}{2} - \frac{1}{\pi}\int_0^\infty \frac{\mathrm{Im}[\phi_{\Omega}(\omega)\mathcal{L}_{I_B}(-j\omega\tau)e^{j\omega\tau N_0}]}{\omega}d\omega,
\end{aligned}
\tag{4.22}
$$

where

$$\phi_{\Omega}(\omega) = \mathbb{E}_{r_{0,0}}[\phi_{\Omega|r_{0,0}}(\omega)] = \mathbb{E}_{r_{0,0}}[e^{-j\omega\Omega}] = \mathbb{E}_{r_{0,0}}[\mathcal{L}_{S_{R_0}|r_{0,0}}\mathcal{L}_{I_R|r_{0,0}}(-j\omega\tau)]. \tag{4.23}$$

Note that $\mathcal{L}_{I_B}(-j\omega\tau) = \mathbb{E}_{d_0}[\mathcal{L}_{I_B|d_0}(-j\omega\tau)]$ is independent of $r_{0,0}$. Substituting (4.19) and (4.9) in (4.23) and then substituting (4.23) and (4.16) in (4.22), I obtain C_{ID}. The distribution of the distance of the nearest IRS at height H_R to the typical user is given as follows: [122]:

$$f_{r_0}(r_{0,0}) = \frac{2Mr_{0,0}}{R^2}\left(1 - \frac{r_{0,0}^2 - H_R^2}{R^2}\right)^{M-1}. \tag{4.24}$$

Also, the distance of the nearest BS at height H_B to the typical user is given as:

$$f_{d_0}(d_0) = 2\pi\lambda_B d_0 e^{-\pi\lambda_B(d_0^2 - H_B^2)}. \tag{4.25}$$

4.5.2   Coverage Probability (Direct Transmission)

The coverage probability of the typical user with the direct mode of communication is defined as $C_{\text{D}} = \Pr(\gamma_D \geq \tau)$, where the SINR of the direct communication mode is given as

$$\gamma_D = \frac{S_{D_0}}{\hat{I}_B + \hat{I}_R + N_0}. \tag{4.26}$$

Now by substituting (4.4), the coverage probability C_{D} can be written as follows:

$$\begin{aligned}
C_{\text{D}} &= \Pr\left(|h_0|^2 \geq d_0^\alpha \frac{\tau\beta^{-2}}{\hat{p}_t}\left(\hat{I}_{\text{B}} + \hat{I}_{\text{R}} + N_0\right)\right) \\
&= \mathbb{E}_{d_0}\left[e^{-\frac{\tau\, d_0^\alpha N_0}{\beta^2 \hat{p}_t}}\, \mathcal{L}_{\hat{I}_B}\left(\frac{\tau\, d_0^\alpha}{\beta^2 \hat{p}_t}\right)\, \mathcal{L}_{\hat{I}_R}\left(\frac{\tau\, d_0^\alpha}{\beta^2 \hat{p}_t}\right)\right],
\end{aligned} \tag{4.27}$$

where $\mathcal{L}(\cdot)$ is the LT and d_0 is the distance between the typical user and the nearest BS, i.e., $d_0 = \sqrt{\ell_0^2 + H_B^2}$. The distribution of the distance of the nearest BS is provided in (4.25).

Corollary 8. *The LT of the aggregate interference to the typical user through all the BSs (except the associated BS_0) $\mathcal{L}_{\hat{I}_B}$ in the the direct mode can then be obtained as follows:*

$$\mathcal{L}_{\hat{I}_B|d_0}(s) = \exp\left(-2\pi\lambda_B \frac{d_0^{2-\alpha} s\hat{p}_t\beta^2}{\alpha - 2}\, {}_2F_1\left(1, \frac{-2+\alpha}{\alpha}; 2 - \frac{2}{\alpha}; -s\, \hat{p}_t\beta^2 d_0^{-\alpha}\right)\right), \tag{4.28}$$

which is similar to (4.16) with p_t replaced with $\hat{p}_t$ for the direct mode.

Corollary 9. *Similar to **Lemma 15**, the LT of interference experienced by the typical user through the all the IRSs and all the BSs $\mathcal{L}_{\hat{I}_R}$ in direct communication mode is given as follows:*

$$\mathcal{L}_{\hat{I}_R}(s) \approx \exp\left(2\pi\lambda_B \frac{4}{\alpha} \sum_{i=1}^{\infty} \frac{\hat{b}_i(s)}{i - \frac{2}{\alpha}} \left(X_R^{i-\frac{2}{\alpha}} - X_0^{i-\frac{2}{\alpha}}\right)\right), \tag{4.29}$$

where $\hat{b}_i(s)$ denotes the Taylor's series expansion coefficients of $\exp(-\hat{k}_1(s)x - \hat{k}_2(s)x^2)$ and $\hat{k}_1(s) = \hat{\mu}_{Z_j} s\, \hat{p}_t / t_j^{-\alpha}$, and $\hat{k}_2(s) = \frac{1}{2t_j^{-2\alpha}} \hat{\sigma}_{Z_j}^2 s^2 \hat{p}_t^2$, $\hat{\mu}_{Z_j} = \mathbb{E}[r_{0,m}^{-\alpha}](Mt_j^2)^{-\alpha/2}(1+\lambda)$ and $\hat{\sigma}_{Z_j}^2 = 2\mathbb{V}[r_{0,m}^{-\alpha}](Mt_j^2)^{-\alpha}(1+2\lambda)$.

Note that the difference arises from the fact that $\hat{I}_R$ has M interfering IRSs in **Corollary 4**, whereas in **Lemma 9**, I have $M-1$ IRSs contributing to the aggregate interference I_R. Finally, substituting (4.28) and (4.29) in (4.27), I obtain the coverage probability of direct link C_D conditioned on the distance d_0.

4.5.3 Ergodic Capacity

The achievable ergodic capacity of a typical user can be given by using the coverage probability expressions as shown below [46]:

$$\mathbb{E}[\log_2(1 + \text{SINR})] = \frac{1}{\ln(2)} \int_0^\infty \frac{P(\text{SINR} > t)}{t} dt.$$

However, the aforementioned evaluation adds one more layer of integration on top of the coverage probability. Therefore, I use an alternative LT-based approach to evaluate ergodic capacity by leveraging on Hamdi's lemma [47] given as follows:

$$\mathbb{E}\left[\ln\left(1 + \frac{X}{Y + N_0}\right)\right] = \int_0^\infty \frac{\mathcal{L}_Y(s) - \mathcal{L}_{X,Y}(s)}{s} \exp(-N_0 s) ds, \tag{4.30}$$

where $\mathcal{L}_Y(s)$ and $\mathcal{L}_{X,Y}(s)$ represent the LT of Y and joint LT of X and Y, respectively. Subsequently, I derive the ergodic capacity of the typical IRS-assisted user as follows:

$$R_{ID} = \int_0^\infty \frac{\mathcal{L}_{I_B}(s)\mathcal{L}_{I_R}(s) - \mathcal{L}_{I_B}(s)\mathcal{L}_{I_R}(s)\mathcal{L}_{S_{R_0}}(s)}{s} \exp(-N_0 s) ds, \tag{4.31}$$

Similarly, the ergodic capacity of the typical user in direct mode R_D is given as follows:

$$R_D = \int_0^\infty \frac{\mathcal{L}_{\hat{I}_B}(s)\mathcal{L}_{\hat{I}_R}(s) - \mathcal{L}_{\hat{I}_B}(s)\mathcal{L}_{\hat{I}_R}(s)\mathcal{L}_{S_{D_0}}(s)}{s} \exp(-N_0 s) ds, \qquad (4.32)$$

where $\mathcal{L}_{S_{D_0}}(s) = \mathbb{E}[\mathcal{L}_{S_{D_0}|d_0}(s)]$ and $\mathcal{L}_{S_{D_0}|d_0}(s) = \frac{1}{1+s\,\hat{P}\beta^2 d_0^{-\alpha}}$.

4.5.4 Energy Efficiency

I define the energy-efficiency of a typical user by dividing the achievable rate with the network power consumption. The energy-efficiency of IRS-assisted user is given as follows:

$$\mathrm{EE}_{\mathrm{ID}} = \frac{\int_0^\infty \frac{\mathcal{L}_{I_B}(s)\mathcal{L}_{I_R}(s) - \mathcal{L}_{I_B}(s)\mathcal{L}_{I_R}(s)\mathcal{L}_{S_{R_0}}(s)}{s} \exp(-N_0 s) ds}{p_{\mathrm{BS}} + p_{\mathrm{U}} + P + p_{\mathrm{IRS}}}, \qquad (4.33)$$

which is obtained by dividing (4.31) with p_{IRS}. Similarly, the energy-efficiency of a typical user in the direct communication mode EE_D can be given by diving (4.32) with the power consumption in the direct mode $\hat{p}_t$ as follows:

$$\mathrm{EE}_{\mathrm{D}} = \frac{\int_0^\infty \frac{\mathcal{L}_{\hat{I}_B}(s)\mathcal{L}_{\hat{I}_R}(s) - \mathcal{L}_{\hat{I}_B}(s)\mathcal{L}_{\hat{I}_R}(s)\mathcal{L}_{S_{R_0}}(s)}{s} \exp(-N_0 s) ds}{p_{\mathrm{BS}} + p_{\mathrm{U}} + \hat{P}}. \qquad (4.34)$$

4.5.5 Overall Network Coverage, Ergodic Capacity, and Energy Efficiency

The overall coverage probability of the typical user is derived as follows:

$$C = (1 - \mathcal{A})C_D + \mathcal{A}C_{ID}, \qquad (4.35)$$

where $\mathcal{A}$ represents the fraction of users in the system performing indirect IRS-assisted transmission, while $(1 - \mathcal{A})$ represents the fraction of users performing direct transmission. Similarly, the overall achievable rate and energy-efficiency of the typical user can be derived as follows: $R = (1 - \mathcal{A})R_D + \mathcal{A}R_{ID}$, and $\mathrm{EE} = (1 - \mathcal{A})\mathrm{EE}_D + \mathcal{A}\mathrm{EE}_{ID}$, respectively.

The fraction of IRS-assisted and direct users can be perceived in many ways. For instance, it can be considered that the fraction of IRS-assisted users is proportional to the

number of IRSs in the network. In this case, $\mathcal{A}$ can be defined as $\frac{\lambda_R}{\lambda_R + \lambda_B}$. As an example, if there are five BSs and five IRSs, then $\mathcal{A} = 0.5$ assuming that one IRS can at-most provide service to one-user at a time. On the other hand, the fraction of IRS-assisted users can be considered proportional to the blocking probability of nearest direct link (as IRS is only associated to BS if there is a blocked direct link). For instance, considering a Boolean blockage model with the assumption that number of blockages follow Poisson distribution [123], the probability of direct transmission can be given as $\exp(-(\eta d_0 + u))$, where η and u are defined on the basis of the shape of considered blockages [124]. Subsequently, the probability of blockages can be written as $\mathcal{A} = 1 - \exp(-(\eta d_0 + u))$. Considering blockage the SINR of the direct mode in (4.26) modifies as $\gamma_D = \mathcal{A} \frac{S_{D_0}}{\hat{I}_B + \hat{I}_R + N_0}$ that results in modified coverage probability C_D in (4.27) as

$$C_{\mathrm{D}} = \mathbb{E}_{d_0} \left[e^{-\frac{\tau\, d_0^\alpha\, N_0}{\mathcal{A}\beta^2 \hat{p}_t}} \; \mathcal{L}_{\hat{I}_B} \left(\frac{\tau\, d_0^\alpha}{\mathcal{A}\beta^2 \hat{p}_t} \right) \; \mathcal{L}_{\hat{I}_R} \left(\frac{\tau\, d_0^\alpha}{\mathcal{A}\beta^2 \hat{p}_t} \right) \right].$$

4.6 Numerical Results and Discussion

In this section, I validate the accuracy of our derived expressions by Monte Carlo (MC) simulations and then obtain useful insights related to different interference scenarios, the total number of IRSs in the setup, number of IRS elements and transmission power for different communication modes. For MC simulations, I first generate the PPP and BPP for the distribution of BSs and IRSs in an observed area of radius $R = 700$ m, respectively. For each instance of MC simulations, first I pick an arbitrary user and then depending on the blockage of nearest BS's line of sight link I associate it to nearest IRS or with the nearest BS and calculate the corresponding instantaneous SINR. This SINR is then utilized to evaluate the performance measures overall coverage probability, overall achievable rate and overall energy efficiency after averaging over 10,000 realizations.
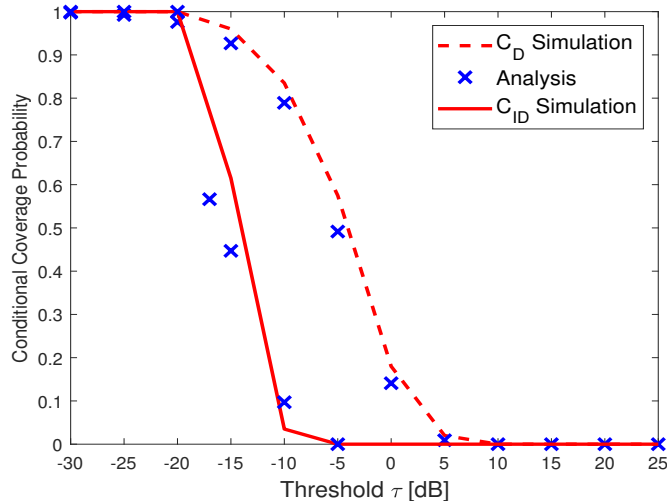
Figure 4.7 Validation of conditional coverage probability in IRS-assisted and direct mode of communications derived in (4.22) and (4.27), using Monte-Carlo simulations.

4.6.1   Simulation Parameters

Unless stated otherwise, the simulation parameters are listed herein. The heights of IRSs and BSs are set to $H_R = 10$ m, and $H_B = 20$ m, respectively. The transmission power for IRS-assisted mode and direct mode is $p_t = 20$ W and $\hat{p}_t = 20$ W, respectively. The static power consumption of BS and user is 40 dBm and 10 dBm, respectively [125], and therefore, $U = 50$ dBm. The phase resolution power consumption for 6- bits $P_r(6) = 78$ mW. The total number of IRS elements per IRS is $N = 50$, BS intensity within the coverage area is $\lambda_B = 10^{-4}$, and the total number of IRSs in the coverage area $M = 1500$ that corresponds to $\lambda_R = M/\pi R^2 \approx 10 \times \lambda_B$. Also, λ_R is IRS intensity, path-loss exponent is $\alpha = 4$, threshold on SINR $\tau = -10$ dB, and noise power spectral density is $N_0 = 10^{-10}$ W/Hz.

4.6.2   Validation of Analysis

Fig. 4.7 compares the coverage probability of IRS-assisted user and the user supported by the direct transmission as a function of the SINR threshold τ considering $p_t = \hat{p}_t = 20$ W.

Numerical results show that our theoretical analysis and Monte-Carlo simulations match well. As expected, the conditional coverage probability decreases with the increase in SINR threshold for both types of users. Nevertheless, the coverage probability of IRS-assisted transmission lags behind the direct transmission even when the intensity of IRSs is higher than the intensity of BSs, i.e., $\lambda_R = 10\lambda_B$. This fact signifies the efficacy of IRS deployments mostly in scenarios when the direct transmission link is blocked.

4.6.3 Impact of BS Transmit Power on Direct Communication

Fig. 4.8 compares the achievable data rate of IRS-assisted communication and the direct mode considering $\hat{p}_t = 1$ W and $\hat{p}_t = 5$ W. I observe that for smaller number of IRS elements, direct transmissions outperform the IRS-assisted transmissions. As the number of IRS elements increases, R_{ID} increases because the IRS link gets stronger with more elements. An increase in IRS interference however degrades the achievable data rate R_{D} in direct links. The figure also depicts that the performance of IRS-assisted communication starts to exceed direct communication with lower IRS elements if the transmit power of BSs is low as can be seen from switching point $N = 30$ and $N = 60$ for $\hat{p}_t = 1$ and $\hat{p}_t = 5$, respectively. I note that, for a given deployment density of BSs and IRSs, IRS-assisted mode is useful for a larger number of IRS elements and low transmit power of BSs in direct mode. Evidently, a higher transmission power of direct user's BSs degrades IRS-assisted communication, which is opposite for direct communication.

Similarly, Fig. 4.9 validates the accuracy of energy-efficiency considering $\hat{p}_t = 1$ W and $\hat{p}_t = 5$ W. As expected, the IRS-assisted mode outperforms the direct mode for $N = 40$ and $N = 100$, for $\hat{p}_t = 1$ W and $\hat{p}_t = 5$ W, respectively. Compared to $\hat{p}_t = 5$ W, energy-efficiency is lower for $\hat{p}_t = 1$ W.
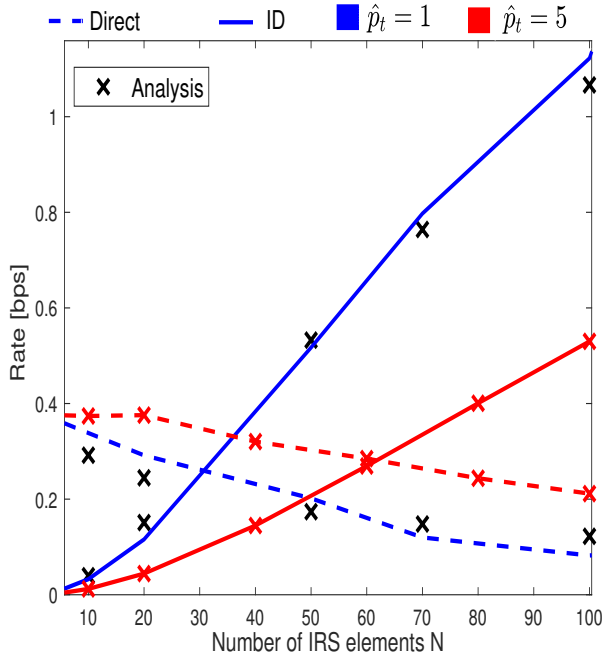
Figure 4.8 Analytical and simulation results on conditional achievable rate in IRS-assisted and direct mode of communications derived in (4.31) and (4.32) with respect to IRS elements (for $\hat{p}_t = 1$ and $\hat{p}_t = 5$).
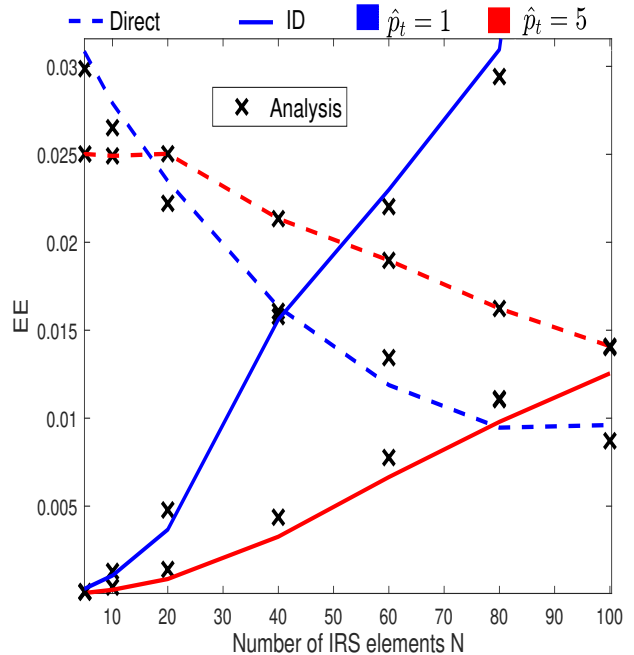
Figure 4.9 Validation of conditional EE for IRS-assisted and direct mode of communications derived in (4.33) and (4.34), using Monte-Carlo simulations (for different number of IRS elements, $\hat{p}_t = 1$ and $\hat{p}_t = 5$).

4.6.4 Impact of IRS Intensity on Direct and IRS-Assisted Communications

Fig. 4.10 compares the coverage probability and rate for direct and IRS-assisted communication as a function of the total number of IRS elements and IRSs with in the cell radius. I note that varying the number of IRS elements per IRS have no significant impact on the coverage probability and rate for sparse deployment of IRSs $M = 300$. However, the coverage probability C_{ID} and achievable rate R_{ID} increases with the increase in number of IRS elements for dense deployment of IRSs $M = 1500$. This is encouraging as it shows that the impact of interference due to dense deployment of IRSs is not significant. On the other hand, the rate of the direct communication decreases with the increasing IRS elements, especially
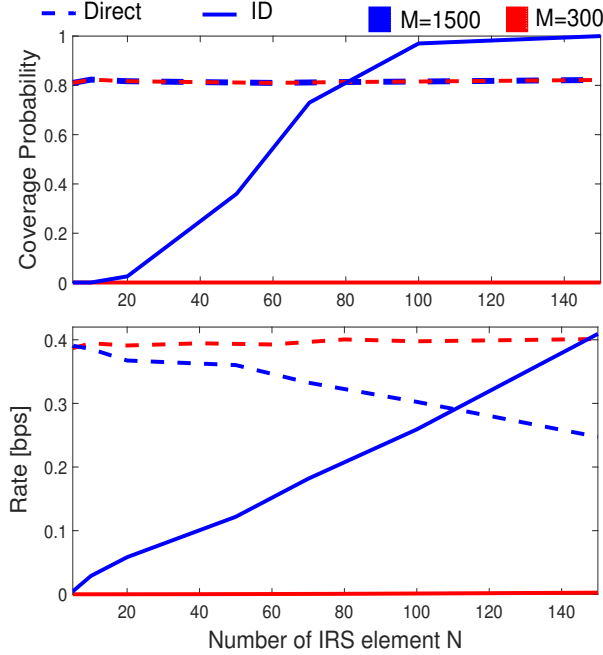
Figure 4.10 Comparison of conditional coverage probability and achievable rate for IRS-assisted mode and direct mode of communications with respect to number of IRS elements (for total number of IRSs $M = 300$ and $M = 1500$).
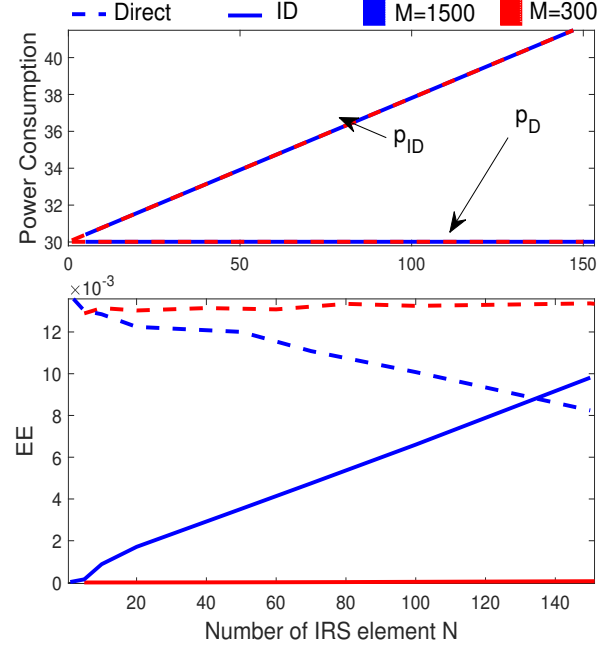
Figure 4.11 Comparison of power consumption and conditional EE for IRS-assisted mode and direct mode of communications with respect to number of IRS elements (for total number of IRSs $M = 300$ and $M = 1500$).

for dense deployment of IRSs since the IRS interference becomes significantly dominant.

Fig. 4.11 shows power consumption and EE for the IRS-assisted and the direct modes of communication with respect to the number of IRSs $M = 300$ and $M = 1500$. The figure presents that the p_{t} increases with the increase in N as expected since $p_{\mathrm{t}} \propto N$. However, the direct mode power consumption $\hat{p}_{\mathrm{t}}$ remains same since $\hat{p}_{\mathrm{t}}$ is not the function of N. It is also clear that M does not have any impact on the power consumption since p_{t} is defined based on total system power consumption per user (refer to Section 3.2.5) and a user is assumed to be connected with only one IRS at a time. The energy-efficiency follows the same trend as conditional rate yet with the smaller slope due to the increasing power of indirect mode that appears in the denominator of EE.
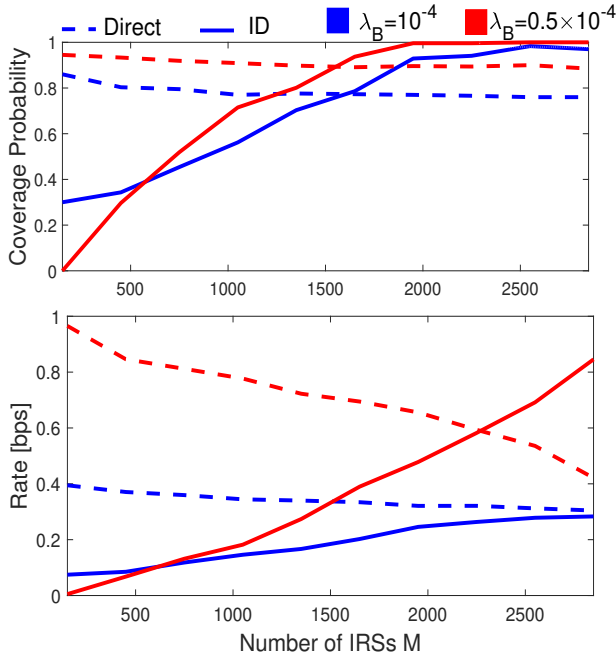
Figure 4.12 Comparison of conditional coverage probability and achievable rate for IRS-assisted mode and direct mode of communications with respect to total number of IRSs (for BS intensity $\lambda_B = 10^{-4}$ and $\lambda_B = 0.5 \times 10^{-4}$, and $N = 100$).
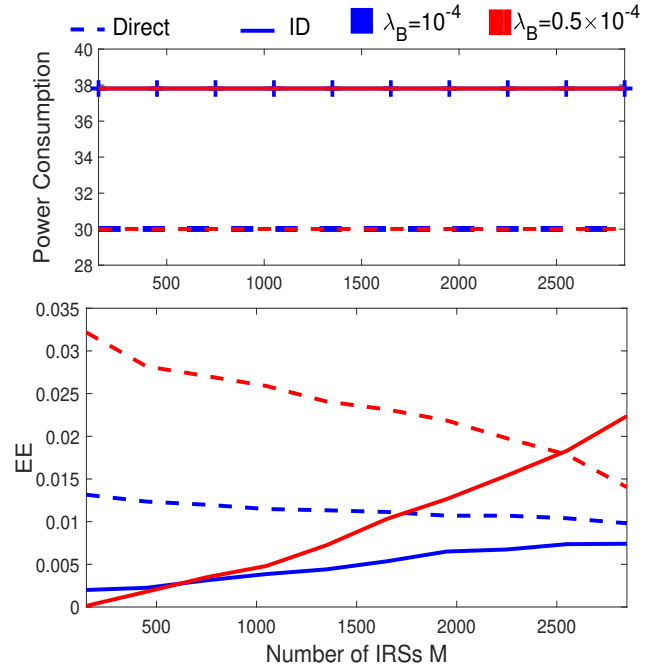
Figure 4.13 Comparison of power consumption and conditional EE for IRS-assisted mode and direct mode with respect to total number of IRSs (for BS intensity $\lambda_B = 10^{-4}$ and $\lambda_B = 0.5 \times 10^{-4}$, and $N = 100$).

4.6.5 Impact of BS Intensity on Direct and IRS-Assisted Communications

Fig. 4.12 compares the coverage probability and ergodic capacity for IRS-assisted and direct communication with respect to total number of IRSs in the coverage area for BS intensity $\lambda_B = 10^{-4}$ and $\lambda_B = 0.5 \times 10^{-4}$. I observe that C_{ID} increases as total number of IRSs in the cell increases. Also, a very subtle decrease in C_{D} is observed for both $\lambda_B = 10^{-4}$ and $\lambda_B = 0.5 \times 10^{-4}$. This is because, as M increases, the IRS density increases and the nearest IRS becomes closer to the user that corresponds to smaller $r_{0,0}$ and higher IRS received signal power that leads to improvement in C_{ID}. Also, an increases in M increases the interference coming from the IRSs for the direct user resulting in a slight decrease in C_{D}. The figure
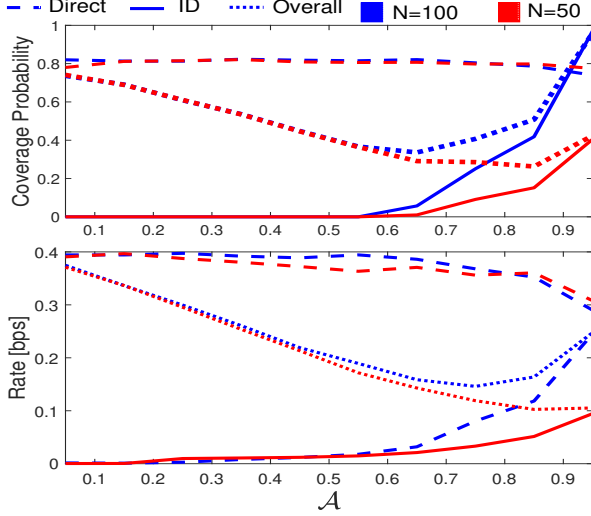
Figure 4.14 Comparison of conditional coverage probability and achievable rate for IRS-assisted mode and direct mode, and overall performance with respect to the fraction of users assisted by IRS $\mathcal{A}$ (for number of IRS elements $N = 50$ and $N = 100$ per IRS surface).
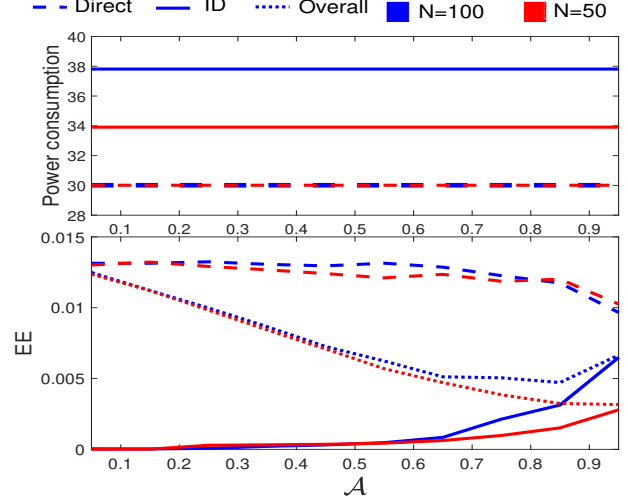
Figure 4.15 Comparison of power consumption, conditional energy-efficiency for IRS-assisted mode, direct mode, and overall EE with respect to the fraction of users assisted by IRS $\mathcal{A}$ (for number of IRS elements $N = 50$ and $N = 100$ per surface).

also shows that a more sparse BS deployment leads to a smaller coverage probability of direct communication mode, and indirect coverage C_{ID} outperforms direct mode coverage for $M > 1700$ for both the values of λ_B. A similar trend can be observed for the achievable rate. This implies that density of deployment of IRSs (i.e., sparse BS deployment or dense IRS deployment) plays a significant role in the performance of IRS-assisted mode.

Fig. 4.13 presents results on power consumption and EE for the direct and indirect modes. Fig. 4.13 follows the same trend of achievable rate as in Fig. 4.12 with the difference in the slope of EE_{ID}.

Fig. 4.14 shows the impact of $\mathcal{A}$ on different system performance measures. The coverage probability of IRS-assisted communication C_{ID} increases with $\mathcal{A}$ because this increases $\lambda_R = \frac{\mathcal{A}}{1-\mathcal{A}} \lambda_B$. The overall system coverage probability C follows C_D when $\mathcal{A} \approx 0$ which corresponds to very few or no IRS in the system. However, C decreases up to $\mathcal{A} = 0.6$ and then it starts

to increase and converges to C_{ID} when $\mathcal{A} \approx 1$ for $N = 100$. Note that, for $\mathcal{A} \approx 0.95$, $\lambda_R = 20\lambda_B$. Moreover, a decrease in direct coverage probability C_D is also visible due to the aggregate interference coming from IRS. A similar trend is observed for $N = 50$ with poorer C_{ID} than C_D due to fewer IRS elements compared to the case when $N = 100$. Also, Fig. 4.15 shows a similar trend in achievable rate because the power consumption does not change significantly.

4.7   Conclusion

I have analyzed the downlink coverage probability, ergodic capacity, and energy-efficiency performance for cellular networks under multi-BS and multi-IRS setup considering both the IRS-assisted communication and direct communication modes. I have observed that using a larger number of IRS elements per IRS are crucial for IRS-assisted communication to outperform direct communication. Also, I have observed that IRS-assisted communication becomes dominant when IRSs are densely deployed (i.e., when IRS intensity is larger than BS intensity). Also, for dense IRS deployment, the impact of IRS-interference significantly decreases the performance of direct communication and enhances IRS-assisted communication because the nearest IRS becomes closer to user. Our results also have demonstrated the impact of fraction of indirect IRS-assisted users on the overall system performance and given insights on how to select the proportion of direct or indirect IRS-assisted users in the network to achieve the desired trade-off between the degradation of direct communication and massive connectivity. The work can be extended to investigate the impact of multi-antennas at the BSs and the user devices.

Chapter Five

Conclusion and Future Research Directions

In this chapter, I conclude the thesis followed by several future directions.

5.1   Conclusion/Summary of the Thesis

The common conclusion drawn from the thesis are as follows:

- The performance of a UAV-assisted communication can be significantly enhanced by optimizing the UAV horizontal and vertical location in 3D.

- The performance of a communication system can be enhanced by integrating UAV and IRS together.

- The IRS-assisted communication performance can be significantly improved in large scale setup of multi BS and multi IRS by increasing the number of IRS elements, dense IRS deployment and sparse BS deployment.

The specific conclusion and summary of each chapter of the thesis is provided next:

The proposed framework of optimal data ferrying in **Chapter two** addresses the challenges given in (1.2.i and 1.2.ii) and is novel in three aspects: (i) performance modeling and optimization of a UAV-assisted data ferrying network with Rician and Rayleigh fading for LoS and NLoS scenarios, respectively, (ii) novel approximations to the derived BER and SNR outage expressions while applying them to optimize data ferrying distance, and (iii) formulation and solution of three different optimization problems, i.e. energy-constrained, outage-constrained, and multi-objective optimization problems.

The highlighted difference in current literature and my work is as follows: Although the optimization problem solved in the work is a single variable optimization but its formulation is significantly challenging compared to typical instantaneous optimization models where the objective function and constraints are defined for each fading channel realization and, subsequently, the optimal solutions are computed per channel realization. To understand the impact of a variety of fading channels, an instantaneous optimization problem needs to be solved for a large number of channel realizations (assuming perfect knowledge of channel state information (CSI)) as compared to only one time in our case. However, the optimization problem I solved is unique since it uses closed-form analytical expressions for the end-to-end outage probability in Rician and Rayleigh fading channels. To deal with the intricate outage expression, I derived novel approximations and transformations to formulate a convex problem.

The proposed framework of integrated UAV-IRS in **Chapter Three** addresses the challenges given in (1.2.ii, 1.2.iii and 1.2.iv) and is novel in the following aspects: (i) Performance modeling and optimization in terms of SNR outage probability, ergodic capacity, and energy efficiency in which end-users (i.e., transmitter and receiver) can communicate in three ways, namely, IRS-only mode, UAV-only mode, and integrated UAV-IRS mode. (ii) I considered the impact of LoS air-to-ground Rician channel and power consumption of both UAV and IRS for each communication mode, (iii) For each communication mode, I formulated and

solved several optimization problems that investigate the effect of major parameters on communication modes (e.g., number of IRS elements and UAV height for IRS-only mode and UAV height for UAV-only mode), and (iv) I provide the impact of critical IRS and UAV parameter on the optimal mode selection criteria based of EE. I also derived novel approximations, and transformations or used fractional programming to obtain the optimization in closed form where applicable.

The developed framework of large-scale IRS-assisted downlink in **Chapter Four** is novel in the following aspects: Performance modeling and characterization of the downlink coverage probability, ergodic capacity, and energy-efficiency for cellular networks under multi-BS and multi-IRS setup considering both the IRS-assisted communication and direct communication users. I consider the impact of critical IRS parameter on IRS-assisted communication, suggesting that the key for dominant IRS-assisted communication (than the direct communication) lies in the followings: (a) larger number of IRS elements, (b) dense deployment of IRSs or sparse deployment of BS (i.e., when IRS intensity is larger than BS intensity). I also present overall system performance measures by taking a fraction of indirect IRS-assisted users and blocking probability in to account.

The highlighted difference in current literature and my work in Chapter Five is as follows: Deriving novel closed-form expressions for (i) received signal through IRS-assisted link in the form of generalized Gamma RV, (ii) modeling the aggregate interference coming from interfering IRSs and interfering BSs with customize-able normal RV depending on IRS-assisted or direct communication scenario, and (iii) the analysis is done considering realistic channel instead of utilizing statistical measure for simplicity, unlike the existing literature. The **Chapter Four** addresses the challenges given in (1.2.iii and 1.2.v)

5.2 Research Outcome: Publication List

All the thesis work is either published or submitted for possible publication. The list of published/submitted papers related to this thesis is given below:

- Journal Publications:

    1. **Taniya Shafique**, Hina Tabassum, and Ekram Hossain. " Stochastic Geometry Analysis of IRS-Assisted Downlink Cellular Networks." Submitted to *IEEE Transactions on Communications*.

    2. **Taniya Shafique**, Hina Tabassum, and Ekram Hossain. " Optimization of wireless relaying with flexible UAV-borne reflecting surfaces." *IEEE Transactions on Communications*, vol. 69, no. 1, pp. 309-325, Oct. 2020.

    3. **Taniya Shafique**, Hina Tabassum, and Ekram Hossain. "End-to-End Energy-Efficiency and Reliability of UAV-Assisted Wireless Data Ferrying." *IEEE Transactions on Communications*, vol. 68, no. 3, pp. 1822-1837, Dec. 2019.

5.3 Future Research Directions

In this section, I provide few possible directions for the future work considering the work done in the thesis.

- *Optimal data ferrying for multi cluster scenario:* As mentioned in **Chapter Two**, end-to-end performance has been studied followed by optimization for UAV data ferrying model in multicasting application in which the UAV can transmit to those receivers for which quality-of-service (QoS) can be met, while traveling towards the destination. However, the considered serving region (i.e. the cell radius) where all receivers are located is very small compared to the traveling distance of UAV. Under this assumption,

the farthest or nearest receiver becomes approximately the same to the receiver who is located at the cell-center. Hence, the problem of optimal UAV-assisted data-ferrying is designed for a single cluster. Therefore, the framework can be extended to a wider coverage region by considering a multi cluster scenario and the optimal UAV trajectory can be optimized based on data-ferry technique.

- *Practical considerations for UAV-based communications:* The performance of the UAV-assisted communication is highly dependent on the energy consumption of the UAVs. There are many factors that affect the energy consumption of a UAV namely, **(i)** Design factor, **(ii)** environmental factors, and **(iii)** drone dynamic factor [126]. The design factor consists of the size and the weight of the UAV, size, the weight and power capacity of the battery, the number and size of rotors, maximum speed, and payload, lift to drag ratio, etc. [127]. The environmental factor consists of wind conditions, weather conditions such as snowy, rainy, etc. temperature, air density and gravitational force. The wind condition is extremely important for the vertical UAV flight [128]. For instance, when the UAV flies up against the wind, the UAV exerts more energy in stabilizing itself and countering the oncoming wind, and therefore, the UAV consumes the battery fast. However, when the UAV flies in the direction of the wind, the UAV battery consumption significantly reduces. Nonetheless, the UAV in the downwind fly is hard to control and prone to turbulence. Also, flying the UAV at a predefined inclined angle stabilizes the UAV in the severe wind scenario [129, 130]. Lastly, the UAV dynamics consists of drone travel speed, drone motion (i.e., take-off/landing, hover, horizontal flight), acceleration, angle of attack and flight altitude. All of these aforementioned factors are interrelated and impact the utility of the UAVs in wireless communication applications by changing the hovering and traveling power consumption of the UAV (please see Section 2.3.4) and hence the energy efficiency and the UAV flying time. Studying the impact of the UAV and environment dynamics can

151

be an interesting future direction.

- *Massive integrated UAV-IRS setup:* The performance gain brought by UAV-assisted communication integrated with Intelligent reflecting surface (IRS) mounted on UAV is studied for single source, single destination, and single UAV-borne IRS. The idea of integrated UAV-IRS can be studied for a correlated fading channel. Also, Multiple integrated UAV-IRS surfaces can be designed to assist wireless communication to multiple ground users. In this case, the assignment of UAV or IRS communication mode to each of the ground users such that overall system performance is optimized can be a potential research direction. The centralized optimization could be time inefficient and higher in complexity so designing such a suboptimal solution that can perform close to the central solution can be a contribution to the 6G networks. The machine learning technique can be a potential candidate for this type of optimization problem.

- *Spherical IRS surface consideration:* The IRS surfaces in existing communication problems are plane meta-surfaces, which consist of a linear array of multiple IRS elements. However, the meta-surface can be designed in different shapes e.g., planner and spherical [131]. Studying the performance comparison due to different shape reflecting surfaces can bring additional performance gain e.g., in beamforming angle, and might introduce diffraction which can help the communication between two different mediums. For instance, an IRS deployed on the water level on sea or ocean can assist underwater and aerial or ground communication.

- *Multi user and multi antenna modeling:* One straightforward future direction is to extend the large scale IRS setup with single antennas presented in the thesis to investigate the impact of multi-antennas at the BSs and the user devices.

Bibliography

[1] J. C. Fahmy. From 1G to 5G: The history of cell phones and their cellular generations. [Online]. Available: https://www.cengn.ca/timeline-from-1g-to-5g-a-brief-history-on-cell-phones/

[2] A. Mourad, R. Yang, P. H. Lehne, and A. De La Oliva, "A baseline roadmap for advanced wireless research beyond 5g," *Electronics*, vol. 9, no. 2, p. 351, 2020.

[3] H. Viswanathan and P. E. Mogensen, "Communications in the 6g era," *IEEE Access*, vol. 8, pp. 57 063–57 074, 2020.

[4] W. Saad, M. Bennis, and M. Chen, "A vision of 6g wireless systems: Applications, trends, technologies, and open research problems," *IEEE network*, vol. 34, no. 3, pp. 134–142, 2019.

[5] L. Song. T07: Aerial access networks for 6g: Integration of uav, hap, and satellite communication networks. [Online]. Available: https://pimrc2020.ieee-pimrc.org/t7-aerial-access-networks-for-6g-integration-of-uav-hap-and-satellite-communication-networks/

[6] M. W. Akhtar, S. A. Hassan, R. Ghaffar, H. Jung, S. Garg, and M. S. Hossain, "The shift to 6g communications: vision and requirements," *Human-centric Computing and Information Sciences*, vol. 10, no. 1, pp. 1–27, 2020.

[7] S. O'Dea. Connection density of 4g, 5g, and 6g mobile broadband technologies. [Online]. Available: https://www.statista.com/statistics/1183690/mobile-broadband-connection-density/

[8] S. Ali, W. Saad, D. Steinbach, I. Ahmad, and J. Huusko, "White paper on machine learning in wireless communication networks," 2020.

[9] T. Yang, K. Yao, Y. Sun, F. Song, Y. Yang, and Y. Zhang, "Joint power and bandwidth allocation for uav backhaul networks: A hierarchical learning approach," *Preprints*, vol. 0, p. 0, 2019.

[10] C. Newton. Facebook takes flight. [Online]. Available: https://www.theverge.com/a/mark-zuckerberg-future-of-facebook/aquila-drone-internet

[11] N. C. Luong, D. T. Hoang, P. Wang, D. Niyato, D. I. Kim, and Z. Han, "Data collection and wireless communication in internet of things (iot) using economic analysis and pricing models: A survey," *IEEE Communications Surveys & Tutorials*, vol. 18, no. 4, pp. 2546–2590, 2016.

[12] S. Eom, H. Lee, J. Park, and I. Lee, "Uav-aided wireless communication designs with propulsion energy limitations," *IEEE Transactions on Vehicular Technology*, 2019.

[13] Y. Zeng and R. Zhang, "Energy-efficient uav communication with trajectory optimization," *IEEE Transactions on Wireless Communications*, vol. 16, no. 6, pp. 3747–3760, 2017.

[14] M. Mozaffari, W. Saad, M. Bennis, and M. Debbah, "Mobile internet of things: Can uavs provide an energy-efficient mobile architecture?" in *Global Communications Conference (GLOBECOM), 2016 IEEE*. IEEE, 2016, pp. 1–6.

[15] C.-M. Cheng, P.-H. Hsiao, H. Kung, and D. Vlah, "Maximizing throughput of UAV-relaying networks with the load-carry-and-deliver paradigm," in *Wireless Commun. and Networking Conf.* IEEE, 2007, pp. 4417–4424.

[16] U. Siddique, H. Tabassum, E. Hossain, and D. I. Kim, "Wireless backhauling of 5g small cells: Challenges and solution approaches," *Transaction on Wireless Commun.*, vol. 22, no. 5, pp. 22–31, 2015.

[17] U. Siddique, H. Tabassum, and E. Hossain, "Downlink spectrum allocation for in-band and out-band wireless backhauling of full-duplex small cells," *IEEE_ J_ WCOM*, vol. 65, no. 8, pp. 3538–3554, 2017.

[18] U. Challita and W. Saad, "Network formation in the sky: Unmanned aerial vehicles for multi-hop wireless backhauling," in *GLOBECOM 2017-2017 IEEE Global Communications Conference.* IEEE, 2017, pp. 1–6.

[19] H. Shakhatreh, A. H. Sawalmeh, A. Al-Fuqaha, Z. Dou, E. Almaita, I. Khalil, N. S. Othman, A. Khreishah, and M. Guizani, "Unmanned aerial vehicles (uavs): A survey on civil applications and key research challenges," *IEEE Access*, vol. 7, pp. 48 572–48 634, 2019.

[20] W. Zhao and M. H. Ammar, "Message ferrying: Proactive routing in highly-partitioned wireless ad hoc networks." in *FTDCS*, vol. 3, 2003, p. 308.

[21] Y. Zeng, J. Xu, and R. Zhang, "Energy minimization for wireless communication with rotary-wing UAV," *IEEE Trans. on Wireless Commun.*, vol. 18, no. 4, pp. 2329–2345, 2019.

[22] Q. Wu and R. Zhang, "Towards smart and reconfigurable environment: Intelligent reflecting surface aided wireless network," *IEEE Communications Magazine*, 2019.

[23] C. Huang, A. Zappone, G. C. Alexandropoulos, M. Debbah, and C. Yuen, "Reconfigurable intelligent surfaces for energy efficiency in wireless communication," *IEEE Transactions on Wireless Communications*, vol. 18, no. 8, pp. 4157–4170, 2019.

[24] C. Liaskos, S. Nie, A. Tsioliaridou, A. Pitsillides, S. Ioannidis, and I. Akyildiz, "A new wireless communication paradigm through software-controlled metasurfaces," *IEEE Communications Magazine*, vol. 56, no. 9, pp. 162–169, 2018.

[25] Q. Wu and R. Zhang, "Intelligent reflecting surface enhanced wireless network via joint active and passive beamforming," *IEEE Transactions on Wireless Communications*, vol. 18, no. 11, pp. 5394–5409, 2019.

[26] C. Huang, G. C. Alexandropoulos, A. Zappone, M. Debbah, and C. Yuen, "Energy efficient multi-user miso communication using low resolution large intelligent surfaces," in *2018 IEEE Globecom Workshops (GC Wkshps)*. IEEE, 2018, pp. 1–6.

[27] R. Méndez-Rial, C. Rusu, N. González-Prelcic, A. Alkhateeb, and R. W. Heath, "Hybrid mimo architectures for millimeter wave communications: Phase shifters or switches?" *Ieee Access*, vol. 4, pp. 247–267, 2016.

[28] E. Vinogradov, H. Sallouha, S. De Bast, M. M. Azari, and S. Pollin, "Tutorial on uav: A blue sky view on wireless communication," *arXiv preprint arXiv:1901.02306*, 2019.

[29] M. Mozaffari, W. Saad, M. Bennis, Y.-H. Nam, and M. Debbah, "A tutorial on uavs for wireless networks: Applications, challenges, and open problems," *IEEE communications surveys & tutorials*, vol. 21, no. 3, pp. 2334–2360, 2019.

[30] B. Ji, Y. Li, B. Zhou, C. Li, K. Song, and H. Wen, "Performance analysis of UAV relay assisted IoT communication network enhanced with energy harvesting," *IEEE Access*, vol. 7, pp. 38 738–38 747, 2019.

[31] L. Zhou, Z. Yang, S. Zhou, and W. Zhang, "Coverage probability analysis of UAV cellular networks in urban environments," in *IEEE Intl. Conf on Commun. Workshops (ICC Workshops)*, 2018, pp. 1–6.

[32] X. Yuan, Z. Feng, W. Xu, W. Ni, J. A. Zhang, Z. Wei, and R. P. Liu, "Capacity analysis of UAV communications: Cases of random trajectories," *IEEE Trans. Veh. Technol.*, vol. 67, no. 8, pp. 7564–7576, 2018.

[33] C. You and R. Zhang, "3D trajectory optimization in Rician fading for UAV-enabled data harvesting," *IEEE Trans. on Wireless Commun.*, 2019.

[34] M. Kim and J. Lee, "Outage probability ofUAVcommunications in the presence of interference," in *2018 IEEE Global Communications Conference (GLOBECOM)*. IEEE, 2018, pp. 1–6.

[35] T. Z. H. Ernest, A. Madhukumar, R. P. Sirigina, and A. K. Krishna, "A power series approach for hybrid-duplex UAV communication systems under Rician shadowed fading," *IEEE Access*, vol. 7, pp. 76 949–76 966, 2019.

[36] J. Lyu, Y. Zeng, and R. Zhang, "Cyclical multiple access in uav-aided communications: A throughput-delay tradeoff," *IEEE Wireless Communications Letters*, vol. 5, no. 6, pp. 600–603, 2016.

[37] Y. Zeng, X. Xu, and R. Zhang, "Trajectory design for completion time minimization in uav-enabled multicasting," *IEEE Trans. Wireless Commun*, vol. 17, no. 4, pp. 2233–2246, 2018.

[38] T. K. Vu, M. Bennis, M. Debbah, M. Latva-Aho, and C. S. Hong, "Ultra-reliable communication in 5G mmWave networks: A risk-sensitive approach," *IEEE Commun. Letters*, vol. 22, no. 4, pp. 708–711, 2018.

[39] M. M. Azari, F. Rosas, K.-C. Chen, and S. Pollin, "Ultra reliable UAV communication using altitude and cooperation diversity," *IEEE Trans. on Commun.*, vol. 66, no. 1, pp. 330–344, 2017.

[40] C. She, C. Yang, and T. Q. Quek, "Joint uplink and downlink resource configuration for ultra-reliable and low-latency communications," *IEEE Trans. on Commun.*, vol. 66, no. 5, pp. 2266–2280, 2018.

[41] A. Mahmood, M. A. Hossain, and M. Gidlund, "Cross-layer optimization of wireless links under reliability and energy constraints," in *IEEE Wireless Commun. and Networking Conf. (WCNC)*, 2018, pp. 1–6.

[42] C. She, C. Liu, T. Q. Quek, C. Yang, and Y. Li, "Ultra-reliable and low-latency communications in unmanned aerial vehicle communication systems," *IEEE Trans. on Commun.*, vol. 67, no. 5, pp. 3768–3781, 2019.

[43] C. Sun, C. She, and C. Yang, "Energy-efficient resource allocation for ultra-reliable and low-latency communications," in *IEEE Global Commun. Conf. (GLOBCOM)*. IEEE, 2017, pp. 1–6.

[44] S. Efazati and P. Azmi, "Performance study of a new cooperative protocol in rician fading channels," in *Telecommunications (IST), 2010 5th International Symposium on*. IEEE, 2010, pp. 280–285.

[45] O. Olabiyi and A. Annamalai, "New exponential-type approximations for the erfc(.) and erfcp(.) functions with applications," in *Intl Wireless Commun. and Mobile Compt. Conf. (IWCMC)*, Aug 2012, pp. 1221–1226.

[46] H. Tabassum and E. Hossain, "Coverage and rate analysis for co-existing RF/VLC downlink cellular networks," *IEEE Trans. Commun.*, vol. 17, no. 4, pp. 2588–2601, 2018.

[47] K. A. Hamdi, "A useful lemma for capacity analysis of fading interference channels," *IEEE Trans. Commun.*, vol. 58, no. 2, pp. 411–416, 2010.

[48] A. Al-Hourani and K. Gomez, "Modeling cellular-to-uav path-loss for suburban environments," *IEEE Wireless Communications Letters*, vol. 7, no. 1, pp. 82–85, 2018.

[49] T. N. Nguyen, P. T. Tran, T. H. Q. Minh, M. Vozňák, and L. Ševčík, "Two-way half duplex decode and forward relaying network with hardware impairment over rician fading channel: system performance analysis," 2018.

[50] M. M. Azari, F. Rosas, K.-C. Chen, and S. Pollin, "Ultra reliable UAV communication using altitude and cooperation diversity," *IEEE Trans. on Commun.*, vol. 66, no. 1, pp. 330–344, 2018.

[51] C. Di Franco and G. Buttazzo, "Energy-aware coverage path planning of uavs," in *Autonomous Robot Systems and Competitions (ICARSC), 2015 IEEE International Conference on.* IEEE, 2015, pp. 111–117.

[52] C. Desset, B. Debaillie, V. Giannini, A. Fehske, G. Auer, H. Holtkamp, W. Wajda, D. Sabella, F. Richter, M. J. Gonzalez *et al.*, "Flexible power modeling of lte base stations," in *Wireless Communications and Networking Conference (WCNC), 2012 IEEE.* IEEE, 2012, pp. 2858–2862.

[53] A. Filippone, *Flight performance of fixed and rotary wing aircraft.* Elsevier, 2006.

[54] T. Shafique, O. Amin, M. Abdallah, I. S. Ansari, M.-S. Alouini, and K. Qaraqe, "Performance analysis of single-photon avalanche diode underwater VLC system using ARQ," *IEEE Photonics Journal*, vol. 9, no. 5, pp. 1–11, 2017.

[55] E. Morgado, I. Mora-Jiménez, J. J. Vinagre, J. Ramos, and A. J. Caamaño, "End-to-end average BER in multihop wireless networks over fading channels," *IEEE trans on wireless commun*, vol. 9, no. 8, pp. 2478–2487, 2010.

[56] M. Chiani and D. Dardari, "Improved exponential bounds and approximation for the q-function with application to average error probability computation," in *Global Telecommunications Conference, 2002. GLOBECOM'02. IEEE*, vol. 2.   IEEE, 2002, pp. 1399–1402.

[57] T. Shafique, A. M. Abdelhady, O. Amin, and M.-S. Alouini, "Energy efficiency, spectral efficiency and delay analysis for selective ARQ multi-channel systems," *IEEE Trans. Green Commun. and Networking*, 2018.

[58] A. C. J. Samarasekera, "The performance of dual-hop decode-and-forward underlay cognitive relay networks with interference power constraints over weibull fading channels," 2014.

[59] M. R. Bhatnagar, "On the capacity of decode-and-forward relaying over rician fading channels," *IEEE Communications Letters*, vol. 17, no. 6, pp. 1100–1103, 2013.

[60] T. Nguyen, T. Quang Minh, P. Tran, and M. Vozňák, "Energy harvesting over rician fading channel: A performance analysis for half-duplex bidirectional sensor networks under hardware impairments," *Sensors*, vol. 18, no. 6, p. 1781, 2018.

[61] R. Salahat, E. Salahat, A. Hakam, and T. Assaf, "A simple and efficient approximation to the modified bessel functions and its applications to rician fading," in *2013 7th IEEE GCC Conference and Exhibition (GCC)*.   IEEE, 2013, pp. 351–354.

[62] T. Kwon, S. W. Choi, and Y.-H. Shin, "A comprehensive design framework for network-wide cost reduction in random access based wireless IoT networks," *IEEE Communications Letters*, 2019.

[63] J. Tang, D. K. So, E. Alsusa, and K. A. Hamdi, "Resource efficiency: A new paradigm on energy efficiency and spectral efficiency tradeoff," *IEEE Transactions on Wireless Communications*, vol. 13, no. 8, pp. 4656–4669, 2014.

[64] C. A. C. Coello, G. B. Lamont, D. A. Van Veldhuizen *et al.*, *Evolutionary algorithms for solving multi-objective problems.* Springer, 2007, vol. 5.

[65] D. Jiang and Y. Cui, "Enhancing performance of random caching in large-scale wireless networks with multiple receive antennas," *IEEE Trans on Wireless Commun.*, vol. 18, no. 4, pp. 2051–2065, 2019.

[66] P. D. Tao *et al.*, "The DC (difference of convex functions) programming and DCA revisited with DC models of real world nonconvex optimization problems," *Annals of operations research*, vol. 133, no. 1-4, pp. 23–46, 2005.

[67] T. P. Dinh, H. M. Le, H. A. Le Thi, and F. Lauer, "A difference of convex functions algorithm for switched linear regression," *IEEE Trans on Automatic Control*, vol. 59, no. 8, pp. 2277–2282, 2014.

[68] S. Sekander, H. Tabassum, and E. Hossain, "Multi-tier drone architecture for 5G/B5G cellular networks: Challenges, trends, and prospects," *IEEE Commun. Magazine*, vol. 56, no. 3, pp. 96–103, 2018.

[69] L. Yang, J. Chen, M. O. Hasna, and H.-C. Yang, "Outage performance of UAV-assisted relaying systems with RF energy harvesting," *IEEE Commun. Letters*, vol. 22, no. 12, pp. 2471–2474, 2018.

[70] S. Zhang, H. Zhang, Q. He, K. Bian, and L. Song, "Joint trajectory and power optimization for UAV relay networks," *IEEE Commun. Letters*, vol. 22, no. 1, pp. 161–164, 2017.

[71] S. Ahmed, A. Mohamed, K. Harras, M. Kholief, and S. Mesbah, "Energy efficient path planning techniques for UAV-based systems with space discretization," in *Wireless Commun. and Networking Conf. (WCNC), IEEE*, 2016, pp. 1–6.

[72] D. Yang, Q. Wu, Y. Zeng, and R. Zhang, "Energy tradeoff in ground-to-UAV communication via trajectory design," *IEEE Trans. Veh. Technol.*, vol. 67, no. 7, pp. 6721–6726, 2018.

[73] J. Chakareski, S. Naqvi, N. Mastronarde, J. Xu, F. Afghah, and A. Razi, "An energy efficient framework for uav-assisted millimeter wave 5G heterogeneous cellular networks," *IEEE Trans. on Green Commun. and Networking*, vol. 3, no. 1, pp. 37–44, 2019.

[74] J. Lyu, Y. Zeng, R. Zhang, and T. J. Lim, "Placement optimization of uav-mounted mobile base stations," *IEEE Communications Letters*, vol. 21, no. 3, pp. 604–607, 2017.

[75] M. Alzenad, A. El-Keyi, F. Lagum, and H. Yanikomeroglu, "3-d placement of an unmanned aerial vehicle base station (uav-bs) for energy-efficient maximal coverage," *IEEE Wireless Communications Letters*, vol. 6, no. 4, pp. 434–437, 2017.

[76] Z. Yang, C. Pan, K. Wang, and M. Shikh-Bahaei, "Energy efficient resource allocation in uav-enabled mobile edge computing networks," *IEEE Transactions on Wireless Communications*, vol. 18, no. 9, pp. 4576–4589, 2019.

[77] E. Basar, M. Di Renzo, J. De Rosny, M. Debbah, M.-S. Alouini, and R. Zhang, "Wireless communications through reconfigurable intelligent surfaces," *IEEE Access*, vol. 7, pp. 116 753–116 773, 2019.

[78] E. Björnson, Ö. Özdogan, and E. G. Larsson, "Intelligent reflecting surface vs. decode-and-forward: How large surfaces are needed to beat relaying?" *IEEE Wireless Commun. Letters*, vol. 9, no. 2, pp. 244–248, 2020.

[79] S. Li, B. Duo, X. Yuan, Y.-C. Liang, and M. Di Renzo, "Reconfigurable intelligent surface assisted UAV communication: Joint trajectory design and passive beamforming," *IEEE Wireless Commun. Letters*, 2020.

[80] Q. Zhang, W. Saad, and M. Bennis, "Reflections in the sky: Millimeter wave communication with UAV-carried intelligent reflectors," *arXiv preprint arXiv:1908.03271*, 2019.

[81] H. Zhang, B. Di, L. Song, and Z. Han, "Reconfigurable intelligent surfaces assisted communications with limited phase shifts: How many phase shifts are enough?" *IEEE Trans. Vehicular Tech.*, vol. 69, no. 4, pp. 4498–4502, 2020.

[82] A. an, M. Debbah, and M.-S. Alouini, "Intelligent reflecting surface assisted wireless communication: Modeling and channel estimation," *arXiv preprint arXiv:1906.02360*, 2019.

[83] G. Pan, J. Ye, J. An, and M.-S. Alouini, "When full-duplex transmission meets intelligent reflecting surface: Opportunities and challenges," *arXiv preprint arXiv:2005.12561*, 2020.

[84] D. Bharadia, E. McMilin, and S. Katti, "Full duplex radios," in *Proceedings of the ACM Conf. on SIGCOMM*, 2013, pp. 375–386.

[85] Q. Wu and R. Zhang, "Beamforming optimization for intelligent reflecting surface with discrete phase shifts," in *IEEE International Conf. on Acoustics, Speech and Signal Processing (ICASSP)*, 2019, pp. 7830–7833.

[86] J. Lu, S. Wan, X. Chen, and P. Fan, "Energy-efficient 3D UAV-BS placement versus mobile users' density and circuit power," in *2017 IEEE Globecom Workshops (GC Wkshps)*, 2017, pp. 1–6.

[87] A. S. Sedra, D. E. A. S. Sedra, K. C. Smith, and K. C. Smith, *Microelectronic circuits*. New York: Oxford University Press, 1998.

[88] A. Bousia, E. Kartsakli, A. Antonopoulos, L. Alonso, and C. Verikoukis, "Energy efficient schemes for base station management in 4G broadband systems," in *Broadband*

Wireless Access Networks for 4G: Theory, Application, and Experimentation. IGI Global, 2014, pp. 100–120.

[89] B. Talha and M. Pätzold, "On the statistical properties of double Rice channels," in *Proc. 10th Intr. Symposium on Wireless Personal Multimedia Commun., WPMC*, 2007, pp. 517–522.

[90] J. Salo, H. M. El-Sallabi, and P. Vainikainen, "The distribution of the product of independent Rayleigh random variables," *IEEE Trans. Antennas Propag.*, vol. 54, no. 2, pp. 639–643, 2006.

[91] F. Jiang and A. L. Swindlehurst, "Dynamic UAV relay positioning for the ground-to-air uplink," in *IEEE Globecom Workshops*, 2010, pp. 1766–1770.

[92] J. Proakis and M. Salehi, *Digital communications.* McGraw-Hill, 2007.

[93] K. Shen and W. Yu, "Fractional programming for communication systems- Part I: Power control and beamforming," *IEEE Transactions on Signal Processing*, vol. 66, no. 10, pp. 2616–2630, 2018.

[94] A. Zappone, E. Björnson, L. Sanguinetti, and E. A. Jorswieck, "Achieving global optimality for energy efficiency maximization in wireless networks," *IEEE Trans. Signal Process.*, 2016.

[95] Q. Wu, S. Zhang, B. Zheng, C. You, and R. Zhang, "Intelligent reflecting surface aided wireless communications: A tutorial," *IEEE Trans. Commun.*, 2021.

[96] J. Lyu and R. Zhang, "Hybrid active/passive wireless network aided by intelligent reflecting surface: System modeling and performance analysis," *arXiv preprint arXiv:2004.13318*, 2020.

[97] Q. Tao, J. Wang, and C. Zhong, "Performance analysis of intelligent reflecting surface aided communication systems," *IEEE Commun. Letters*, vol. 24, no. 11, pp. 2464–2468, 2020.

[98] D. Kudathanthirige, D. Gunasinghe, and G. Amarasuriya, "Performance analysis of intelligent reflective surfaces for wireless communication," in *IEEE Intl. Conf on Commun. (ICC)*, 2020, pp. 1–6.

[99] L. Yang, F. Meng, Q. Wu, D. B. da Costa, and M.-S. Alouini, "Accurate closed-form approximations to channel distributions of RIS-aided wireless systems," *IEEE Wireless Commun. Letters*, vol. 9, no. 11, pp. 1985–1989, 2020.

[100] A.-A. A. Boulogeorgos and A. Alexiou, "Performance analysis of reconfigurable intelligent surface-assisted wireless systems and comparison with relaying," *IEEE Access*, vol. 8, pp. 94 463–94 483, 2020.

[101] I. Trigui, W. Ajib, and W.-P. Zhu, "A comprehensive study of reconfigurable intelligent surfaces in generalized fading," *arXiv preprint arXiv:2004.02922*, 2020.

[102] H. Ibrahim, H. Tabassum, and U. T. Nguyen, "Exact coverage analysis of intelligent reflecting surfaces with Nakagami-m channels," *IEEE Trans. Vehicular Technol.*, vol. 70, no. 1, pp. 1072–1076, 2021.

[103] T. Van Chien, A. K. Papazafeiropoulos, L. T. Tu, R. Chopra, S. Chatzinotas, and B. Ottersten, "Outage probability analysis of IRS-assisted systems under spatially correlated channels," *IEEE Wireless Commun. Letters*, 2021.

[104] Z. Peng, T. Li, C. Pan, H. Ren, W. Xu, and M. Di Renzo, "Analysis and optimization for RIS-aided multi-pair communications relying on statistical CSI," *IEEE Trans. Vehicular Technol.*, 2021.

[105] L. Yang, Y. Yang, D. B. da Costa, and I. Trigui, "Outage probability and capacity scaling law of multiple RIS-aided networks," *IEEE Wireless Commun. Letters*, 2020.

[106] D. L. Galappaththige, D. Kudathanthirige, and G. A. A. Baduge, "Performance analysis of distributed intelligent reflective surface aided communications," in *IEEE Global Commun. Conf. (GLOBECOM)*, 2020, pp. 1–6.

[107] T. N. Do, G. Kaddoum, T. L. Nguyen, D. B. da Costa, and Z. J. Haas, "Multi-RIS-aided wireless systems: Statistical characterization and performance analysis," *arXiv preprint arXiv:2104.01912*, 2021.

[108] Y. Zhu, G. Zheng, and K.-K. Wong, "Stochastic geometry analysis of large intelligent surface-assisted millimeter wave networks," *IEEE J. Select Area. Commun.*, vol. 38, no. 8, pp. 1749–1762, 2020.

[109] M. Afshang and H. S. Dhillon, "Fundamentals of modeling finite wireless networks using binomial point process," *IEEE Trans. Wireless Commun.*, vol. 16, no. 5, pp. 3355–3370, 2017.

[110] S. N. Chiu, D. Stoyan, W. S. Kendall, and J. Mecke, *Stochastic Geometry and its Applications*. John Wiley & Sons, 2013.

[111] J. G. Andrews, F. Baccelli, and R. K. Ganti, "A tractable approach to coverage and rate in cellular networks," *IEEE Trans. Commun.*, vol. 59, no. 11, pp. 3122–3134, 2011.

[112] A. AlAmmouri, H. ElSawy, O. Amin, and M.-S. Alouini, "In-band α-duplex scheme for cellular networks: A stochastic geometry approach," *IEEE Trans. Wireless Commun.*, vol. 15, no. 10, pp. 6797–6812, 2016.

[113] E. Björnson and L. Sanguinetti, "Power scaling laws and near-field behaviors of massive MIMO and intelligent reflecting surfaces," *arXiv preprint arXiv:2002.04960*, 2020.

[114] H. Lu, Y. Chen, and N. Cao, "Accurate approximation to the pdf of the product of independent rayleigh random variables," *IEEE Antennas Wireless Propag. Letters*, vol. 10, pp. 1019–1022, 2011.

[115] E. W. Stacy *et al.*, "A generalization of the gamma distribution," *The Annals of mathematical statistics*, vol. 33, no. 3, pp. 1187–1192, 1962.

[116] A. Jeffrey and D. Zwillinger, *Table of integrals, series, and products.* Elsevier, 2007.

[117] S. P. Boyd and L. Vandenberghe, *Convex Optimization.* Cambridge University Press, 2004.

[118] "*NIST Digital Library of Mathematical Functions*," http://dlmf.nist.gov/, Release 1.1.1 of 2021-03-15, f. W. J. Olver, A. B. Olde Daalhuis, D. W. Lozier, B. I. Schneider, R. F. Boisvert, C. W. Clark, B. R. Miller, B. V. Saunders, H. S. Cohl, and M. A. McClain, eds. [Online]. Available: http://dlmf.nist.gov/

[119] T. Shafique, H. Tabassum, and E. Hossain, "Optimization of wireless relaying with flexible UAV-borne reflecting surfaces," *IEEE Trans. Commun.*, vol. 69, no. 1, pp. 309 – 325, 2021.

[120] M. A. Kishk and M.-S. Alouini, "Exploiting randomly-located blockages for large-scale deployment of intelligent surfaces," *arXiv preprint arXiv:2001.10766*, 2020.

[121] M. Di Renzo and P. Guan, "Stochastic geometry modeling of coverage and rate of cellular networks using the Gil-Pelaez inversion theorem," *IEEE Commun. Letters*, vol. 18, no. 9, pp. 1575–1578, 2014.

[122] S. Srinivasa and M. Haenggi, "Distance distributions in finite uniformly random networks: Theory and applications," *IEEE Trans. Vehicular Technol.*, vol. 59, no. 2, pp. 940–949, 2009.

[123] J. Sayehvand and H. Tabassum, "Interference and coverage analysis in coexisting RF and dense Terahertz wireless networks," *IEEE Wireless Commun. Letters*, vol. 9, no. 10, pp. 1738–1742, 2020.

[124] T. Bai, R. Vaze, and R. W. Heath, "Analysis of blockage effects on urban cellular networks," *IEEE Trans. Wireless Commun.*, vol. 13, no. 9, pp. 5070–5083, 2014.

[125] M. Zhang, L. Tan, K. Huang, and L. You, "On the trade-off between energy efficiency and spectral efficiency in RIS-aided multi-user MISO downlink," *Electronics*, vol. 10, no. 11, p. 1307, 2021.

[126] J. Zhang, "Economic and environmental impacts of drone delivery," 2021.

[127] S. Delbecq, M. Budinger, A. Ochotorena, A. Reysset, and F. Defaÿ, "Efficient sizing and optimization of multirotor drones based on scaling laws and similarity models," *Aerospace Science and Technology*, vol. 102, p. 105873, 2020.

[128] maxdarrow01. Drone weather forecast: A complete guide. [Online]. Available: https://blog.flykit.app/drone-weather-forecast-complete-guide/

[129] R. Mahony, V. Kumar, and P. Corke, "Multirotor aerial vehicles: Modeling, estimation, and control of quadrotor," *IEEE Robotics and Automation magazine*, vol. 19, no. 3, pp. 20–32, 2012.

[130] H. Huang, G. M. Hoffmann, S. L. Waslander, and C. J. Tomlin, "Aerodynamics and control of autonomous quadrotor helicopters in aggressive maneuvering," in *2009 IEEE international conference on robotics and automation*. IEEE, 2009, pp. 3277–3282.

[131] S. Hu, "Spherical large intelligent surfaces," *arXiv preprint arXiv:1907.02699*, 2019.

APPENDIX

Appendix A

Convexity of $E_{tot}(z)$

The second derivative of $E_{tot}(z)$ is $\frac{2}{\alpha}z^{\frac{2}{\alpha}-2}\left[\frac{T_u P_h}{H}\left(\frac{2}{\alpha}-1\right) + \frac{A}{H^2}z^{4/\alpha}\left(z^{-2}-\frac{2}{\alpha}\right) + \left(\frac{4}{\alpha}-1\right)A\right]$, where $A = \frac{P(v)z^{2/\alpha}H^2}{(z^{4/\alpha}-H^2)^{3/2}}$. The convexity is not conclusive from the second derivative for all values of z. However we verified the convexity on MATHEMATICA and CVX for different values of H, D and α. We can check the convexity of $E_{tot}(z)$ in CVX by writing the following problem:

$$\min_{z} \quad E_{tot}(z) = T_u P_h \frac{z^{2/\alpha}}{H} + P(V)(D - \sqrt{z^{4/\alpha} - H^2}) + C$$

$$\text{s.t.} \quad z \leq (H^2 + D^2)^{\alpha/4}, z \geq H^{\alpha/2}$$

in CVX, using auxiliary variable W, as shown below:

$$\min_{z} \quad \frac{P_h T_u z^{2/\alpha}}{H} + \frac{P(V)(D - W)}{V}$$

$$\mathbf{C3} : (z^{2/\alpha} - H)(z^{2/\alpha} + H) \geq W^2$$

$$\mathbf{C2} : z \leq (H^2 + D^2)^{\alpha/4}, z \geq H^{\alpha/2}$$

which is convex and solvable in CVX.

Appendix B

Monotonicity of $E_{tot}(z)$ in (2.65)

I demonstrate that $E_{tot}(z)$ is monotonically decreasing for all values of α, H, and D given $P_h, P(V), P_c$. We first substitute $y = z^{2/\alpha}$ and show that $E_{tot}(y)$ is monotonically decreasing if $E'_{tot}(y) = \frac{P_h T u}{H} - \frac{P(V)}{V} \frac{y}{\sqrt{y^2 - H^2}} \leq 0$. That is, $\frac{P_h T u V}{H P(V)} \leq \frac{y}{\sqrt{y^2 - H^2}}$. Since $P_h < P(V)$, T_u is in order of msec, V is of order of thousands, the product $T_u V$ is always less than the altitude H. As such, L.H.S. is upper bounded by 1. On the other hand, we note that the R.H.S. $\frac{y}{\sqrt{y^2 - H^2}} > 1$. Starting from $y = z^{2/\alpha} = H$, we see that the R.H.S becomes infinity. Then, for $y = H + 1$, we see that the R.H.S becomes $\frac{H+1}{\sqrt{2H+1}}$ for all y, which is greater than 1. Then, we substitute $y = H + n$, where $n \geq 2$ which gives $\frac{H+n}{\sqrt{2H+n}} > 1$. Therefore, L.H.S.< R.H.S. and the function is monotonically decreasing.

Appendix C

Monotonicity of Outage probability of (2.51)

To prove outage probability for v_1 (2.51) and v_3 is an increasing function w.r.t. z, we take the derivative as follows:

$$\frac{dO_k(v_i, z)}{dz} = -U \sum_{\ell=0}^{\infty} \sum_{m=0}^{\ell} f(m, \ell) 2z^{2m+1} e^{-b_d \Gamma'_k z^2} \left(\frac{m}{z^2} - b_k \Gamma'_k \right), \qquad i = 1, 3.$$

That is, (2.51) is as an increasing function of z if $\frac{dO_k(v_i, z)}{dz} \geq 0$ which is true if $\left(\frac{m}{z^2} - b_k \Gamma'_k \right) < 0$. This is due to the reason that in $\frac{dO_k(v_i, z)}{dz}$ functions e.g., $f(m, \ell)$, z^{2m+1}, and $e^{-b_k \Gamma'_k z^2}$ are non negative for all m, and z therefore $\left(\frac{m}{z^2} - b_k \Gamma'_k \right)$ is the only term that can change sign. Thus the first derivative will remain positive only if $(m - b_k \Gamma'_k z^2) < 0$. Note that m is in the range $m \in [0\ 20]$ for evaluations, $b_k \in \{0, \infty\}$, and the range of z is $z \in \{H^{\alpha/2}\ (H^2 + D^2)^{\alpha/4}\}$. Therefore, it is evident that P_c and the contribution of Γ'_k is less dominant than z^2. Hence the condition satisfies for our range of variables.

Appendix D

Ratio of concavity-convexity of (3.44)

We write $-\frac{1}{2}\alpha_i(h)\log(\hat{z}_i^2 + h^2) = \frac{-O_i(h)}{R_i(h)}$. The numerator $-O_i(h)$ is concave when the second derivative is $-\frac{d^2 O_i(h)}{dh^2} \leq 0$. This is true if,

$$
\begin{aligned}
&-\Bigg[4A_i\hat{z}_i^5 + \hat{z}_i^4\left(-2B_i + 5A_i\sqrt{\hat{z}_i^2 + h^2}\right) + \hat{z}_i^3\left(8A_ih^2 - B_i\sqrt{\hat{z}_i^2 + h^2}\right) + h^2\hat{z}_i^2\left(-4B_i + 5(3A_i + C_i)\sqrt{\hat{z}_i^2 + h^2}\right) \\
&\quad + h^4\left(-2B_i + 3(4A_i + C_i)\sqrt{\hat{z}_i^2 + h^2}\right) + \hat{z}_u\left(4A_ih^4 + B_ih^2\sqrt{\hat{z}_i^2 + h^2}\right) + (\hat{z}_i^2 + h^2)\log(\hat{z}_i^2 + h^2) \\
&\quad \times \left(2A_iz_{us}^3 + (4A_i + C_i)h^2\sqrt{\hat{z}_i^2 + h^2} + \hat{z}_i^2\left(-B_i + (4A_i + C_i)\sqrt{\hat{z}_i^2 + h^2}\right)\right)\Bigg] \leq 0.
\end{aligned}
$$

$$(D.1)$$

Starting from (D.1), we use $\log(\hat{z}_i^2 + x^2) \geq \log(\hat{z}_u) + \frac{x^2}{x^2 + \hat{z}_i^2}$ and $\log(\hat{z}_i) \geq 1$ when $\hat{z}_i \geq 10$ and $\min(\hat{z}_i) > 10$ which shows that source and UAV should be at least 10m distance apart in the horizontal plane (which gives one of the condition to prove concave numerator). Under this condition, we obtain,

$$
\begin{aligned}
&-\Bigg[6\hat{z}_i^5 A_i + 12A_ih^2\hat{z}_i^3 + 5h^4(4A_i + C_i)\sqrt{\hat{z}_i^2 + h^2} + \hat{z}_i^4(9A_i + C_i)\sqrt{\hat{z}_i^2 + h^2} + \hat{z}_i^2 h^2(27A_i + 8C_i)\sqrt{\hat{z}_i^2 + h^2} + \\
&\hat{z}_i(4A_ih^4 + B_ih^2\sqrt{\hat{z}_i^2 + h^2}) - \hat{z}_i^3 B_i\sqrt{\hat{z}_i^2 + h^2} - 2B_ih^4 - 3B_i\hat{z}_i^4 - 6B_i\hat{z}_i^2 h^2\Bigg] \leq 0.
\end{aligned}
$$

$$(D.2)$$

Substituting the lower bound $\sqrt{\hat{z}_i^2 + h^2} \geq \max(\hat{z}_i, h)$, which does not change the negativity of the expression, we have

$$
\begin{aligned}
&6\hat{z}_i^5 A_i + 12A_ih^2\hat{z}_i^3 + 5h^4(4A_i + C_i)\max(\hat{z}_i, h) + \hat{z}_i^4((9A_i + C_i)\max(\hat{z}_i, h)) + \hat{z}_i^2 h^2(27A_i + 8C_i)\times \\
&\max(\hat{z}_i, h) + \hat{z}_i(4A_ih^4 + B_ih^2\max(\hat{z}_i, h)) - \hat{z}_i^3 B_i\max(\hat{z}_i, h) - 2B_ih^4 - 3B_i\hat{z}_i^4 - 6B_i\hat{z}_i^2 h^2 \geq 0.
\end{aligned}
$$

$$(D.3)$$

To simplify the expression, we consider **case (i)** when $\hat{z}_i > h$, and substitute $\max(\hat{z}_i, h) = \hat{z}_i$ that yields:

$$(15A_i + C_i)\hat{z}_i^5 + (24A_i + 5C_i)\hat{z}_i h^4 + 39A_i h^2 \hat{z}_i^3 + 8C_i h^2 \hat{z}_i^3 - 4B_i \hat{z}_i^4 - 5B_i \hat{z}_i^2 h^2 - 2B_i h^4 \geq 0.$$

Replacing $\hat{z}_i$ by h in the positive terms and h by $\hat{z}_i$ in negative terms, we get

$$11B_i \hat{z}_i^4 - (78A_i + 14C_i)h^5 > 0 \implies z_i \geq h^{5/4} \left(\frac{78A_i + 14C_i}{11B_i} \right)^{1/4}. \tag{D.4}$$

Similarly, for **case (ii): when** $h > \hat{z}_i$**:** we substitute $\max(\hat{z}_i, h) \geq h$ in (D.3), replacing h by $\hat{z}_i$ in the positive terms and $\hat{z}_i$ by h in negative terms and simplification gives

$$= - \left[6\hat{z}_i^5 A_i + 12A_i \hat{z}_i^5 + 5\hat{z}_i^5(4A_i + C_i) + \hat{z}_i^5(9A_i + C_i) + \hat{z}_i^5(27A_i + 8C_i) + 4A_i \hat{z}_i^5 + B_i \hat{z}_i^4 - 12B_i h^4 \right] \leq 0$$

$$\implies h \geq \hat{z}_i \left(\frac{78A_i \hat{z}_i + B_i + 14C_i \hat{z}_i}{12B_i} \right)^{1/4}. \tag{D.5}$$

However, the denominator $R_i(h) = (1 + \varsigma_i)(\hat{z}_i + 2\sqrt{\hat{z}_i^2 + h^2})^2 - B_i' h \left(\hat{z}_i + 2\sqrt{\hat{z}_i^2 + h^2} \right) + C_i' h^2$ is convex when the second derivative of $R_i(h)$ is positive. The term $\frac{d^2 R_i(h)}{dh^2} \geq 0$ is positive when $2\hat{z}_i^3 A_i + (\hat{z}_i^2 + h^2)(4A_i + C_i)\sqrt{\hat{z}_i^2 + h^2} \geq \hat{z}_i^2 B_i$ which is true since $2A_i \hat{z}_i > B_i$ because A_i, B_i, C_i are order of tens but z_i is in order of hundreds and thousands, hence $R_i(h)$ is convex.

Hence, (D.4) and (D.5) under the constraint $\min(\hat{z}_i) > 10$ gives the condition on concavity of $-O_i(h)$.